General Disclaimer

One or more of the Following Statements may affect this Document

- This document has been reproduced from the best copy furnished by the organizational source. It is being released in the interest of making available as much information as possible.

- This document may contain data, which exceeds the sheet parameters. It was furnished in this condition by the organizational source and is the best copy available.

- This document may contain tone-on-tone or color graphs, charts and/or pictures, which have been reproduced in black and white.

- This document is paginated as submitted by the original source.

- Portions of this document are not fully legible due to the historical nature of some of the material. However, it is the best reproduction available from the original submission.

RADIATIVE TRANSFER, CHEMICAL NON-EQUILIBRIUM, AND TWO-TEMPERATURE EFFECTS BEHIND A REFLECTED SHOCK WAVE IN NITROGEN

Leland A. Carlson
The Ohio State University

12

RADIATIVE TRANSFER, CHEMICAL NONEQUILIBRIUM, AND TWO-TEMPERATURE EFFECTS BEHIND A REFLECTED SHOCK WAVE IN NITROGEN

DISSERTATION

Presented in Partial Fulfillment of the Requirements for the Degree Doctor of Philosophy in the Graduate School of The Ohio State University

By

Leland Arnold Carlson, B.A.A.E., M.S.

******

The Ohio State University
1969

NGR-36-008-106

Approved by

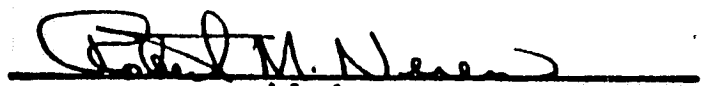

Adviser
Department of Aeronautical and Astronautical Engineering

ACKNOWLEDGMENTS

The author wishes to express his appreciation to Dr. Robert M. Nerem of The Department of Aeronautical and Astronautical Engineering for his encouragement and support.

This research was supported by Grant No. NGR-36-008-106 of the National Aeronautics and Space Administration, Washington, D. C. Partial support for the numerical calculations was furnished by the Numerical Computation Laboratory of The Ohio State University.

VITA

[redacted] . . .	Born - [redacted]
1965	B.A.A.E., The Ohio State University, Columbus, Ohio
	M.S., The Ohio State University, Columbus, Ohio
1965-1966	National Science Foundation Fellow
1966-1968	Research Assistant, Aeronautical and Astronautical Research Laboratory, The Ohio State University, Columbus, Ohio
1968-1969	Graduate Research Associate, Aeronautical and Astronautical Research Laboratory, The Ohio State University, Columbus, Ohio

PUBLICATIONS

"Numerical Calculations of Relaxation Phenomena Behind Normal Shock Waves in a Dissociated Free Stream," M.S. Thesis, The Ohio State University, 1965.

"Radiating Shock Layer of a Cylindrical Blast Wave," AIAA Student Journal, Vol. 4, No. 2, April 1966, pp 32-37.

"Chemical Relaxation Phenomena Behind Normal Shock Waves in a Dissociated Free Stream," Co-authors, R. M. Nerem and J. E. Hartsel, AIAA Journal, Vol. 5, No. 5, May 1967, pp. 910-916.

"Equilibrium Air Stagnation Point Boundary-Layer Calculations Using a Variable Heat of Dissociation Model," Co-author, R. M. Nerem, International Journal of Heat and Mass Transfer, Vol. 11, pp. 699-707, 1968.

FIELDS OF STUDY

Major Field: Aeronautical and Astronautical Engineering

Studies in Heat Transfer and Radiative Gasdynamics. Professor Robert M. Nerem

Studies in Aerothermochemistry. Professor Rudolph Edse

Studies in Viscous Aerodynamics. Professor John D. Lee

TABLE OF CONTENTS

LIST OF ILLUSTRATIONS

LIST OF SYMBOLS

b	Collision impact parameter
B_ν, B_λ	Black body radiative intensity function
C_2	Arbitrary constant used in coordinate transformation, Equation (106)
C_I	Ion drift velocity in the plasma sheath
c_{p_i}	Specific heat at constant pressure of species i
D_{ij}	Diffusion coefficient
e_i	Internal energy of species i
E_{il}	Energy of the l^{th} electronic level of j^{th} species
$E_n(z)$	Exponential integral function of order n
f_i	Velocity distribution function for species i
F_j	j^{th} component of external force
$\vec{g}_{ij}$	Relative velocity of approach, defined by Equation (6)
g	Magnitude of $\vec{g}_{ij}$
$\vec{G}$	Mass center velocity, defined by Equation (7)
g_{il}	Degeneracy of l^{th} electronic level of i^{th} species
h	Static enthalpy; also Planck's constant
h_i	Static enthalpy of species i
$\vec{J}_i$	Momentum change of species i due to inelastic collisions

K_ν, K_λ	Spectral absorption coefficient
K_i	Absorption coefficient for wavelength region i, Equation (84); also equilibrium constant for reaction
K	Collision parameter, defined by Equation (22)
k_{fi}, k_{bi}	Forward and backward reaction rate coefficients
k	Boltzmann constant
M_i	Molecular weight of species i
m_i	Mass of species i
N_i	Number density of species i
p	Static pressure
p_i	Static pressure of species i
$[P_i]$	Pressure tensor
P_{ij}	Momentum exchange between species i and j due to elastic collisions
p_i	Pressure ahead of incident shock
Q_i	Energy change of species i due to inelastic collisions
q_R	Radiative heat transfer
$\vec{q}_i$	Heat transfer of species i
R	Universal gas constant
$\vec{r}$	Position vector
S, S_{pq}	General black body source function
S_{ij}	Momentum collision cross section for species i and j
s, t	Time after reflection of shock wave
T	Temperature

T_i	Temperature of species i
$\vec{u}$	Mixture mass average velocity vector
u_j	j^{th} component of u
$\vec{u}_i$	Average velocity of species i
U_s, U_1	Incident shock velocity
$\vec{U}_i$, U_i	Diffusion velocity of species i
$\vec{V}_i$	Particle velocity of species i
$\vec{V}_i$	Peculiar velocity of species i, defined by Equation (2)
W	Shock wave velocity
$\dot{w}_i$	Volumetric rate of mass production of species i
X_i	External force on species i
x	Distance measured from end-wall
x_j	j^{th} component of r
Z_i	Partition function for species i
ϵ	Electronic charge; also angular coordinate
η	Transformed variable, defined by Equation (106)
θ_r	Characteristic rotational temperature of molecular nitrogen
θ_v	Characteristic vibrational temperature of molecular nitrogen
λ	Wavelength
λ_i	Thermal conductivity of species i
μ_i	Coefficient of viscosity of species i
ν_i	Collision frequency of species i

ν_{ij}, ν^*_{ij}	Stoichiometric coefficients of j^{th} species in i^{th} reaction
ζ_{ij}	Elastic energy exchange term, defined in Equations (I-34) and (I-35)
ρ_i	Density of species i
τ_ν	Optical thickness, defined by Equation (81)
ϕ	Sheath potential
ϕ_i	Species property in Equation (1)

Subscripts

1	Conditions ahead of incident shock wave
2	Conditions behind incident shock wave
5	Conditions behind reflected shock wave
R	Refers to reflected shock wave
s	Conditions immediately behind reflected shock wave
w	Conditions at the end-wall

CHAPTER I

INTRODUCTION

In the near future the exploration of not only the moon but also the various planets in our solar system may become a reality. Unmanned spacecraft will be used to investigate the atmosphere and environment surrounding the planets, and in order to obtain accurate information concerning them the actual return of these vehicles to earth may be required. The recovery of planetary probes will involve re-entry into the earth's atmosphere at high super-orbital velocities, possibly approaching fifteen kilometers per second. At such high re-entry velocities, the equilibrium temperature in the bow shock region can reach twenty thousand degrees Kelvin; and the heat transfer to the vehicle and the flow field around it will be dominated by thermal radiation. The probability also exists that in part of the flow around the vehicle chemical nonequilibrium and two-temperature effects will be significant. As a consequence several investigations have been carried out at The Ohio State University[1,2,3] with the purpose of gaining a better understanding of the various radiative and nonequilibrium phenomena present in

high-temperature gas flows.

For the study of high-temperature gases, the flow behind a planar shock wave which has reflected from an isothermal wall is attractive. The main advantage of the reflected shock problem is that its one-dimensionality makes the integro-differential nature of the governing energy equation, which includes radiative emission and absorption, more amenable to solution. Furthermore, this problem can be studied experimentally in a shock tube;[4] and the conditions generated behind a reflected shock wave simulate those encountered at the stagnation point of a space vehicle re-entering at super-orbital velocity.

As a consequence of these desirable features, Anderson[3] in 1965 investigated the radiating reflected shock flow field and obtained numerical calculations using a two-step absorption coefficient model to represent the non-gray characteristics of air. Later, however, the spectral properties of radiating high-temperature air and nitrogen were more accurately represented by an absorption coefficient model using five wavelength regions.[5] Consequently Anderson's numerical scheme was modified and expanded to include such a radiation model. The resulting computer program allowed the calculation of the flow field between a reflected shock wave and the shock tube end-wall as a function of time, including the effects of radiative

transport, and the prediction of the end-wall radiative heat transfer and intensity in each wavelength region. In this program the reflected shock wave velocity was also considered to be a variable since from a physical viewpoint it would be expected to decrease with time due to radiative cooling. Furthermore, if desired, results could be obtained for either a five-step transparent gas radiation model or an equivalent gray gas model.

All of the numerical solutions obtained with this extended program were limited in that they assumed complete chemical and thermodynamic equilibrium. In addition, since the program numerically solved the reflected shock problem by means of a finite difference approach based upon a coarse physical coordinate system, it was incapable of computing accurate temperature derivatives at the wall; and thus it yielded only approximate values for the conductive heat transfer.

Some typical results obtained with this five-step equilibrium reflected shock wave program are shown in Figures 1 and 2. In Figure 1 the temperature is plotted as a function of distance from the shock tube end-wall for various times after reflection. The sharp decrease in temperature immediately behind the reflected shock front is indicative of the marked effects of radiative cooling. Figure 2 compares experimentally obtained shock

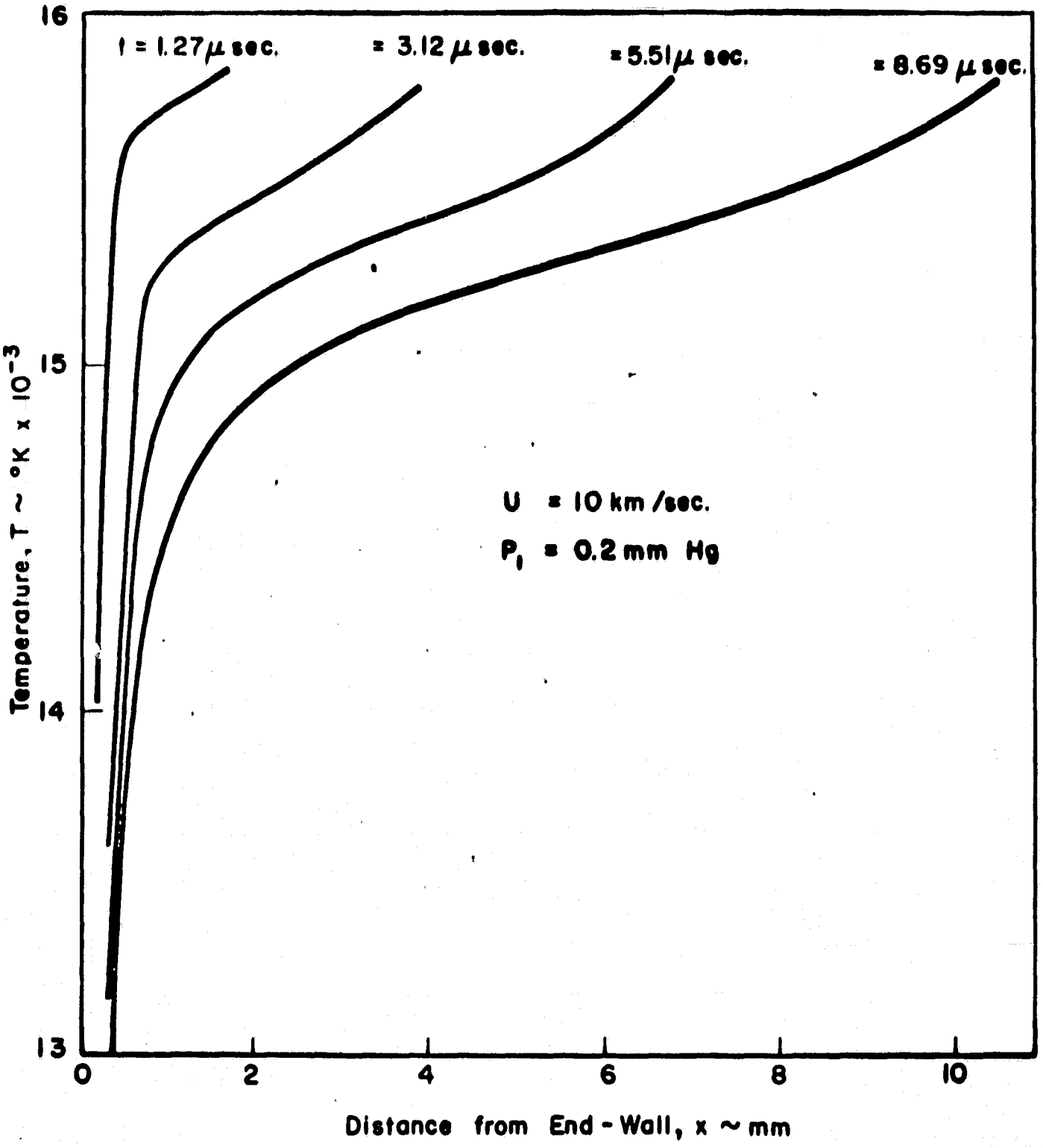

Fig. 1.--Temperature Profiles Behind a Reflected Shock Wave in Equilibrium Air

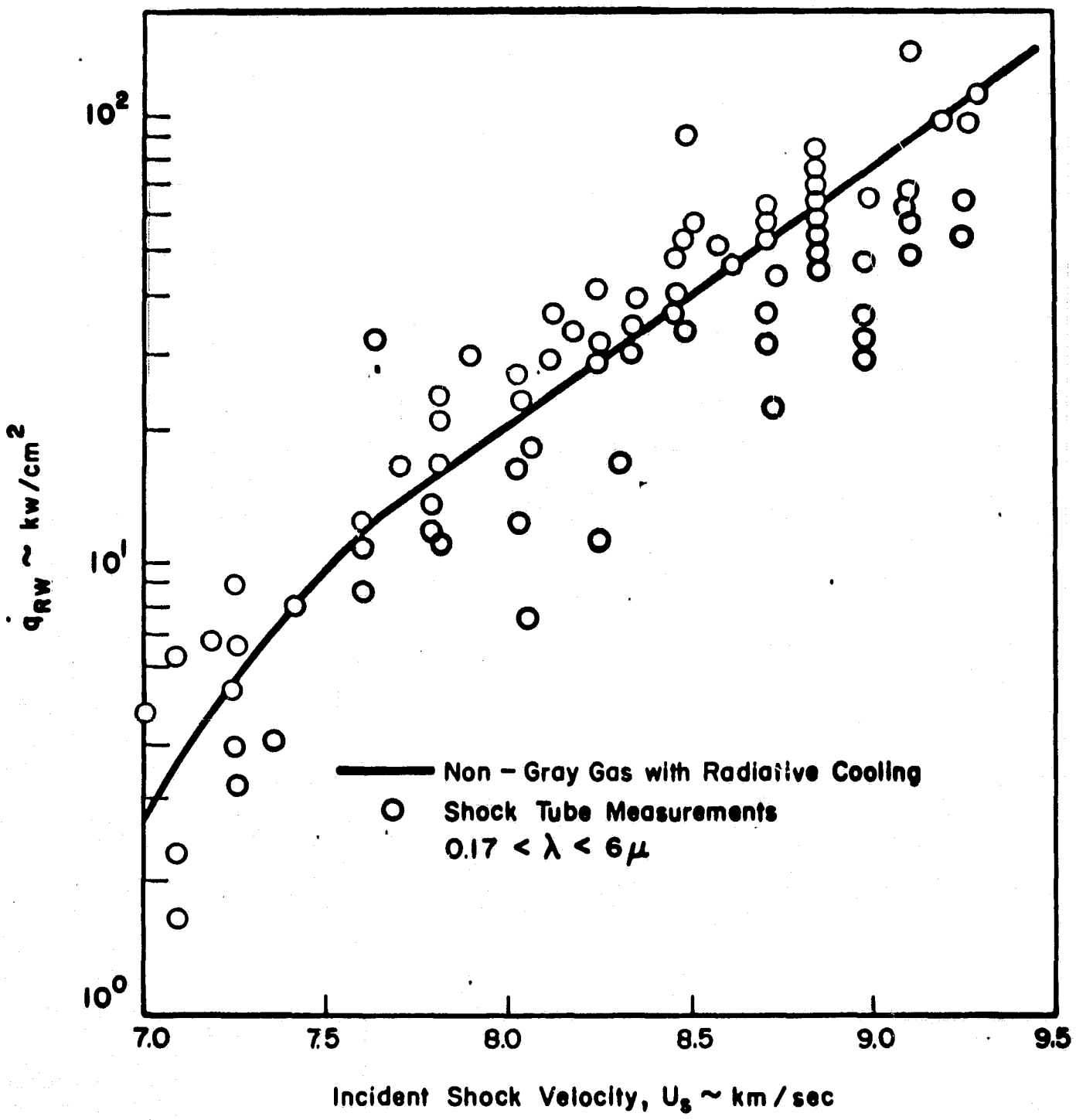

Fig. 2.--Comparison of Shock-Tube End-Wall Radiative Heat Transfer Measurements With Theoretical Calculations for a Time of 10 Microseconds After Shock Wave Reflection

tube end-wall radiative heat transfer measurements with the non-gray gas equilibrium calculations. In general, the agreement is reasonable.

Even though equilibrium calculations have yielded acceptable results for these relatively high pressure conditions, it has been shown[2] that at the low pressures corresponding to conditions of interest in atmospheric entry there are portions of the reflected shock flow field in which chemical nonequilibrium effects can be significant. For example, in the region immediately behind a reflected shock front large gradients in temperature and species concentration can occur. Any such chemical nonequilibrium would, of course, affect the radiative heat transfer through changes in the concentration and temperature of the radiating species; and thus it would be desirable to obtain solutions which include these variations. Similar effects might also be expected in the end-wall boundary layer.

Variable properties in front of the reflected wave, resulting from the nonequilibrium region behind the incident shock wave, might also have an effect on the flow behind the reflected shock wave. Presley and Hanson[6] have shown that such pre-shock nonequilibrium can cause variations of up to a factor of almost two in the post-shock pressure distribution. It should be noted that the

equilibrium calculations discussed above assumed no pressure variation with distance.

Besides chemical nonequilibrium, it is possible for a partially ionized gas to have regions of thermal nonequilibrium between electrons and the other heavier species. This type of nonequilibrium results because the rate of energy exchange between electrons and heavy particles is very slow due to the large mass differences in the species, and it is characterized by different electron and heavy body temperatures. Thermal nonequilibrium of this nature has been observed[7] and predicted[8] in the region behind a shock front, and Camac and Kemp[9] have obtained numerical solutions which indicate its presence in a boundary layer on a cold wall. Since radiation is primarily governed by the electron temperature, any thermal nonequilibrium might have a significant effect on the nature and magnitude of the end-wall radiative heat transfer.

In order to further investigate these nonequilibrium phenomena for the case of the reflected shock wave the present study has been initiated. The primary purposes of this study are as follows:

(1) To develop a solution to the reflected shock problem including chemical nonequilibrium and two-temperature effects.

(2) To gain a better understanding of the chemical

processes in and their effect on the structure of the reflected shock flow field.

(3) To determine the extent of thermal nonequilibrium behind a reflected shock wave and its relative effect on the end-wall radiative heat transfer.

It should be noted that previous solutions to the reflected shock problem have not included nonequilibrium effects of this type.

In this investigation the fundamental equations and boundary conditions governing the flow between a reflected shock wave and an end-wall have been formulated including chemical nonequilibrium, two-temperature, and radiative-gasdynamic coupling effects. In obtaining these equations one dimensionality has been assumed, precursor effects on the gas in front of the shock wave have been ignored, and the gas has been treated as being non-gray spectrally. Furthermore, the gas in front of the reflected wave has been considered to be in complete equilibrium. This condition has been assumed in order to facilitate the determination of which effects are due to nonequilibrium behind the shock and which are due to phenomena in front of it. In addition, the exchange of momentum and energy due to elastic collisions between particles has been included, and the associated collision integrals have been formulated and evaluated.

The resulting equations have been transformed into a boundary layer type of coordinate system, and a solution technique based upon a forward-in-time finite-difference scheme has been postulated. A calculation neglecting the end-wall boundary layer has been carried out for a reflected shock wave resulting from an incident shock travelling at 11 km/sec into quiescent nitrogen at a pressure of 10^{-3} cm of mercury. The results of this calculation have been used to discuss the nature and extent of nonequilibrium phenomena behind such a reflected shock wave.

CHAPTER II

FORMULATION OF THE GENERAL CONSERVATION EQUATIONS FOR A MULTI-TEMPERATURE GAS

The primary aim of this investigation is to analyze the reflected shock problem for the case where the electrons may be at a temperature different from that of the heavier particles. Thus, species conservation equations expressed in terms of species properties must be obtained. These equations can be derived from the general equation of change, as obtained from the Boltzmann equation, and introducing into it the various species quantities.

The general equation of change can be written[10]

$$\frac{\partial}{\partial t}(N_i \overline{\phi_i}) + \sum_{j=1}^{3} \frac{\partial}{\partial x_j}(N_i \overline{\phi_i u_j}) - N_i \left\{ \overline{\frac{\partial \phi_i}{\partial t}} + \sum_{j=1}^{3} \overline{u_j \frac{\partial \phi_i}{\partial x_j}} + \sum_{j=1}^{3} F_j \overline{\frac{\partial \phi_i}{\partial u_j}} \right\} = N_i \Delta \overline{\phi_i} \tag{1}$$

where ϕ_1 is a species property, either scalar or vector, and the bar over a term indicates averaging. In Equation (1) the terms involving magnetic and electric fields have been neglected because this type of external force does not

exist in the present reflected shock problem. However, the general force term involving F has been retained; and its actual form will be derived and discussed in Chapter IV.

The single term on the right hand side of Equation (1) represents the change in the mean value of property ϕ_1 due to encounters between particles of type i and the other particles in the gas. This term can be evaluated either by the energy-loss factor technique, which uses experimentally determined expressions and quantities, or by direct manipulation of collision integral expressions (see Appendix I and also Chapter III). While the energy-loss factor method is more direct and simpler in application, particularly when inelastic effects are important, the required experimental coefficients have not yet been obtained for the high temperatures typical of conditions behind reflected shock waves.[11] Consequently, the collision integral approach will be used in this investigation.

In the application of the general equation of change a choice exists between expressing the results in terms of a species average velocity, $\vec{u}_i$, or in terms of a mean average velocity, $\vec{u}$, combined with a species diffusion velocity, $\vec{U}_i$. Since it would be desirable to compare any solutions obtained in this study with experimental results and since the macroscopic velocity observed experimentally is the mass average velocity, the equations have been

formulated in terms of this latter quantity. Being consistent with this choice, the peculiar velocity used in the definition of the pressure tensor, heat flux vector, etc., is as follows

$$\vec{V}_i = \vec{v}_i - \vec{u} \tag{2}$$

It should be noted that a formulation in terms of mass average velocity is in contrast to the approach of several previous investigators of two-temperature gas problems.[8,12,13]

Now if ϕ_i is set equal to m_i, then the general equation of transfer yields the mass conservation equation for species i, providing that the mass production of species i due to chemical reactions is included. This latter effect can be represented by a production term $\dot{w}_i$ with the result that

$$\frac{\partial \rho_i}{\partial t} + \frac{\partial}{\partial \vec{r}} \cdot \left[\rho_i (\vec{u} + \vec{V}_i)\right] = \dot{w}_i \tag{3}$$

where the fact that $\rho_i = N_i m_i$ has been utilized. The form of $\dot{w}_i$ depends upon the chemical changes considered. An expression for it will be derived in Chapter IV.

In the derivation of the species momentum equation some authors[9] have set $\vec{\phi}_i = m_i \vec{v}_i$. However, since in the present problem there will probably be some induced mass

motion due to the retardation of the reflected shock wave by radiation cooling, the more suitable form for ϕ_1 is $m_1\vec{v}_1$. The introduction of this form into Equation (1) yields, after simplification via the species continuity equation, the species momentum equation

$$\rho_i \frac{D\vec{u}}{Dt} + \frac{D}{Dt}(\rho_i \vec{U}_i) + \rho_i \vec{U}_i \left(\frac{\partial}{\partial \vec{r}} \cdot \vec{u}\right) + \rho_i \left(\vec{U}_i \cdot \frac{\partial}{\partial \vec{r}}\right)\vec{u}$$

$$+ \frac{\partial}{\partial \vec{r}} \cdot [P_i] - N_i \vec{X}_i + \dot{w}_i \vec{u} = \sum_j \vec{P}_{ij} + \vec{J}_i \qquad (4)$$

The terms on the right hand side of Equation (4) represent respectively the rate of change of momentum of species i due to elastic collisions and due to inelastic collisions. A complete derivation of Equation (4) is given in Appendix I.

In a similar manner the equation representing the conservation of species energy can be derived from the general transfer equation by setting ϕ_1 equal to $\frac{1}{2}m_1 v_1^2$. The result as derived in Appendix I is

$$\frac{D}{Dt}(\rho_i h_i) - \frac{D p_i}{Dt} + \frac{\partial}{\partial \vec{r}} \cdot \vec{q}_i + \rho_i h_i \left(\frac{\partial}{\partial \vec{r}} \cdot \vec{u}\right) + \rho_i \vec{U}_i \cdot \frac{D\vec{u}}{Dt}$$

$$+ [\tau_i] : \left[\frac{\partial}{\partial \vec{r}} ; \vec{u}\right] - N_i \vec{X}_i \cdot \vec{U}_i - \dot{w}_i \frac{u^2}{2} = \sum_j \zeta_{ij} + \vec{U}_i \cdot \sum_j \vec{P}_{ij} + Q_i \qquad (5)$$

The terms on the right hand side of Equation (5) are collision interaction terms. The first one represents the rate of energy gain by species i due to elastic encounters between species i and the other species because of thermal

motion of the particles. The second is the rate at which work is done on species i due to elastic interactions between species i and the other species because of relative motion of the particles. The last signifies the rate of energy exchange occurring because of inelastic collisions. Expressions for the elastic terms will be derived in the next chapter.

CHAPTER III

THE ELASTIC INTERACTION TERMS

As indicated in the last chapter, when the conservation equations for momentum and energy are applied to individual species, they contain terms that express the change in these properties due to particle encounters. In this chapter the collision integral approach will be used to derive expressions for those terms associated with elastic collisions. Discussion of inelastic effects will be deferred until the actual consideration and formulation of the reflected shock wave problem.

Some useful definitions and relationships associated with collision processes are as follows:

Relative Velocity

$$\vec{g}_{ij} = \vec{v}_i - \vec{v}_j \;,\; \vec{g}'_{ij} = \vec{v}_i' - \vec{v}_j'$$
$$g = |\vec{g}_{ij}| = |\vec{g}'_{ij}| \tag{6}$$

Mass Center Velocity

$$\vec{G} = \frac{m_i \vec{v}_i + m_j \vec{v}_j}{m_i + m_j} = \frac{m_i \vec{v}_i' + m_j \vec{v}_j'}{m_i + m_j} \tag{7}$$

$$\vec{v}_i = \vec{G} + m_i \vec{g}_{ij} / (m_i + m_j) \tag{8}$$

Particle Velocities

$$\vec{v}_i' = \vec{G} + m_j \vec{g}'_{ij} / (m_i + m_j) \tag{9}$$

$$\vec{v}_j = \vec{G} - m_i \vec{g}_{ij} / (m_i + m_j) \tag{10}$$

Particle Velocities (Continued)

$$\vec{v}_j' = \vec{G} - m_i \vec{g}_{ij}' / (m_i + m_j) \tag{11}$$

For the case of energy change due to elastic collisions, the portion resulting from random motion is shown in Appendix I to be

$$\xi_{ij} = \int\int\int\int (\tfrac{1}{2} m_i v_i'^2 - \tfrac{1}{2} m_i v_i^2 + m_i (\vec{v}_i - \vec{v}_i') \cdot \vec{u}_i) f_i f_j g \, b \, db \, d\theta \, d\epsilon \, d\vec{v}_i \, d\vec{v}_j \tag{12}$$

By applying Equations (6)-(11) this equation can be written as

$$\xi_{ij} = \int\int\int\int \frac{m_i m_j}{m_i + m_j} [\vec{g}_{ij}' - \vec{g}_{ij}] \cdot [\vec{G} - \vec{u}_i] f_i f_j g \, b \, db \, d\theta \, d\epsilon \, d\vec{v}_i \, d\vec{v}_j \tag{13}$$

Now it would be desirable to have the integrand in Equation (13) entirely in terms of quantities before the collision. In order to perform this transformation the geometry of the collision must be considered. Since $\vec{g}_{ij}'$ is a vector, it

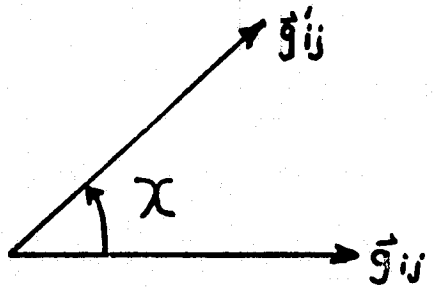

can be reduced to two components -- one perpendicular and one parallel to $\vec{g}_{ij}$. From the sketch the parallel

component can be expressed as

$$\vec{g}'_{ij,\parallel} = g \cos\chi \left(\frac{\vec{g}_{ij}}{g}\right) \tag{14}$$

If the integration variable $\vec{v}_i$ and $\vec{v}_j$ are changed to $\vec{g}_{ij}$ and $\vec{v}_j$ and the integration over all possible angles ϵ is carried out, then the various contributions due to the components of $\vec{g}'_{ij}$ perpendicular to $\vec{g}_{ij}$ will cancel out. Hence $g'_{ij,\perp}$ need no longer be considered. Thus, using Equation (14), Equation (13) becomes

$$\begin{aligned} \S_{ij} = \frac{-m_i m_j}{m_i + m_j} \iiint [\iiint (1 - \cos\chi) b\, db\, d\epsilon] \\ \cdot [\vec{g}_{ij} \cdot (\vec{G} - \vec{u}_i)] f_i f_j g\, d\vec{v}_i\, d\vec{v}_j \end{aligned} \tag{15}$$

The expression in the first set of brackets above is defined[14] as the collision cross-section, and in general it is a function of the relative velocity, g. It will subsequently be designated by $S_{ij}(g)$.

Before actually changing the variables of integration, consideration should be given to the form of the distribution functions f_i and f_j. In principle these should be the total distribution functions for the particles under consideration. In practice, however, such distributions are either not precisely known or would make the above integrals too complicated to be evaluated. Fortunately, the individual species should be relatively close to

equilibrium with respect to themselves; and thus a Maxwell-Boltzmann equilibrium distribution in a coordinate system relative to the individual particles should serve as a good approximation to the actual distribution function. Consequently, the following form was selected.

$$f_i = N_i \left[\frac{m_i}{2\pi k T_i}\right]^{3/2} \exp\left[\frac{-m_i (\vec{v}_i - \vec{u}_i)^2}{2 k T_i}\right] \tag{16}$$

As indicated above, the next step is to change the variables of integration from $\vec{v}_1$ and $\vec{v}_j$ to $\vec{g}_{ij}$ and $\vec{v}_j$. Converting $\bar{G}(\vec{v}_1, \vec{v}_j)$ to $\vec{G}(\vec{g}_{ij}, \vec{v}_j)$ by using Equation (8) and proceeding in a straightforward manner yields

$$\begin{aligned} \zeta_{ij} = {} & \frac{-m_i m_j}{m_i + m_j} \iint \left[\frac{m_i}{m_i + m_j} g^2 + \vec{g}_{ij} \cdot (\vec{v}_j - \vec{u}_i)\right] N_i \left(\frac{m_i}{2\pi k T_i}\right)^{3/2} \\ & \cdot \exp\left\{\frac{-m_i}{2 k T_i}\left((\vec{v}_j - \vec{u}_i)^2 + 2(\vec{v}_j - \vec{u}_i)\cdot \vec{g}_{ij} + g_{ij}^2\right)\right\} \\ & \cdot N_j \left(\frac{m_j}{2\pi k T_j}\right)^{3/2} \exp\left\{\frac{-m_j}{2 k T_j}\left((\vec{v}_j - \vec{u}_i)^2 - 2(\vec{v}_j - \vec{u}_i)\cdot(\vec{u}_j - \vec{u}_i)\right.\right. \\ & \left.\left. + (\vec{u}_j - \vec{u}_i)^2\right\} S_{ij}(g)\, g\, d\vec{g}_{ij}\, d\vec{v}_j \end{aligned} \tag{17}$$

This equation can be simplified somewhat by letting $\vec{X} = \vec{v}_j - \vec{u}_1$, which results in

$$\mathcal{J}_{ij} = \frac{-m_i m_j}{m_i + m_j} N_i N_j \left(\frac{m_i}{2\pi k T_i}\right)^{3/2} \left(\frac{m_j}{2\pi k T_j}\right)^{3/2}$$
$$\cdot \iint \left\{\frac{m_i}{m_i + m_j} g^2 + \vec{g}_{ij} \cdot \vec{X}\right\} \exp\left\{\frac{-m_i}{2k T_i}\left(X^2 + 2\vec{X}\cdot\vec{g}_{ij} + g^2\right)\right\} \cdot \exp\left\{\frac{-m_j}{2k T_j}\left(X^2 - 2\vec{X}\cdot\Delta\vec{U} + \Delta U^2\right)\right\} \qquad (18)$$
$$\cdot S_{ij}(g)\, g\, d\vec{g}_{ij}\, d\vec{X} \,.$$

where

$$\Delta\vec{U} = \vec{u}_j - \vec{u}_i \qquad (19)$$

In order to simplify the evaluation of Equation (18) it has been assumed that the particles involved in a collision behave as rigid spheres and, thus, that the collision cross-section, S_{ij}, is independent of velocity.

By expanding Equation (18) into the various x components and by using the following integral relationships, the integration over $\vec{X}$ can be carried out.

$$\int_{-\infty}^{+\infty} e^{-ax^2-2bx-c}\, dx = \sqrt{\frac{\pi}{a}}\, e^{\frac{b^2-ac}{a}}$$
$$\int_{-\infty}^{+\infty} x\, e^{-ax^2-2bx-c}\, dx = -\frac{b}{a}\sqrt{\frac{\pi}{a}}\, e^{\frac{b^2-ac}{a}} \qquad (20)$$

Equation (21) gives the result.

$$\mathfrak{J}_{ij} = \frac{-m_i m_j}{m_i + m_j} N_i N_j \left(\frac{1}{2\pi k}\right)^3 \left(\frac{m_i m_j \pi}{T_i T_j}\right)^{3/2} \left(\frac{m_i}{2kT_i} + \frac{m_j}{2kT_j}\right)^{-3/2}$$

$$\cdot S_{ij} \left\{ \int_{-\infty}^{+\infty} \frac{m_i}{m_i + m_j} g^3 \exp\left[-Kg^2 - K\Delta U^2 - 2K(\vec{g}_{ij} \cdot \Delta\vec{U})\right] d\vec{g}_{ij} \right.$$

$$\left. + \int_{-\infty}^{+\infty} \left(\frac{m_j T_i}{m_i T_j + m_j T_i} g(\vec{g}_{ij} \cdot \Delta\vec{U}) - \frac{m_i T_j g^3}{m_i T_j + m_j T_i} \right) \right. \qquad (21)$$

$$\left. \cdot \exp\left[-Kg^2 - K\Delta U^2 - 2K(\vec{g}_{ij} \cdot \Delta\vec{U})\right] d\vec{g}_{ij} \right.$$

In this equation

$$K = \left[\frac{2kT_i}{m_i} + \frac{2kT_j}{m_j} \right]^{-1} \qquad (22)$$

Since the above integration is over all velocity space, the orientation of a Cartesian coordinate system is arbitrary. Thus, a spherical coordinate system in which the z-axis is in the direction of the $\Delta\vec{U}$ vector has been used. In this manner the dot products appearing in Equation (21) reduce to $g\,\Delta U\cos\phi$, and dg_{ij} becomes $g^2 \sin\phi d\phi d\theta dg$. The orientation of the spherical angles is shown in the sketch,

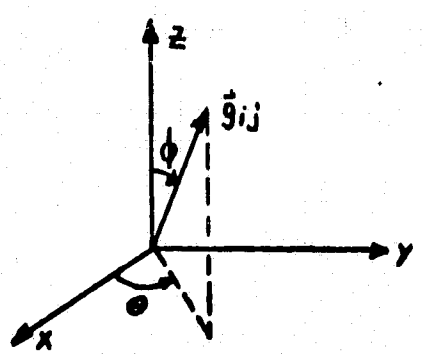

and the resulting expression for $\mathcal{S}_{ij}$ is given by Equation (23)

$$\mathcal{S}_{ij} = \frac{-m_i m_j}{m_i + m_j} N_i N_j \left(\frac{1}{2\pi k}\right)^3 \left(\frac{m_i m_j \pi}{T_i T_j}\right)^{3/2} \left(\frac{m_i}{2kT_i} + \frac{m_j}{2kT_j}\right)^{-3/2} S_{ij}$$
$$\cdot \left\{ \int_0^\infty \int_0^{2\pi} \int_0^{\pi} \frac{m_i}{m_i + m_j} g^6 \exp\left[-Kg^2 - K\Delta U^2 - 2Kg\Delta U\cos\phi\right] \sin\phi \, d\phi \, d\theta \, dg \right.$$
$$+ \int_0^\infty \int_0^{2\pi} \int_0^{\pi} \left(\frac{m_j T_i}{m_i T_j + m_j T_i} g^4 \Delta U \cos\phi - \frac{m_i T_j}{m_i T_j + m_j T_i} g^5 \right) \tag{23}$$
$$\left. \exp\left[-Kg^2 - K\Delta U^2 - 2Kg\Delta U\cos\phi\right] \sin\phi \, d\phi \, d\theta \, dg \right\}$$

Evaluation of the integrals with respect to θ and ϕ can be easily accomplished, and Equation (24) shows the result.

$$\mathcal{S}_{ij} = \frac{(m_i m_j)^{5/2} N_i N_j \, 2\pi \, S_{ij}}{(m_i + m_j)^2 (m_i T_j + m_j T_i)^{5/2} (2\pi k)^{3/2}}$$
$$\cdot \left\{ \frac{m_i m_j (T_j - T_i)}{K\Delta U} \int_0^\infty g^4 e^{-K(g^2 + \Delta U^2)} \sinh(2Kg\Delta U) \, dg \right.$$
$$+ \frac{m_j T_i (m_i + m_j) \Delta U^2}{2K^2 \Delta U^3} \int_0^\infty g^2 e^{-K(g^2 + \Delta U^2)} \left[2Kg\Delta U \cosh(2Kg\Delta U)\right. \tag{24}$$
$$\left. \left. - \sinh(2Kg\Delta U)\right] dg \right\}$$

A procedure identical to that which led from Equation (11) to Equation (24) can be applied to the rate of change of momentum due to elastic collisions. The result is expressed in Equation (25).

$$\vec{P}_{ij} = \frac{(m_i m_j)^{5/2} N_i N_j S_{ij} \Delta\vec{U}}{(m_i+m_j)(\pi)^{1/2}(2k)^{3/2}(m_i T_j + m_j T_i)^{3/2} \Delta U^3 K^2} \cdot \int_0^\infty g^2 e^{-Kg^2 - K\Delta U^2} (2K_g \Delta U \cosh(2K_g \Delta U) - \sinh(2K_g \Delta U)) dg \tag{25}$$

Equations (24) and (25) have previously been derived by Cravath[15] and also by Morse.[16] Cravath subsequently evaluated the integrals in the ζ_{ij} equation for the case $\Delta\vec{U}$ zero, and Morse evaluated both ζ_{ij} and $\vec{P}_{ij}$ with the restriction that $K \Delta U^2$ be small. However, the present investigation has revealed that the above integrals can be evaluated directly and that no restriction need be placed on K or $\Delta\vec{U}$.

The first step in the integration procedure is to express the hyperbolic sines and cosines in terms of exponentials. Then with the aid of the following indefinite integrals

$$\int e^{-ax^2-2bx-c} dx = \frac{1}{2}\sqrt{\frac{\pi}{a}}\, e^{\frac{b^2-ac}{a}} erf(\sqrt{a}x + \frac{b}{\sqrt{a}})$$

$$\int erf\, x\, dx = x\, erf\, x + \frac{1}{\sqrt{\pi}} e^{-x^2} \tag{26}$$

and repeated application of integration by parts to the g^n terms, the integrations can be carried out. For example, the first term in the first integral of Equation (24)

becomes

$$\int_0^\infty \frac{g}{2}^4 e^{-Kg^2+2K\Delta U g}\,dg =$$

$$e^{K\Delta U^2}\sqrt{\frac{\pi}{K}}\,\mathrm{erfc}\left(-\sqrt{K}\Delta U\right)\left\{\frac{\Delta U^4}{4}+\frac{3\Delta U^2}{4K}+\frac{3}{16K^2}\right\} \qquad (27)$$

$$+\sqrt{\frac{\pi}{K}}\left\{\frac{\Delta U^3}{4\sqrt{\pi K}}+\frac{5}{8}\,\frac{\Delta U}{K\sqrt{\pi K}}\right\}$$

In a like manner, the rest of the terms can be evaluated. While these integrations are straight forward, it should be realized that they are tedious and quite complicated. The final results are as follows:

$$\xi_{ij} = \frac{(m_i m_j)^{5/2} N_i N_j 2\pi S_{ij}}{(m_i+m_j)^2 (m_i T_j + m_j T_i)^{5/2} (2\pi k)^{3/2}}$$

$$\cdot\left\{\frac{m_i m_j (T_j - T_i)}{K\Delta U}\left[\sqrt{\frac{\pi}{K}}\left(\frac{\Delta U^4}{4}+\frac{3\Delta U^2}{4K}+\frac{3}{16K^2}\right)\cdot\right.\right.$$

$$\left.\cdot 2\,\mathrm{erf}\left(\sqrt{K}\Delta U\right)+e^{-K\Delta U^2}\,2\sqrt{\frac{\pi}{K}}\left(\frac{\Delta U^3}{4\sqrt{\pi K}}+\frac{5}{8}\frac{\Delta U}{K\sqrt{\pi K}}\right)\right] \qquad (28)$$

$$\cdot\frac{m_j T_i (m_i+m_j)}{2K^2\Delta U}\left[\sqrt{\frac{\pi}{K}}\,\mathrm{erf}\left(\sqrt{K}\Delta U\right)\left(K\Delta U^4+\Delta U^2-\frac{1}{4K}\right)\right.$$

$$\left.\left.+e^{-K\Delta U^2}\Delta U^3+e^{-K\Delta U^2}\frac{\Delta U}{2K}\right]\right\}$$

and

$$\vec{P}_{ij} = \frac{(m_i m_j)^{5/2} N_i N_j \Delta\vec{U} S_{ij}}{(m_i + m_j)\sqrt{\pi}\,(2k)^{3/2}(m_i T_j + m_j T_i)^{3/2}\Delta U^3} \cdot \left(\frac{2 m_j k T_i + 2 m_i k T_j}{m_i m_j}\right)^2 \left\{ erf(\sqrt{K}\Delta U)\left(\sqrt{\frac{\pi}{K}} K \Delta U^4 + \Delta U^2 \sqrt{\frac{\pi}{K}} - \frac{1}{4K}\sqrt{\frac{\pi}{K}}\right) + e^{-K\Delta U^2}\left(\Delta U^3 + \frac{\Delta U}{2K}\right)\right\} \tag{29}$$

To this author's knowledge this is the first time that expressions for the exchange of energy and momentum due to elastic collisions have been obtained in this form.

Finally, it should be pointed out that both Equation (28) and Equation (29) take on the forms given by Cravath[15] and Morse[16] for the cases $\Delta\vec{U}$ zero and $K\,\Delta U^2$ small.

CHAPTER IV

FORMULATION OF THE TWO-TEMPERATURE, NONEQUILIBRIUM, RADIATING REFLECTED SHOCK PROBLEM

A. Background

Before engaging in a discussion of the specific assumptions and equations utilized in the present investigation of the reflected shock problem, a brief review of pertinent previous work relating to high temperature shock waves is in order. In the period 1955-1957 Petschek and Byron[17] analyzed the phenomena associated with the approach to equilibrium behind strong shock waves and determined that for argon the dominant mechanism of ionization is electron-atom collisions. More significantly, they showed that their experimental results could be best explained by an analysis which allowed the electron temperature to be different from that of the atoms and ions. They explained this possible difference by noting that an electron requires approximately 10^5 collisions with atoms to lose its energy, but only one collision with an electron to approach a Maxwellian distribution. Thus, they reasoned that a separate electron temperature can exist if electron self-collision occurs at least once per every 10^5 atom

collisions. For argon, these conditions are satisfied when the degree of ionization is greater than 10^{-8}.

In 1964 Jaffrin and Probstein[12] reported their multi-temperature analysis of the structure of a steady state shock wave. Again the gas considered was argon, and it was assumed to be fully ionized. This effort was subsequently extended by Jaffrin[11] to the partially ionized gas case, although frozen chemistry was still assumed. In both of these investigations the primary interest was in shock structure, precursor effects, and induced electric fields. From the present viewpoint, however, their results are significant in that they indicate that in the relaxation region behind a planar shock front the electron temperature can indeed be different from the temperature of the other particles.

Recently Chapin[8] examined the same problem but including the effects of chemical nonequilibrium and thermal radiation. While again the primary interest was in the argon shock structure and precursor effects, his results showed that both chemical and thermal nonequilibrium effects are important and coupled together in the relaxation zone. Further, he deduced that radiation cooling can be significant and can affect the ionization rate as equilibrium is approached. Radiation cooling refers to the actual physical cooling of the gas due to energy losses by

radiation. In his analysis Chapin used a gray gas radiation model, but as he admits such a model is not an accurate representation of the actual radiation processes which occur.

To this author's knowledge there has been only one previous two-temperature analysis of the flow behind a reflected shock wave. In 1964 Camač and Kemp[9] published an analysis for the end-wall boundary layer behind a reflected shock front and gave a sample calculation of boundary layer profiles and heat transfer. The gas considered was argon at a time of one microsecond after shock reflection. Unfortunately, due to numerical difficulties they were forced to assume frozen chemistry and negligible collision exchange effects. Nevertheless, their analysis was the first to consider a two-temperature time dependent problem with a plasma in the presence of a cold wall. As will be discussed later in this chapter, the existence of a wall adjacent to the plasma creates a region called the plasma sheath in which a continuum description with charge neutrality fails to apply.

As has been indicated, each of these previous investigators performed their analyses assuming that the test gas was argon. The primary reason for this choice was that the properties of argon are from a comparative viewpoint well-known. Furthermore, since it is a monoatomic gas, its

chemistry is simple--being limited only to ionization. If, however, the results of the present investigation are to have some applicability to the phenomena associated with post-Apollo re-entry, then a gas must be chosen which is reasonably similar to air. With respect to molecular weight, existence of dissociation and ionization, and radiative properties, nitrogen is very similar to air; but yet its chemistry is still reasonably simple. Consequently nitrogen has been selected as the test gas for this study.

B. Conservation Equations

In the shock tube the reflected shock wave problem is a two-dimensional unsteady problem in x and r. However, in the vicinity of the shock tube center-line, the flow is essentially one-dimensional in x; and, thus, in the interest of simplification the present problem will be treated as one-dimensional. This approach not only serves to simplify the equations but also makes the integrals in the radiation terms easier to evaluate (see Section I of this chapter). The distance, x, is measured from the end-wall, and the time, t, is counted from the instant of shock reflection. All of the fluid dynamic properties between the shock wave and the end-wall are functions of distance and time, and the velocity of the reflected shock front is assumed to be a function of time. This time

dependence is necessary in order to account for any shock attenuation effects resulting from radiation cooling.

In Chapter II the general fluid dynamic conservation equations for a multi-temperature gas were derived and discussed. Application of the equation for the conservation of mass of each species to the one-dimensional case yields

$$\frac{\partial \rho_i}{\partial t} + \frac{\partial (\rho_i u)}{\partial x} + \frac{\partial (\rho_i v_i)}{\partial x} = \dot{w}_i \qquad (30)$$

while the global continuity equation can be expressed as

$$\frac{\partial \rho}{\partial t} + \frac{\partial (\rho u)}{\partial x} = 0 \qquad (31)$$

In the species momentum equation, Equation (4), there appears an external force which for the case of no externally applied electric or magnetic fields results from the electrostatic forces between electrons and ions. In the electron equation this force term has the form[9]

$$\vec{X}_e = -\epsilon \vec{E} \qquad (32)$$

where ϵ is the magnitude of the electronic charge and $\vec{E}$ is the induced electric field. When Equation (32) is substituted into the species momentum equation and all terms of order m_e and smaller are neglected, the electron momentum equation reduces to simply

$$\frac{\partial p_e}{\partial \vec{r}} = -\epsilon \vec{E} N_e \qquad (33)$$

where the viscous term has also been neglected since the velocity gradients in the reflected shock flow field are extremely small. Equation (33), which relates the electric field between electrons and ions to the electron pressure, can thus be used in the external force term in the species energy equation.

Likewise the one-dimensional global momentum equation is

$$\rho \frac{\partial u}{\partial t} + \rho u \frac{\partial u}{\partial x} = -\frac{\partial p}{\partial x} \qquad (34)$$

where again the viscous term has been neglected as small. Note that no external force term appears in Equation (34) since the electrostatic force between the electrons and ions balances out and does not affect the momentum of the fluid as a whole.

Since it is the primary aim of this study to investigate the reflected shock wave region including the effects of thermal nonequilibrium, there should in principle be an energy equation for each species. However, since the exchange of energy in elastic collisions is dependent upon the mass ratio of the colliding particles, it is reasonable to expect that for particles of almost the same mass the

temperature equilibrates in a few collisions. Thus, in an ionized gas the heavy particles (i.e., atoms, molecules, and ions) should all be characterized by the same temperature T_H; but the electrons may have a different temperature T_e. Hence, only two conservation of energy equations are needed. Obviously, one is the electron species energy equation, which can be obtained by applying Equation (5) to electrons and neglecting terms of order (m_e/m_a).

$$\rho_e \frac{\partial h_e}{\partial t} + \rho_e u \frac{\partial h_e}{\partial x} + \frac{\partial}{\partial x}\left(-\lambda_e \frac{\partial T_e}{\partial x}\right) + \frac{\partial}{\partial x}\left(\rho_e v_e h_e\right)$$

$$- \frac{\partial p_e}{\partial t} - u \frac{\partial p_e}{\partial x} + \dot{w}_e h_e - h_e \frac{\partial}{\partial x}(\rho_e v_e) - \dot{w}_e \frac{u^2}{2} \qquad (35)$$

$$= v_e \frac{\partial p_e}{\partial x} + \sum_{j=1}^{s} \vec{J}_{ej} + v_e \sum_{j=1}^{s} P_{ej} + Q_e$$

The first term on the right-hand-side of Equation (35) represents the effect of external forces, and it is obtained by using Equation (32) and (33) to express the force $\vec{X}_e$ in terms of the electron pressure. The second term, $\sum_{j=1}^{s} J_{ej}$, is the rate of energy gain by electrons due to elastic encounters because of thermal motion of the particles; while the third term accounts for the energy gain resulting from elastic collisions because of the relative fluid motion of the electrons. The last term, Q_e, represents energy change due to inelastic encounters. Its nature and origin will be discussed in Section F below.

For the second energy expression either a heavy-body energy equation (summation of the respective heavy-body species equations) or a global energy equation may be used. For this investigation the global energy equation has been used due to its slightly simpler form. This equation is obtained by applying Equation (5) to each species and then summing over all species. The result, which is presented in Equation (36), has been further modified by using the species continuity equation.

$$\rho \frac{\partial h}{\partial t} + \rho u \frac{\partial h}{\partial x} + \frac{\partial}{\partial x}\left[\sum_{i=1}^{s}\left(-\lambda_i \frac{\partial T_i}{\partial x}\right)\right] + \frac{\partial}{\partial x}\left[\sum_{i=1}^{s} \rho_i v_i h_i\right]$$

$$+ \frac{\partial q_R}{\partial x} - \frac{\partial p}{\partial t} - u \frac{\partial p}{\partial x} = -\sum_{i=1}^{s} \dot{w}_i h_i^{\circ} \qquad (36)$$

In both Equation (35) and Equation (36) the viscous stress terms have been omitted because their expected effect in the reflected shock region is negligible. Also a radiative heat transfer term appears only in the global energy equation because it has been assumed that the radiation effect on electron energy is negligible. This assumption will be discussed in more detail in Section I of this chapter.

Finally, in Equation (36)

$$\rho h = \sum_{i=1}^{s} \rho_i h_i \qquad (37)$$

The form of h_1 and its relationship to the species temperature will be discussed in the next section.

C. Thermodynamics

The enthalpy-temperature relationship used in this formulation is that obtained by application of statistical mechanics. By definition

$$h_i = e_i + \frac{k T_i}{m_i} \tag{38}$$

and from statistical mechanics

$$e_i = \frac{k T_i^2}{m_i} \left(\frac{\partial \ln Z_i}{\partial T_i} \right)_{VOLUME} \tag{39}$$

where Z_i is the complete partition function for the ith species. Substitution of the appropriate partition functions[18] into Equations (38) and (39) and carrying out the indicated operations yields

$$h_i = \frac{5 + (n_i - 1)2}{2} \frac{kT_i}{m_i} + \frac{(n_i - 1)\theta_{vi} k}{(e^{\theta_{vi}/T_i} - 1) m_i} + \frac{\sum_{\ell=1}^{n} g_{i\ell} \frac{E_{i\ell}}{k} e^{-E_{i\ell}/kT_e}}{\sum_{\ell=1}^{n} g_{i\ell} e^{-E_{i\ell}/kT_e}} \frac{k}{m_i} \tag{40}$$

where n_i is the number of particles per molecule of species i and T_i is the species temperature (either T_H or T_e) associated with the mixture mass average velocity. Since at the conditions of interest in this study the amount of molecular nitrogen present is usually negligible, the contribution of the vibrational term to the overall

enthalpy is small; and it need only be approximately represented. Thus, the simple harmonic oscillator approximation has been used with the assumption that the vibrational mode is in equilibrium at the heavy particle temperature. Furthermore, the electronic terms have been formulated using the electron temperature, assuming that the electronic levels are in equilibrium with the free electrons.

The equation of state is simply

$$p_i = \rho_i \frac{k T_i}{m_i} \tag{41}$$

and by Dalton's principle

$$p = \sum_{i=1}^{s} p_i \tag{42}$$

D. Transport Properties

The transport coefficients for this study have been derived from elementary kinetic theory relationships which have been suitably modified for mixture effects. The kinetic theory result for the viscosity of a pure gas is

$$\mu_i = \frac{5\pi}{32} \rho_i \left(\frac{8kT_i}{\pi m_i}\right)^{\frac{1}{2}} \frac{1}{\nu_i} \tag{43}$$

Fay,[19] however, has proposed that this expression is suitable for use in a mixture of gases providing that the collision frequency has the following form

$$\nu_i = \sum_k N_i S_{ik} \left(\frac{8kT_i}{\pi m_i} + \frac{8kT_k}{\pi m_k} \right)^{1/2} \frac{2m_k}{m_i + m_k} \qquad (44)$$

Application of this procedure will yield the appropriate collision frequencies, ν_1, and hence μ_1. In the course of the derivation of the various ν_1, however, terms of the form $((T_e/m_e) + (T_H/m_A))$ are frequently encountered; and a comparison of the respective particle masses indicates that these terms can be accurately approximated by T_e/m_e as long as $T_e >> 10^{-5}\ T_H$. Similarly in the heavy particle collision frequencies examination of the terms resulting from encounters with electrons indicates that they too can be neglected provided T_e is less than $10^2\ T_H$. Since the electron and heavy body temperatures are expected to be the same order of magnitude, neglecting these terms poses no serious problem. Furthermore dropping terms of the second type can be justified from a theoretical viewpoint. Hansen[18] points out that the collision frequency in Equation (43) should really only count those collisions which are effective at transferring momentum. In general all collisions do this, but in the collision of a heavy particle with a very light particle the change is so insignificant that the collision should really not be counted. By dropping the electron contribution to the ν_1 of the heavy particle, this argument is satisfied.

The resulting expressions for the respective collision frequencies are given in the following equations:

$$\nu_M = \left[\frac{8kT_N}{\pi m_A}\right]^{1/2}\left\{\frac{\rho_M}{m_M} S_{MM} + \sqrt{\frac{2}{3}}\frac{\rho_A}{m_A} S_{AM} + \sqrt{\frac{2}{3}}\frac{\rho_I}{m_I} S_{MI}\right\}$$

$$\nu_A = \left[\frac{8kT_N}{\pi m_A}\right]^{1/2}\left\{2\sqrt{\frac{2}{3}}\frac{\rho_M}{m_M} S_{MA} + \sqrt{2}\frac{\rho_A}{m_A} S_{AA} + \sqrt{2}\frac{\rho_I}{m_I} S_{AI}\right\}$$

$$\nu_I = \left[\frac{8kT_N}{\pi m_A}\right]^{1/2}\left\{2\sqrt{\frac{2}{3}}\frac{\rho_M}{m_M} S_{MI} + \sqrt{2}\frac{\rho_A}{m_A} S_{AI} + \sqrt{2}\frac{\rho_I}{m_I} S_{II}\right\} \qquad (45)$$

$$\nu_e = 2\frac{\rho_M}{m_M} S_{Me}\left[\frac{8kT_e}{\pi m_e}\right]^{1/2} + 2\frac{\rho_A}{m_A} S_{Ae}\left[\frac{8kT_e}{\pi m_e}\right]^{1/2}$$

$$+ 2\frac{\rho_I}{m_I} S_{Ie}\left[\frac{8kT_e}{\pi m_e}\right]^{1/2} + \frac{\rho_e}{m_e} S_{ee}\left[\frac{16kT_e}{\pi m_e}\right]^{1/2}$$

These four equations can thus be used with Equation (43) to calculate the various viscosity coefficients.

In a similar manner kinetic theory yields for the thermal conductivity of species i

$$\lambda_i = \frac{15}{4}\frac{k}{m_i}\mu_i Eu \qquad (46)$$

where Eu is the Eucken correction factor. This factor, which is non-unity only for molecular nitrogen, has been formulated in several ways. However, since the amount of diatomic nitrogen present in the reflected shock flow field is small, the simple form originally attributed to Eucken will be used.[20]

$$Eu = \frac{3}{5} + \frac{4}{15}\frac{c_{vM}\, m_M}{k} \qquad (47)$$

The specific heat at constant volume, c_{vM}, of molecular nitrogen can be obtained by differentiation from Equation (39).

The only other transport coefficient required in the present analysis is the diffusion coefficient. As will be discussed, only binary diffusion will be considered, and thus only one diffusion coefficient will be needed. To a first approximation this coefficient can be represented as[21]

$$D_{AM} = \frac{3\pi}{8\left(\frac{\rho_A}{m_A} + \frac{\rho_M}{m_M}\right) S_{MA}} \left\{\frac{kT_H\,(m_A + m_M)}{2\pi\, m_A m_M}\right\}^{1/2} \qquad (48)$$

E. Chemical Kinetics

Several species and many chemical reactions could be used to formulate a model for reacting nitrogen. However, for the conditions which are of interest here the following four species and six reactions should be sufficiently representative of high-temperature reacting nitrogen.

Species:

Molecular Nitrogen	-- N_2
Atomic Nitrogen	-- N
Nitrogen Ion	-- N^+
Electron	-- e

Reactions:

$$
\begin{aligned}
N_2 + N &\rightleftharpoons 2N + N \\
N_2 + N_2 &\rightleftharpoons 2N + N_2 \\
N_2 + M &\rightleftharpoons 2N + M \\
N + N^+ &\rightleftharpoons 2N^+ + e \\
N + e &\rightleftharpoons N^+ + 2e \\
N + N &\rightleftharpoons N^+ + e + N
\end{aligned}
\tag{49}
$$

Another species which might possibly be included is the molecular ion, N_2^+. If present in sufficient numbers, this ion can have an effect on the type of dissociation and ionization reactions which occur. However, for equilibrium conditions in front of and behind a typical reflected shock wave its concentration is extremely small. Thus, its inclusion was not felt to be warranted, expecially considering the additional reaction complexity which would result from its introduction. In the reaction system the first three account for the dissociation of nitrogen, and the last three represent the ionization processes.

Now the primary quantity desired from the chemical kinetic analysis is the volumetric rate of mass production of each species j, $\dot{w}_j$, which is found by considering the production rate from each reaction i. That is

$$\dot{W}_j = \sum_{i=1}^{r} \dot{w}_{ij} \tag{50}$$

where r is the number of reactions considered. For a general reaction of the form

$$\sum_{j=1}^{s} \nu_{ij} A_j \rightleftharpoons \sum_{j=1}^{s} \nu_{ij}^{*} A_j \tag{51}$$

kinetics[22] yields that

$$\dot{w}_{ij} = \eta_j (\nu_{ij}^{*} - \nu_{ij}) k_{fi} \rho^{\sum \nu_{ij}} \prod_{\alpha=1}^{s} \left(\frac{\rho_\alpha}{\rho \eta_\alpha}\right)^{\nu_{i\alpha}} \cdot \left[1 - \frac{\rho^{\Sigma(\nu_{ij}^{*} - \nu_{ij})}}{K_i} \sum_{\alpha=1}^{s} \left(\frac{\rho_\alpha}{\rho \eta_\alpha}\right)^{\nu_{i\alpha} - \nu_{i\alpha}^{*}}\right. \tag{52}$$

where k_{fi} is the forward rate constant for reaction i. Here K_i is the equilibrium constant in terms of concentrations, and it has been assumed that

$$K_i = k_{fi}/k_{bi} \tag{53}$$

The validity of Equation (53) in nonequilibrium situations has often been questioned. However, C. W. Chu[23] has demonstrated that as long as the reaction rate constants are functions only of temperature, then Equation (53) is not only valid but also compatible with Equation (52).

The equilibrium constant can be expressed in terms of the partial pressure equilibrium constant as

$$K_i = K_{p_i} (RT)^{-\sum (\nu_{ij}'' - \nu_{ij})} \tag{54}$$

which in turn can be obtained from free energy and statistical mechanical considerations as follows[22]

$$\ln K_{p_i} = \sum_{j=1}^{s} (\nu_{ij}'' - \nu_{ij}) \left\{ \frac{3}{2} \ln\left(\frac{2\pi m_j k}{h^2}\right) + \ln k + \left(\frac{5 + 2(n_j - 1)}{2}\right) \ln T - (n_j - 1) \ln \theta_{r_j} + (n_j - 1) \ln\left[\frac{1}{1 - e^{-\theta_{v_j}/T}}\right] + \ln\left[\sum_{l=1}^{n} g_{i,l}\, e^{-\varepsilon_{j,l}/kT}\right] \right\} - \sum_{j=1}^{s} (\nu_{ij}'' - \nu_{ij}) \frac{H_j^\circ}{RT_j} \tag{55}$$

Equations (52)-(55) will be used for the dissociation reactions. Furthermore, since the concentration of molecular nitrogen in the region behind the reflected shock wave is low, vibration-dissociation coupling effects have been ignored.

Unfortunately Equation (52) does not adequately describe the mass production rates for the ionization reactions because these reactions involve two steps, proceeding via excitation of the nitrogen atom to the $3s^4P$ state and subsequent rapid ionization.[24] For example, the atom-atom reaction proceeds as follows

$$N(\text{ground}) + N \rightleftharpoons N(\text{excited}) + N \tag{56}$$

$$N(excited) \rightleftharpoons N^+ + e \qquad (57)$$

Now by assuming that the first step in the chain is rate determining, that $(dN_{N_{excited}}/dt)$ is approximately zero, and that the ground state concentration equals the atom concentration, kinetics yields

$$\dot{w}_{N(ex),Total} = \eta_N \left[k_{f_a} [N]^2 - k_{b_a} [N(ex)][N] + \dot{w}_{N(ex),57} \right] \qquad (58)$$

where brackets have been used to denote concentration. However by assumption

$$\dot{W}_{N(ex),Total} = 0$$

so that

$$\dot{w}_{N(ex),57} = -\eta_N \left[k_{f_a} [N(ground)][N] - k_{b_a} [N(ex)][N] \right] . \qquad (59)$$

where k_{fa} and k_{fb} are related by the equilibrium constant for reaction (56). Since at equilibrium the population of the various levels is described by a Boltzmann distribution, this equilibrium constant can be expressed as

$$K_{eq} = \frac{g_{ex} \exp(-E_{ex}/kT_H)}{g_{ground}}$$

Accordingly Equation (59) becomes

$$\dot{W}_{N(ex),57} = -\eta_N [N(ground)][N] k_{f_a} \left[1 - \frac{g_{ground}}{g_{ex}} \frac{e^{E_{ex}/kT_H} [N(ex)]}{[N(ground)]}\right] \qquad (60)$$

Now if it is assumed that the excited state is in equilibrium with the electrons at the electron temperature T_e, then from the Saha equation

$$\frac{N_e^2}{N_{N(excited)}} = 2\left(\frac{2\pi m_e k T_e}{h^2}\right)^{3/2} \frac{Q_{elec,I}\, e^{-\chi_{ex}/kT_e}}{g_{ex}} \qquad (61)$$

where χ_{ex} is the ionization potential from the excited state and $Q_{elec,N_{ex}}$ has been approximated by g_{ex}. The electron production rate is related to the excited atom production rate as follows

$$\dot{W}_{N(ex),57} = m_A \dot{N}_{N(ex),57} = -m_A \dot{N}_{e,57} = -\frac{m_A}{m_e} \dot{W}_{e,AA} \qquad (62)$$

Substituting this expression and Equation (61) into Equation (60) yields for the atom-atom reaction, assuming $[N(ground)]$ equals $[N]$

$$\dot{W}_{e,AA} = \eta_e k_f \frac{\rho_A^2}{\eta_A^2} \left[1 - \frac{g_{ground}\, e^{E_{ex}/kT_H + \chi_{ex}/kT_e} N_{AV} \rho_e^2 h^3 \eta_A}{\rho_A \eta_e^2\, 2 (2\pi k T_e m_e)^{3/2} Q_{elec,I}}\right]$$

$$\dot{W}_{I,AA} = \dot{W}_{e,AA} \frac{m_I}{m_e} \quad ; \quad \dot{W}_{A,AA} = -\dot{W}_{e,AA} \frac{m_A}{m_e} \qquad (63)$$

A similar analysis applied to the electron-atom reaction results in the following set of equations

$$\dot{w}_{e,eA} = k_f \frac{\rho_A}{m_A} \rho_e \left\{ 1 - \frac{g_{ground}\, e^{I/kT_e} N_{Av} \rho_e^2 h^3 m_A}{\rho_A m_e^2 2 (2\pi m_e k T_e)^{3/2} Q_{elec,I}} \right\} \tag{64}$$

$$\dot{w}_{I,eA} = \dot{w}_{e,eA} \frac{m_I}{m_e} \quad ; \quad \dot{w}_{A,eA} = -\dot{w}_{e,eA} \frac{m_A}{m_e}$$

Notice that $\dot{w}_{e,AA}$ is governed by both the electron and the heavy body temperatures, while the production rate for the atom-electron reaction involves only the electron temperature. Likewise consideration of the atom-ion reaction yields

$$\dot{w}_{e,AI} = m_e k_f \frac{\rho_A \rho_I}{m_A m_I} \left\{ 1 - \frac{Q_{A,elec}\, e^{E_{ex}/kT_H + T_{ex}/kT_e} N_{Av} \rho_e^2 h^3 m_A}{\rho_A m_e^2 2 (2\pi k T_e m_e)^{3/2} Q_{elec,I}} \right\}$$

F. Inelastic Collision Effects

Any collision or interaction in which the internal energy of the colliding particles is changed is an inelastic interaction, and the magnitude of this change must be accounted for in the energy equations. In any global equation such as the overall energy equation conservation of energy requires that all collision effects

sum to zero. Thus, inelastic collision terms appear only in the electron energy equation; and only those inelastic collisions which affect the energy of the electrons need to be considered. Radiative effects, which are some times considered as inelastic effects, are included in the radiation model described in Section I.

In the reaction system described in Equations (49) only the last three involve inelastic collisions affecting electrons. First consider the electron-atom reaction. When an electron is created by this process, the electron which caused the ionization will lose energy equivalent to the ionization potential, E_I, plus the energy of the created electron, which on the average is say $\bar{\varepsilon}$. The original N_e electrons will rapidly equilibrate themselves by elastic collisions and consequently they will have collectively lost energy $E_I + \bar{\varepsilon}$ in creating an electron of average energy $\bar{\varepsilon}$. The subsequent equilibration between the N_e original electrons and the newly created electron will not affect the energy per unit volume since it only involves a transfer of energy from one particle to another. Thus the net energy loss per unit volume resulting from this process is simply E_I. Since $\dot{w}_{e,ea}/m_e$ is the rate of production of electrons by this process, the total energy loss is -- $w_{e,ea}E_I/m_e$.

Similarly, every time the atom-atom process occurs

an electron of average energy $\bar{\varepsilon}_{AA}$ is created. Hence the total energy gain from the atom-atom collision is $\dot{w}_{e,AA}\ \bar{\varepsilon}_{AA}/m_e$. A similar expression results from the atom-ion process. The overall net result is

$$Q_e = -\frac{\dot{w}_{e,eA}\,E_I}{m_e} + \frac{\dot{w}_{e,AA}\,\bar{\varepsilon}_{AA}}{m_e} + \frac{\dot{w}_{e,AI}\,\bar{\varepsilon}_{AI}}{m_e} \qquad (65)$$

Chapin,[8] however, has calculated that $\bar{\varepsilon}_{AA}$ is on the order of kT_e or less. Thus, since for present conditions of interest the electron-atom process is usually the dominant ionization mechanism, the terms containing $\bar{\varepsilon}_{AA}$ and $\bar{\varepsilon}_{AI}$ will usually be negligible in comparison. For those parts of the flow field in which the atom-atom reaction is important, the concentration of electrons should be so low that any error in the calculation of the electron temperature resulting from neglection of the $\bar{\varepsilon}_{AA}$ term should be slight and have a negligible effect overall. A similar conclusion can be drawn for the $\bar{\varepsilon}_{AI}$ term. Consequently only the first term in Equation (65) will be retained.

G. Collision Cross Section

In the formulation of the collision interaction terms in Chapter III one of the quantities which appears in the results is the momentum collision cross section, S_{ij}. An approximate method of determining average cross sections

for uncharged particles has been discussed by Hansen[18] and also by Fay.[19] In this method the effective collision diameter is obtained by equating the average potential function for the collision to kT; i.e.

$$V(R) = kT \tag{66}$$

The average cross section is then πR^2.

Using the potential function given by Vanderslice, Mason, and Lippincott,[25] application of this technique yields for the molecule-molecule interaction

$$S_{MM} = 0.4423\left[\ln(1.0427 \times 10^{-7} T_N)\right]^2 \times 10^{-16} cm^2 \tag{67}$$

Likewise the cross section for the atom-molecule collision is expressible as

$$S_{AM} = (0.4206 \times 10^{-16})\left\{\ln[2.222 \times 10^{-7} T_N]\right\}^2 cm^2 \tag{68}$$

For the unlike particle collision it is commonly assumed that the effective collision diameter is equal to the mean of those for the like-particle collisions.[19] That is, in terms of cross sections

$$2(S_{AM})^{1/2} = (S_{AA})^{1/2} + (S_{MM})^{1/2} \tag{69}$$

While this relationship does not apply in general it should be sufficiently accurate to serve for the evaluation of the

atom-atom cross section, S_{AA}.

For the electron-molecule and electron-atom collisions the results of Shkarofsky et al[26] have been correlated to yield the following results.

$$\left.\begin{array}{c} T_e \leq 3095\ ^\circ K \\ S_{eM} = (-0.863 + 0.5153 \log_{10} T_e)\, 10^{-15}\ cm^2 \\ 3095\ ^\circ K < T_e \leq 7737\ ^\circ K \\ S_{eM} = 0.818 \times 10^{-15} + 0.377 \times 10^{-19}\, T_e\ cm^2 \\ T_e > 7737\ ^\circ K \\ S_{eM} = 0.5355 \times 10^{-19}\, T_e + 0.696 \times 10^{-15}\ cm^2 \end{array}\right\} \qquad (70)$$

$$\begin{array}{c} T_e \leq 1500\ ^\circ K \\ S_{eA} = 1.26 \times 10^{-15}\ cm^2 \\ 1500\ ^\circ K < T_e \leq 9200\ ^\circ K \\ S_{eA} = 0.333 \times 10^{-15} (0.642 + \log_{10} T_e)\ cm^2 \\ T_e > 9200\ ^\circ K \\ S_{eA} = 1.52 \times 10^{-15}\ cm^2 \end{array} \qquad (71)$$

In collisions in which both partners are charged, the dominant forces involved are long range electrostatic forces and the potential function is coulombic. The cross section resulting from applying a coulombic potential in Equation (66) must, however, be modified to account for the charge shielding effect which occurs in a finite density plasma. While some disagreement exists concerning

the magnitude of this correction, a form proposed by Jaffrin[12] approximates the mean of the various other estimates; and it has been used in the present analysis. The end results are

$$S_{ee} = \frac{\pi \epsilon^4}{2(kT_e)^2} \ln\left[\frac{9k^3 T_e^3 m_e}{4\pi \rho_e \epsilon^6}\right]^{1/2} \tag{72}$$

$$S_{II} = \frac{\pi \epsilon^4}{2(kT_N)^2} \ln\left[\frac{9k^3 T_N^3 m_I}{4\pi \rho_I \epsilon^6}\right]^{1/2} \tag{73}$$

$$S_{Ie} = S_{ee} \tag{74}$$

The atom-ion cross section, S_{AI}, has been approximated as[19]

$$S_{AI} = 140 \times 10^{-16} cm^2 \tag{75}$$

While this value may not be precisely correct, it does have the correct magnitude relative to the other cross sections and should lead to good results. Finally, lacking any other indication, the ion-molecule cross section, S_{MI}, has arbitrarily been set equal to S_{AM}.

H. Diffusion Term and Approximations

In formulating the diffusion velocity expressions, a modified ambipolar diffusion model as postulated by Fay and Kemp[27] for ionized nitrogen has been used. In this model it is assumed that the charge-exchange cross section between atoms and ions is high enough to insure that they have the same diffusion velocity. Since ions and electrons always have equal diffusion velocities within a diffusion layer which is thick compared to the Debye distance, this assumption means that the atoms, ions, and electrons diffuse as a single component and with the same velocity. The other oppositely directed component is composed of molecules.

From Chapman and Cowling[28] the general binary diffusion equation is

$$\vec{U}_1 - \vec{U}_2 = \frac{-N^2}{N_1 N_2} D_{12} \left\{ \frac{\partial}{\partial \vec{r}} \left(\frac{N_1}{N} \right) + \frac{N_1 N_2 (m_2 - m_1)}{N \rho} \frac{\partial \ln p}{\partial \vec{r}} \right. \qquad (76)$$

$$\left. - \frac{\rho_1 \rho_2}{p \rho} (\vec{F}_1 - \vec{F}_2) + k_T \frac{1}{T} \frac{\partial T}{\partial \vec{r}} \right\}$$

Applying Equation (76) to ionized nitrogen in the manner of Fay and Kemp[27] and considering the effects of thermal diffusion and external forces as negligible yields

$$U_M - U_e = \frac{(N_A + N_I + N_M) D_{N-N_2}}{(N_A + N_I) N_M k T_H} \cdot \left\{ \frac{\partial}{\partial x} (p_A + p_I + p_e) - \frac{p_A + p_e + p_I}{p} \frac{\partial p}{\partial x} \right\} \tag{77}$$

Since

$$\rho_m U_m + (\rho_I + \rho_A + \rho_e) U_e = 0 \tag{78}$$

Equation (77) can be solved for the electron diffusion velocity. The effect of considering a two-temperature gas appears by expressing the partial pressure in terms of the temperature and number densities. The results are

$$U_A = U_I = U_e = \frac{-m_m}{(N_A + N_I + 2N_M) m_A} \left(\frac{N_M + N_A + N_I}{N_A + N_I} \right) \cdot \frac{D_{N-N_2}}{k T_H} \left\{ \frac{\partial}{\partial x} \left(k T_H \left(N_A + N_I + N_e \frac{T_e}{T_H} \right) \right) - \frac{(N_A + N_I + N_e T_e / T_H)}{(N_M + N_A + N_I + N_e T_e / T_H)} \frac{\partial p}{\partial x} \right\} \tag{79}$$

$$U_M = \frac{-(N_A + N_I) m_A U_A}{N_M m_M}$$

where terms of order m_e have been neglected.

In Equation (79) the diffusion coefficient should be a binary diffusion coefficient. However, since the atom-molecule and ion-molecule cross sections are assumed equal, the binary diffusion coefficient becomes simply D_{N-N_2}. The form of this coefficient has been given in Equation (48).

I. Radiation Model

The form of the radiation term, $\partial q_R / \partial x$, in the overall energy equation for the case where the absorption coefficient is represented by a multi-step model has been derived in detail and discussed previously by Anderson.[3] Therefore, only a brief outline of the derivation will be presented here.

In general, assuming that the end-wall is non-emitting and non-reflective, the spectral radiative energy transfer at any point is

$$-\dot{q}_{R_\nu}(\tau_\nu) = 2\pi \int_{\tau_\nu}^{\tau_{s\nu}} B_\nu(z) E_2(z-\tau_\nu)\, dz - 2\pi \int_0^{\tau_\nu} B_\nu(z) E_2(\tau_\nu - z)\, dz \tag{80}$$

where τ_ν is the optical length. The optical length is related to physical length via the absorption coefficient by

$$d\tau_\nu = K_\nu\, dx \tag{81}$$

Differentiation of Equation (80) with respect to x yields

$$-\frac{d\dot{q}_{R\nu}}{dx} = -4\pi K_\nu B_\nu(\tau_\nu) + 2\pi K_\nu \int_0^{\tau_{s\nu}} B_\nu(z) E_1(|\tau_\nu - z|)\, dz \qquad (82)$$

Subsequent integration over all wavelengths results in the total radiative flux

$$-\frac{d\dot{q}_R}{dx} = -4\pi \int_0^\infty K_\nu B_\nu\, d\nu + 2\pi \int_0^\infty K_\nu \int_0^{\tau_{s\nu}} B_\nu E_1(|\tau_\nu - z|)\, dz\, d\nu \qquad (83)$$

In this expression the first term represents the loss of energy due to radiative emission, and the second term accounts for the energy gain from radiative absorption.

In principle the exact spectral dependence of q_r could be determined by carrying out the integration in Equation (83) at each point in the flow. From a computational viewpoint, however, this is impractical due to the large amount of information required for the determination of the absorption coefficient, K_ν , and the black-body function, B_ν . In order to simplify the problem the spectrum is divided into a series of finite length steps. In each step for a given set of state conditions the absorption coefficient is assumed to be a constant given by

$$K_i = \frac{\int_{\lambda_i}^{\lambda_{i+1}} K_\lambda B_\lambda \, d\lambda}{\int_{\lambda_i}^{\lambda_{iH}} B_\lambda \, d\lambda} \tag{84}$$

Likewise the black body function for the region is defined as

$$B_i = \int_{\lambda_i}^{\lambda_{i+1}} B_\lambda \, d\lambda \tag{85}$$

Using these expressions and the assumption that $B_1(z)$ can be represented by a series of straight line segments, the integrals in Equation (83) can be carried out. The result is

$$-\frac{dq_R}{dx} = 2\pi \left\{ -\sum_i 2K_i B_i + \sum_i K_i \left\{ 2B_i - B_i(0) E_2(\tau_i) \right.\right.$$
$$- B_i(\tau_i) E_2(\tau_{si} - \tau_i) - \sum_{j=0}^{j=I} \frac{B_{i\,j+1} - B_{ij}}{z_{j+1} - z_j} \tag{86}$$
$$\left.\left. \cdot \left[E_3(|\tau_i - z_{j+1}|) - E_3(|\tau_i - z_j|) \right] \right\} \right\}$$

where I is the point immediately behind the shock wave. The summation over i is over the various wavelength steps, while that over j accounts for the x integration.

In order to accurately represent the non-gray absorption characteristics of high temperature nitrogen the

spectrum has been subdivided into the following five wavelength regions:

Region	Wavelength Interval
1	620 - 1100 Å
2	1100 - 1300 Å
3	1300 - 1570 Å
4	1570 - 7870 Å
5	7870 - 9552 Å

For each wavelength region an average absorption coefficient and a black body function, as defined in Equations (84) and (85), have been computed and correlated as functions of temperature and number density; and these functions are then used in the actual computation of optical lengths and radiative heat flux. Typical results are shown in Figures 3 and 4.

In the five step model, wavelength regions three and five are based solely upon atomic lines. While these two regions only include eleven nitrogen lines, an analysis[4] of other lines indicates that they are relatively important. The remaining regions -- one, two, and four -- are based solely on bound-free and free-free atomic nitrogen processes.

In principle the source or black body function and the absorption coefficient should be modified to include

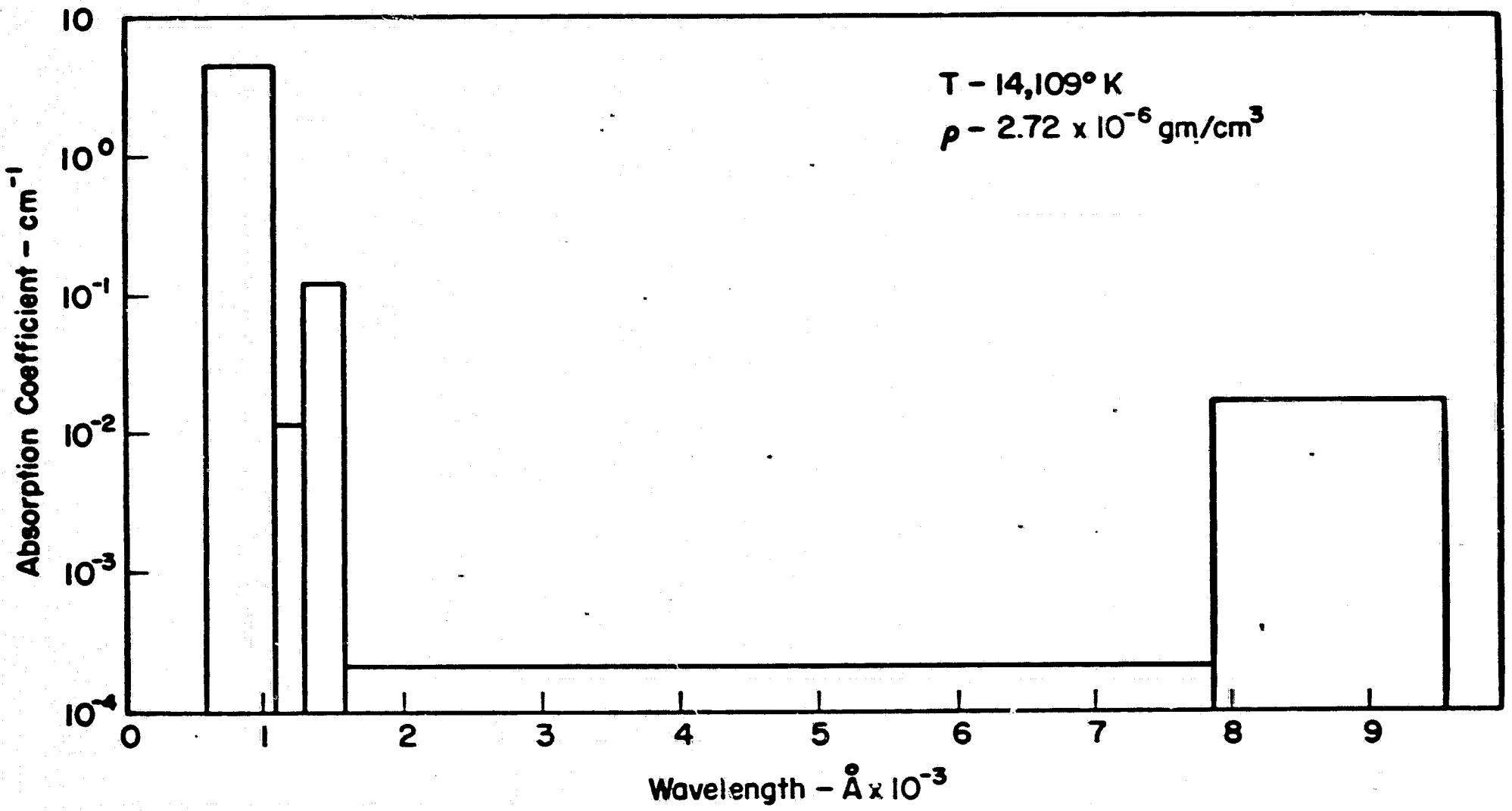

Fig. 3.--Illustration of Five-Step Absorption Coefficient Model for Typical Reflected Shock Wave Conditions

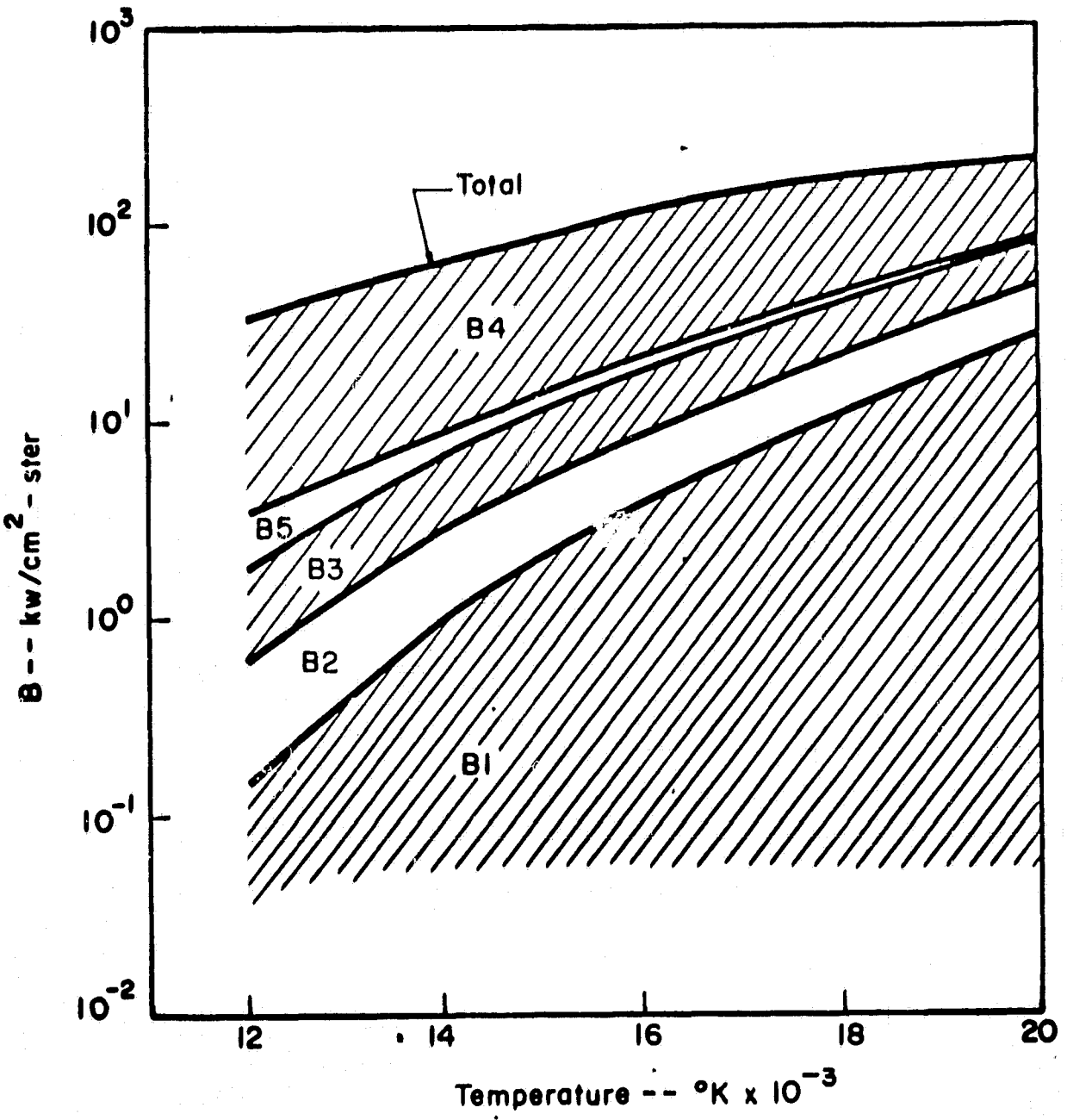

Fig. 4.--Five-Step Black-Body Source Function Model Showing Contributions From Each Wavelength Region

two temperature effects. Chapin[8] has carried out a general derivation of these functions for the thermal nonequilibrium case. The result for the bound-free source function is

$$S = \frac{[N_A(p)]_e \, 2h\nu^3}{N_A(p) \, c^2} \left(e^{h\nu/kT_e} - \frac{N_A(p)_E}{N_A(p)} \right)^{-1}$$

where $N_A(p)_E$ is the population of state p which would exist if state p were in equilibrium with the ions and electrons.

As in the discussion on ionization it is assumed that all the excited states of the atoms are in equilibrium with the electrons and ions. Thus the source function for bound-free radiation differs from the black body function only for those frequencies which originate from radiation due to photoionization from the ground state. That is, no correction need be applied for wavelengths greater than that of the ionization edge because such radiation results from the excited states, which are in equilibrium. In the case of nitrogen the ionization wavelength is 855 Å, and thus any required correction would only affect a small portion of region one. Since the thermal nonequilibrium correction itself is at most a few percent and since the affected region is small, the correction has been neglected.

Likewise, an analysis of nonequilibrium effects upon the source function for bound-bound radiation yields that

its correct form is[8]

$$S_{pq} = \frac{N_A(q)}{N_A(p)} \frac{g_p}{g_q} \cdot \frac{2h\nu^3}{c^2}\left[1 - \frac{N_A(q)}{N_A(p)} \frac{g_p}{g_q}\right]^{-1}$$

However if it is assumed that the individual state populations correspond to a Boltzmann distribution at the electron temperature, then this equation can be rewritten as

$$S_{pq} = e^{-\Delta E/kT_e} \frac{2h\nu^3}{c^2}\left[1 - e^{-\Delta E/kT_e}\right]^{-1}$$

But since ΔE is the energy of the jump, it is equivalent to $h\nu$. So

$$S_{pq} = \frac{2h\nu^3}{c^2}\left[e^{h\nu/kT_e} - 1\right]^{-1}$$

which is the usual black body function. Thus no correction is required for bound-bound radiation.

It should be noted that in the present analysis, the temperature to be used for calculating the absorption coefficients in region one, two, and four should be the electron temperature since the free-bound and free-free transitions are generally governed by electron encounters. On the other hand, the appropriate temperature for regions

three and five is not so obvious. However, experimental results at AVCO[24] indicate that nitrogen bound-bound transitions are probably closely coupled to the electron temperature. Consequently, as a result of this coupling, the q_R term in the overall energy equation will be dependent upon electron temperature.

In this analysis the effects of Bremsstrahlung on total electron energy have been assumed negligible. Hence, a radiation term only appears in the overall energy equation.

It should be noted that the present absorption coefficient model is accurate only for an electron temperature range from approximately 8000°K to 20,000°K. Below eight thousand degrees processes involving molecular nitrogen become important, and above twenty thousand the nitrogen double ion can be influential. Neither type of process has yet been included in the model. However, for the conditions and chemical model of interest at present, the above absorption coefficient scheme should be sufficient.

J. Wall Sheath Description and Boundary Conditions

If it is desired to formulate the problem including the end-wall boundary layer, then consideration must be given to the plasma sheath which is adjacent to the end-wall. While the properties of a plasma sheath surrounding an object in contact with a plasma have been analysed by

many investigators, the model of most interest is the approximation of Schultz and Brown.[29] In their analysis it is postulated that a sheath, which is on the order of a Debye length in thickness, forms adjacent to the wall and that in the sheath charge neutrality and the continuum equations fail to apply. Furthermore there appears between the sheath and the continuum flow a very thin transition region. Throughout it is assumed that the electrons are isothermal and that the sheath develops an electric potential between itself and the plasma so as to maintain charge neutrality and zero charge flux at the sheath edge.

Camac and Kemp[9] have successfully utilized this model by ignoring the transition region, and Dix[30] has also shown that inclusion of the transition region has a negligible effect on the results. Thus the transition region will also be neglected in the present analysis. Now in order to maintain zero charge flux at the sheath edge, the sheath potential must adjust itself so that the positive current, consisting of electron emission from the surface and diffusing ions, equals the electron current. That is,

$$\frac{N_e c_e}{4} \exp\left(\frac{-\epsilon\phi}{k T_e}\right) = \frac{N_I c_I}{4} + J \qquad (87)$$

where ϕ is the sheath potential, $\bar{c}_e$ the electron thermal velocity, c_I the ion drift velocity in the sheath, and J

the wall emission. Note that Equation (87) inherently assumes that the wall is catalytic to electron recombination since no term has been included to account for the reflection of electrons from the wall.

The ion drift velocity, c_I, depends upon the number of collisions an ion has in passing through the sheath. For the case of many collisions, this is simply the ion thermal velocity. For the collisionless case, however, the results of Schultz and Brown[29] indicate that

$$c_I = 4\sqrt{\frac{k T_e}{m_I}} \tag{88}$$

The present analysis includes the option of using either value.

If in the interest of simplification the wall electron emission is assumed negligible, then Equation (87) can be solved for the sheath potential in terms of properties at the sheath edge. Using the fact that charge neutrality exists at the sheath edge this assumption leads to

$$\phi = \frac{k T_e}{\epsilon} \ln\left(\frac{1}{c_I}\sqrt{\frac{8 k T_e}{\pi m_e}}\right) \tag{89}$$

This result for ϕ will subsequently be used in the boundary conditions.

Since the thickness of the plasma sheath is negligible

in comparison to that of the end-wall boundary layer, the edge of the sheath can be construed as being physically at the wall. Thus, the inner boundary conditions on the continuum equations which correspond to properties at the sheath edge, can be applied at x equal to zero. These boundary conditions are obtained by matching at the sheath edge the molecular description in the plasma sheath to the corresponding usual continuum description at the wall. One quantity which can be matched in this manner is the ion mass flux. Equating the two corresponding expressions yields

$$\frac{m_I N_I c_I}{4} = -\rho_I v_I \tag{90}$$

The electron energy flux can be likewise considered. Those electrons which get to the wall enter the sheath with an average energy of $2kT_e + |e\phi|$, and their corresponding flux is $(N_e \bar{c}_e/4)\exp(-|e\phi|/kT_e)$. Hence the continuity of electron energy flux requires

$$\left(\lambda_e \frac{\partial T_e}{\partial x} - \rho_e v_e h_e\right)_{x=0} = (2kT_e + |e\phi|) \cdot \frac{N_e c_e}{4} \exp\left(\frac{-|e\phi|}{kT_e}\right) \tag{91}$$

where the sheath potential ϕ is obtained from Equation (89).

At the wall the molecules, being unaffected by the sheath, are in good contact with the wall and thus have the wall temperature. By assumption the ions are, at least in regions where the continuum description holds, in thermal equilibrium with the molecules. Thus, at the wall the ions should also be at the wall temperature. In this analysis the wall will be assumed catalytic and all atoms at the wall will recombine to form molecules. With these considerations there results the two additional boundary conditions

$$(T_H)_{x=0} = T_W \tag{92}$$

and

$$(\rho_A)_{x=0} = 0 \tag{93}$$

Equations (89)-(93) complete the specification of the inner boundary conditions for the case where the end-wall boundary layer is included in the analysis.

On the other hand when it is desirable, e.g. from a computational standpoint, to calculate only the inviscid portion of the flow field, the above boundary conditions are not applicable. In that case, however, the second derivatives of the flow field variables at the outer edge of the boundary layer should be negligible. Therefore, for

the inviscid case the inner boundary conditions on all the variables except the velocity can be approximated by requiring the second derivatives to be zero. The velocity should still be assumed to be exactly zero.

The outer boundary conditions correspond to the properties immediately behind the reflected shock front. These conditions can be obtained as a function of properties in front of the shock wave by assuming frozen flow and matching of total enthalpy across the wave. The details of this procedure will be presented in the next chapter.

CHAPTER V

A SOLUTION FOR THE TWO-TEMPERATURE REFLECTED SHOCK PROBLEM

A. Treatment of Boundary Conditions

In obtaining the outer boundary conditions, that is the conditions immediately behind the shock wave, three distinct cases must be considered. Ideally these conditions correspond to the situation where the gas is chemically frozen prior to chemical relaxation. However, there may be conditions of interest where the relaxation distance is so short that it would be more practical to assume that equilibrium immediately exists. Likewise, since chemical relaxation often proceeds in stages, other conditions could cause the dissociation processes to be in local equilibrium while ionization is still frozen. In order to give versatility to the present solution, schemes to calculate the post-shock conditions for each of these cases have been developed, assuming that the gas in front of the shock wave is in complete equilibrium and that precursor effects are negligible. These methods are referred to as the frozen, equilibrium, and partially frozen cases.

In each case the basic equations that are used are the conservation equations of mass, momentum, and energy across

the shook front. Using the subscript 2 to denote conditions behind the wave, these equations are

$$\rho_2 (W_s + V_2) = \rho_s (W_s + V_s) \tag{94}$$

$$p_2 + \rho_2 (W_s + V_2)^2 = p_s + \rho_s (W_s + V_s)^2 \tag{95}$$

$$h_2 + \frac{1}{2}(W_s + V_2)^2 = h_s + \frac{1}{2}(W_s + V_s)^2 \tag{96}$$

By estimating the pressure behind the wave, Equations (94) and (95) can be rearranged so as to yield estimates for ρ_5 and V_5.

$$V_s = V_2 - (p_s - p_2)/\rho_2 (W_s + V_2) \tag{97}$$

$$\rho_s = \rho_2 (W_s + V_2)/(W_s + V_s) \tag{98}$$

If the flow has been assumed to be frozen, then the corresponding species densities can be calculated from the fact that the mass fractions are constant across the shook front. That is,

$$\rho_{i_5} = (\rho_{i_2}/\rho_2)\rho_5 \tag{99}$$

Now in traversing the shock the requirement on electron energy is

$$h_{e_2} + \frac{1}{2}(W_5 + V_2)^2 = h_{e_5} + \frac{1}{2}(W_5 + V_5)^2 \tag{100}$$

which after substituting the continuity equation can be re-expressed as

$$h_{e_5} = h_{e_2} + \frac{1}{2}(W_5 + u_2)^2\left[1 - \rho_2^2/\rho_5^2\right] \tag{101}$$

When an order of magnitude analysis is applied to Equation (101), it turns out that the first term on the right-hand-side, h_{e_2}, is approximately 10^5 larger than the second term. Hence to a first approximation the electron static enthalpy is unchanged across the shock wave. In other words,

$$T_{e_5} = T_{e_2} \tag{102}$$

With this information, the initial estimate for pressure, and the resulting species densities (Equation (99)), the equation of state can be solved for a heavy body

temperature. All of these values can then be used to see if Equation (96) is satisfied. If it is, then the correct post-shock values have been found. If not, then some type of iteration must be employed.

In the present investigation a simple Newton iteration scheme based upon total enthalpy conservation and pressure has been selected. To start the procedure a second estimate of the post-shock pressure is made that is arbitrarily five percent larger than the first. The post-shock variables are then computed in the same manner as before, and the total enthalpy difference across the wave calculated. A new pressure estimate is then obtained by

$$p_{s_{i+2}} = p_{s_{i+1}} - \frac{\Delta H_{i+1}\,(p_{s_{i+1}} - p_{s_i})}{\Delta H_{i+1} - \Delta H_i} \qquad (103)$$

where the subscripts indicate the estimate and ΔH_i refers to the associated enthalpy difference. The entire procedure, Equations (97) thru (103), is then repeated for as many times as is necessary until Equation (96) is satisfied. This was assumed to occur when the difference in the two sides of the equation was less than one-half percent.

For the equilibrium case the procedure is the same through Equation (98). At that point a temperature estimate is also selected and the corresponding equilibrium

composition computed by application of the law of mass action to the dissociation and ionization reactions. The actual equations used are those which have been presented by Fay and Kemp.[27]

Since this approach requires two post-shock variables to be estimated, two criteria are needed to check the validity of the guesses. As in the frozen case, one check is the energy equation across the shock wave, Equation (96). The second one is obtained by comparing the density calculated via Equation (98) and the one computed using the calculated composition and the equation of state. If either one of the criteria is not met, then an iteration is started. In the iteration scheme, which is of the Newton two variable type, the required partial derivatives -- $\partial \rho / \partial p$, $\partial \rho / \partial T$, $\partial (H_5 - H_2)/\partial p$, $\partial (H_5 - H_2)/\partial T$, -- are evaluated by separately computing the post-shock conditions for a pressure five percent above the initial value and a temperature five percent above the first guess. Thus, each iteration step requires three calculations of post-shock values. Nevertheless, the approach to convergence is almost as fast as in the frozen case.

For the partially frozen case, a mixture of the above methods is used. Those species which are considered to be chemically frozen have their densities calculated from Equation (99), while those for the equilibrium constituents

are obtained from the law of mass action. The iterative procedure and convergence criteria are the same as for the equilibrium case.

The inner boundary conditions on the electron temperature and density are determined in the viscous case by the flux of ion mass and electron energy across the outer edge of the plasma sheath. The basic equations for these and the other inner boundary conditions were presented in Chapter IV, Section J. Unfortunately the equations for the viscous case are highly non-linear, and thus the edge values for electron temperature and density can only be obtained through iteration. However, Knight[31] has pointed out that for many conditions these equations may be simplified. Combination of Equation (90) and (91) yields that

$$\frac{\partial T_e}{\partial x} = \frac{-\rho_I C_I}{4 \lambda_e} \left[\frac{1}{2} \frac{k T_e}{m_I} - \frac{|\epsilon \phi|}{m_I} \right] \tag{104}$$

If ρ_I were sufficiently small, then Equation (104) indicates that quite possibly the approximation could be made that

$$\left(\frac{\partial T_e}{\partial x} \right)_{x=0} \cong 0 \tag{105}$$

at least in comparison to the heavy body temperature

gradient. This approximation greatly simplifies the inner boundary conditions for the boundary layer case and completely eliminates the need for iteration. Since the number of ions in the boundary layer and adjacent to the sheath edge should be very small due to the low heavy body temperature which exists there, Equation (105) should be a good approximation. Of course, in the inviscid case the second derivative approximation postulated in Section J of the last chapter will suffice.

B. Transformation of the Conservation Equations

In the past, formulations to the reflected shock problem have always been in a physical coordinate system based upon the distance from the shock-tube end-wall. While such a coordinate system is convenient from an equation viewpoint, it may be a disadvantage in a numerical solution becuase it does not provide additional points in regions of high gradients. Thus, it might be advantageous to transform the equations into a coordinate system which provides additional points in at least some of the high gradient regions. A suitable transformation is the reflected shock similarity transformation

$$\eta = \left[\frac{C_2}{2\rho_2 t}\right]^{1/2} \int_0^x \rho(x',t)\,dx' \qquad (106)$$

$$s = t$$

Being of the "boundary layer type" this particular transformation should greatly facilitate any calculations which include an end-wall thermal boundary layer. Furthermore, it may be advantageous even in a pure inviscid calculation in that a solution in η will facilitate determination of boundary layer edge gradients, which may then be used in a separate boundary layer calculation. (In any flow with extensive radiation cooling non-zero boundary layer edge gradients usually exist.)

The transformation given in Equation (106) does, however, have one possibly serious disadvantage. If the solution is obtained in η, then the corresponding x points must be obtained by integration. Since the reflected shock velocity is obtained from the rate of change with respect to time of the shock position measured in x, any error in the integration could cause a serious error in the shock velocity. In spite of this possible difficulty, the present solution has been formulated in an η - s coordinate system. The relative merits of this coordinate system based on the computational results obtained will be discussed in Appendix II.

In the η - s coordinate system the governing equations for the reflected shock problem are as follows:

Species Continuity

$$\frac{\partial \rho_i}{\partial s} - \frac{n}{2s}\frac{\partial \rho_i}{\partial \eta} + \left[\frac{c_2}{2\rho_2 s}\right]^{1/2}\rho\rho_i\frac{\partial u}{\partial \eta} + \left[\frac{c_2}{2\rho_2 s}\right]^{1/2}\rho\frac{\partial}{\partial \eta}(\rho_i V_i) = \dot{w}_i \tag{107}$$

Momentum

$$\rho\frac{\partial u}{\partial s} - \frac{\rho n}{2s}\frac{\partial u}{\partial \eta} = -\left[\frac{c_2}{2\rho_2 s}\right]^{1/2}\rho\frac{\partial p}{\partial \eta} \tag{108}$$

Electron Energy

$$\rho_e c_{pe}\frac{\partial T_e}{\partial s} - \frac{n}{2s}\rho_e c_{pe}\frac{\partial T_e}{\partial \eta} + \left[\frac{c_2}{2\rho_2 s}\right]\rho\frac{\partial}{\partial \eta}\left(-\lambda_e\rho\frac{\partial T_e}{\partial \eta}\right)$$

$$+\left[\frac{c_2}{2\rho_2 s}\right]^{1/2}\rho\rho_e c_{pe}V_e\frac{\partial T_e}{\partial \eta} - \frac{\partial p_e}{\partial s} + \frac{n}{2s}\frac{\partial p_e}{\partial \eta}$$

$$-\left[\frac{c_2}{2\rho_2 s}\right]^{1/2}\rho V_e\frac{\partial p_e}{\partial \eta} = \dot{w}_e\frac{u^2}{2} + \sum \xi_{ej} + V_e\sum P_{ej} \tag{109}$$

$$-\frac{\dot{w}_{e,ea}}{m_e}E_I - c_{pe}T_e\dot{w}_e$$

Energy

$$\sum_i \rho_i c_{pi} \frac{\partial T_i}{\partial s} + \sum_i h_i \frac{\partial \rho_i}{\partial s} - h \frac{\partial \rho}{\partial s}$$

$$- \frac{n}{2s} \left\{ \sum_i \left(\rho_i c_{pi} \frac{\partial T_i}{\partial \eta} + h_i \frac{\partial \rho_i}{\partial \eta} \right) - h \frac{\partial \rho}{\partial \eta} \right\}$$

$$- \rho \left[\frac{c_2}{2 \rho_2 s} \right] \frac{\partial}{\partial \eta} \left[\sum_i \lambda_i \rho \frac{\partial T_i}{\partial \eta} \right] + \rho \left[\frac{c_2}{2 \rho_2 s} \right]^{1/2} \frac{\partial}{\partial \eta} \left[\sum_i \rho_i h_i V_i \right] \qquad (110)$$

$$+ \rho \left[\frac{c_2}{2 \rho_2 s} \right]^{1/2} \frac{\partial q^R}{\partial \eta} - \frac{\partial p}{\partial s} + \frac{n}{2s} \frac{\partial p}{\partial \eta}$$

$$= - \dot{w}_I h_I^\circ - \dot{w}_A h_A^\circ$$

These four equations combined with the equations of state (Equations (41)-(42)), diffusion relationships (Equation (79)), enthalpy expressions (Equation (40)), chemical production terms (Equation (50)) and

$$\sum_{i=1}^{s} \rho_i = \rho \qquad (111)$$

essentially define the problem for the basic unknowns ρ_1, ρ, u, T_e, T_H, p_e, and p.

If in addition it is desired to permit the reflected shock velocity to be variable and thus the shock position to be a non-linear function of time, then two additional

equations are required. The first equates the mass flux across the shock front to the time rate of change of mass behind the wave. That is

$$\rho_2 (W_s + V_2) = \frac{d}{dt} \int_0^{x_s(t)} \rho(x,t)\, dx \qquad (112)$$

which in the η - s system becomes

$$\rho_2 (W_s + V_2) = \left[\frac{2\rho_2 s}{c_2}\right]^{1/2} \frac{d\eta_s}{dt} + \frac{\eta_s}{2}\left[\frac{2\rho_2}{c_2 s}\right]^{1/2} \qquad (113)$$

Here one of the advantages of the transformed system becomes apparent because the integral in Equation (112) has been rewritten in differential form; and if a finite difference scheme is employed, Equation (113) is readily solved for the shock position η_s at time t + Δt in terms of properties at time t. The second equation yields the shock velocity in terms of the change in physical shock position

$$W_p = \frac{dx_s}{dt} \qquad (114)$$

C. Method of Solution

Since the governing set of simultaneous equations is highly non-linear, some sort of numerical technique must be used to obtain solutions. Basically the method employed in the present investigation is a forward finite difference technique whereby if the flow field is known at some time s for all η between the shock wave and the wall, the difference technique will yield the flow field values for all η at time $s + \Delta s$. In this approach all first and second order derivatives with respect to η which appear in Equations (107) thru (110) are replaced by central difference approximations. For example $\partial T_e/\partial \eta$ and $\partial^2 T_e/\partial \eta^2$ are represented as

$$\frac{\partial T_e(\eta,s)}{\partial \eta} \cong \frac{T_e(\eta+\Delta\eta,s) - T_e(\eta-\Delta\eta,s)}{2\Delta\eta} \tag{115}$$

$$\frac{\partial^2 T_e(\eta,s)}{\partial \eta^2} \cong \frac{T_e(\eta+\Delta\eta,s) - 2T_e(\eta,s) + T_e(\eta-\Delta\eta,s)}{(\Delta\eta)^2} \tag{116}$$

On the other hand, the time derivatives in these same equations are represented by forward differences

$$\frac{\partial T_e(\eta,s)}{\partial s} \cong \frac{T_e(\eta,s+\Delta s)-T_e(\eta,s)}{\Delta s} \tag{117}$$

Since only time derivatives of the first order appear in the set of differential equations, each equation in its finite difference form can be algebraically solved for one of the unknowns at time s + Δs. As an example, consider application of this procedure to the electron continuity equation

$$\frac{\partial \rho_e}{\partial s} - \frac{\eta}{2s}\frac{\partial \rho_e}{\partial \eta} + \left[\frac{c_2}{2\rho_2 s}\right]^{1/2}\rho\rho_e\frac{\partial u}{\partial \eta} + \left[\frac{c_2}{2\rho_2 s}\right]^{1/2}\rho\frac{\partial}{\partial \eta}(\rho_e v_e) = \dot{w}_e \tag{118}$$

Rewriting this equation, but with the derivatives replaced by their finite difference forms, yields

$$\frac{\rho_e(\eta,s+\Delta s)-\rho_e(\eta,s)}{\Delta s} - \frac{\eta}{2s}\frac{\rho_e(\eta+\Delta\eta,s)-\rho_e(\eta-\Delta\eta,s)}{2\Delta\eta} + \left[\frac{c_2}{2\rho_2 s}\right]^{1/2}\rho(\eta,s)\rho_e(\eta,s)\frac{u(\eta+\Delta\eta,s)-u(\eta-\Delta\eta,s)}{2\Delta\eta} + \left[\frac{c_2}{2\rho_2 s}\right]^{1/2}\rho(\eta,s)\left\{v_e(\eta,s)\frac{\rho_e(\eta+\Delta\eta,s)-\rho_e(\eta-\Delta\eta,s)}{2\Delta\eta}\right. \tag{119}$$

continued on the next page

$$-\rho_e(\eta,s)\,\frac{U_e(\eta+\Delta\eta,s)-U_e(\eta-\Delta\eta,s)}{2\Delta\eta}\Big\} = \dot{w}_e(\eta,s) \tag{119}$$

and subsequent solving for $\rho_e(\eta, s+\Delta s)$ gives

$$\rho_e(\eta,s+\Delta s)=\rho_e(\eta,s)+\Delta s\Big\{\frac{n}{2s}\,\frac{\rho_e(\eta+\Delta\eta,s)-\rho_e(\eta-\Delta\eta,s)}{2\Delta\eta}$$

$$-\rho(\eta,s)\rho_e(\eta,s)\Big[\frac{C_2}{2\rho_2 s}\Big]^{1/2}\frac{u(\eta+\Delta\eta,s)-u(\eta-\Delta\eta,s)}{2\Delta\eta}+\dot{w}_e(\eta,s)$$

$$-\Big[\frac{C_2}{2\rho_2 s}\Big]^{1/2}\rho(\eta,s)\Big\{U_e(\eta,s)\,\frac{\rho_e(\eta+\Delta\eta,s)-\rho_e(\eta-\Delta\eta,s)}{2\Delta\eta} \tag{120}$$

$$-\rho_e(\eta,s)\,\frac{U_e(\eta+\Delta\eta,s)-U_e(\eta-\Delta\eta,s)}{2\Delta\eta}\Big\}\Big\}$$

In a like manner Equation (108) can be solved for $u(\eta, s+\Delta s)$, Equation (109) for $T_e(\eta, s+\Delta s)$, and Equation (110) for $T_H(\eta, s+\Delta s)$.

Now let IS represent the point immediately behind the shock wave at time s, and let I = 1 represent the wall. Then with this set of equations and a known solution as a function of η at some time s, a solution at time $s+\Delta s$ can be found via the following scheme:

1. Use the finite difference form of the shock mass flux balance to find the new shock location η_s.

   For points I = 2 to I = IS - 1

2. Use the electron, atom, and molecule species continuity equations in finite difference form to obtain $\rho_e(\eta, s + \Delta s)$, $\rho_a(\eta, s + \Delta s)$, and $\rho_m(\eta, s + \Delta s)$.
3. Find ρ_I from $\rho_I = m_I \rho_e / m_e$.
4. Find $\rho(\eta, s + \Delta s)$ from $\Sigma \rho_i = \rho$.
5. Express h_e and p_e in terms of T_e.
6. Use the electron energy equation in finite difference form to calculate T_e, and hence also p_e and h_e.
7. Use the overall energy equation in finite difference form to calculate $T_H(\eta, s + \Delta s)$.
8. Compute $p(\eta, s + \Delta s)$, $h_i(\eta, s + \Delta s)$, and $h(\eta, s + \Delta s)$.
9. Use the momentum equation to obtain $u(\eta, s + \Delta s)$.

   For the points between I = IS - 1 and the shock wave

10. Obtain the values of all the properties immediately behind the shock wave using the normal shock calculation procedure.
11. Use interpolation to compute the value of the individual flow variables for the points between

I = IS - 1 and the shock wave.

The values for I = 1 are obtained by applying the appropriate inner boundary conditions.

12. By inversion of Equation (106) and numerical integration obtain the physical shock wave location $x_s(s + \Delta s)$.

13. Obtain $W_R(s + \Delta s)$ from $x_s(s + \Delta s) - x_s((s))/\Delta s$.

This procedure can then be repeated for each new time until the desired final time is reached.

D. Starting Solution

Obviously in order to use the above described finite difference technique, some type of starting solution at some time s must be known. If it is desired to make only inviscid calculations, then the starting solution can be composed of a constant property flow field with values equivalent to those immediately behind the shock wave. While such a flow field is not exactly correct, it should serve as a good approximation if the initial time is selected short enough. In any case it is felt that the solution should approach the actual case after a few finite difference time increments.

In the case where it is desired to include an end-wall thermal boundary layer, then the above approach can still serve as the starting solution for the inviscid

portion of the flow. The boundary layer itself must, however, be treated separately. The transformation into the η - s coordinate system facilitates this because it casts the equations into a pseudo-similar form. If the boundary layer is assumed frozen, radiative transfer processes neglected, collision interaction effects ignored, and a local-similarity concept applied for some small time s, then the equations become ordinary differential equations. While these assumptions are only approximately valid, it is felt that the resulting simplification and the fact that the results will only be used for starting profiles warrants their use.

The resulting set of non-linear ordinary differential equations could be solved by any of several numerical methods. One possible approach is to use finite differences. In this case evaluation of the derivatives of the unknown variables via central differences causes each equation to take on a tri-diagonal nature. For example, the electron species continuity equation has the algebraic form

$$A_{j,i-1}\rho_{e_{i-1}} + A_{ji}\rho_{e_i} + A_{j,i+1}\rho_{e_{i+1}} = B_j \qquad (121)$$

where the coefficients A_{ji} and B_j are functions of the flow field properties at point i. If the A's and B's are evaluated using some previous solution, then the resulting A

matrix can be inverted and a new approximation to the electron density solution obtained. A similar procedure can be applied to the remaining equations to obtain new approximations for the rest of the flow field variables. These improved solutions can in turn be used to evaluate new A and B coefficients, and the process repeated until convergence is obtained.

The asymptotic form of the governing equations in the outer regions of the boundary layer should provide good initial guesses for the tri-diagonal iteration scheme. For example, the outer form of the starting solution energy equation is

$$\frac{\eta}{C_2}\frac{dT_H}{d\eta} + C_3\frac{d^2T_H}{d\eta^2} = 0 \qquad (122)$$

where C_2 and C_3 are constants evaluated at the edge of the boundary layer. This simplified equation has an exact solution of

$$T_H(\bar{\eta}) = (T_{edge} - T_{wall})\frac{2}{\sqrt{2\pi}}\int_0^{\bar{\eta}} e^{-\bar{\eta}^2/2}d\bar{\eta} + T_{wall} \qquad (123)$$

where

$$\bar{\eta} = n / \sqrt{C_2 C_3} \qquad (124)$$

and the integral is directly proportional to the error function. By calculating appropriate values for C_2 and C_3 an estimate for the corresponding boundary layer thickness can be obtained. Inspection of the other equations reveals that the remaining variables all have asymptotic solutions of the same form. Since the end wall problem is probably dominated by thermal conduction, it is felt that all of the zero order solutions should be normalized to the boundary layer thickness predicted by Equations (123) and (124).

E. Determination of Condition for Initial Calculations

In selecting a test condition which is compatible with the aims of this investigation several items must be considered. First, the equilibrium temperature behind the shock wave should be sufficiently high that radiative processes and radiation heat transfer are significant. Second the characteristic chemical relaxation times should be long enough so that nonequilibrium chemistry effects can be observed, and finally the pressure and enthalpy in the shocked flow should correspond to a flight condition which is of interest. In addition it would be desirable, although not essential, to select a condition which could

be experimentally investigated in the OSU shock tube facility and at which chemical and thermal nonequilibrium effects might exist in combination with radiative cooling.

One method of determining the relative effects which exist at a given condition is to calculate and compare characteristic times for radiation cooling, chemical recombination, and thermal equilibration. A characteristic radiation time can be obtained by considering the heavy body energy equation for the case where the state of the gas is assumed to vary only with time. By assuming that the gas is transparent to radiation, the fastest possible cooling rate will be represented; and the resultant calculated time will be a lower limit. If the variables appearing in the derivatives are normalized the equation takes the form,

$$\left(\rho_I c_{p_I} + \rho_A c_{p_A} + \rho_m c_{p_m}\right) \frac{T_s}{\tau_{rad}} \frac{\partial (T/T_s)}{\partial (t/\tau_{rad})} = 4\pi \int K_\lambda B_\lambda \, d\lambda$$

Then by assuming that the derivative is of order one the equation can be solved for a characteristic time. The expression for this time is

$$\tau_{rad} = \frac{\sum \rho_i c_{p_i} T_s}{4\pi \int K_\lambda B_\lambda d\lambda} \tag{125}$$

It should be noted that τ_{rad} is in actuality a measure of the time required for complete cooling.

In a like manner a chemical time can be obtained by considering the rate equation for the deionization phase of

$$N + M \rightleftharpoons N^+ + e + M \tag{126}$$

The result is

$$\tau_{chem} = \frac{m_e m}{k_r \rho_{e_s} \rho_s} \tag{127}$$

where τ_{chem} is related to the time required for complete deionization.

The determination of a thermal equilibration time is a little more complicated because both chemical and collisional effects affect the time required for the electron and heavy body temperatures to equalize. However, if chemical and diffusion effects are ignored and a limiting form of the collision interaction terms considered, then

the electron energy equation yields a characteristic collision equilibration time. The result is

$$\tau_{collision} = \frac{\frac{3}{16 m_e}\left[\frac{\pi m_e}{2kT_e}\right]^{1/2}}{\frac{\rho_A}{m_A^2} S_{eA} + \frac{\rho_I}{m_I^2} S_{eI} + \frac{\rho_M}{m_M^2} S_{eM}} \qquad (128)$$

Here S_{ij} represents the collision cross section for particles i and j.

Equations (125), (127) and (128) have been evaluated for equilibrium conditions behind reflected shock waves resulting from incident shocks of 8 km/sec and 11 km/sec and a range of pressures. The resulting characteristic times are plotted on Figure 5. These curves reveal that the collision equilibration times are always extremely short; and, thus, that unless chemical nonequilibrium or large external effects exist, extensive thermal nonequilibrium will not exist. On the other hand, they also show that the characteristic chemical recombination times at a pressure of ten microns of mercury are quite long, indicating that extensive chemical nonequilibrium can occur. In fact the chemical times are sufficiently longer than the radiation ones to indicate that possibly some chemical nonequilibrium can be induced by radiation cooling.

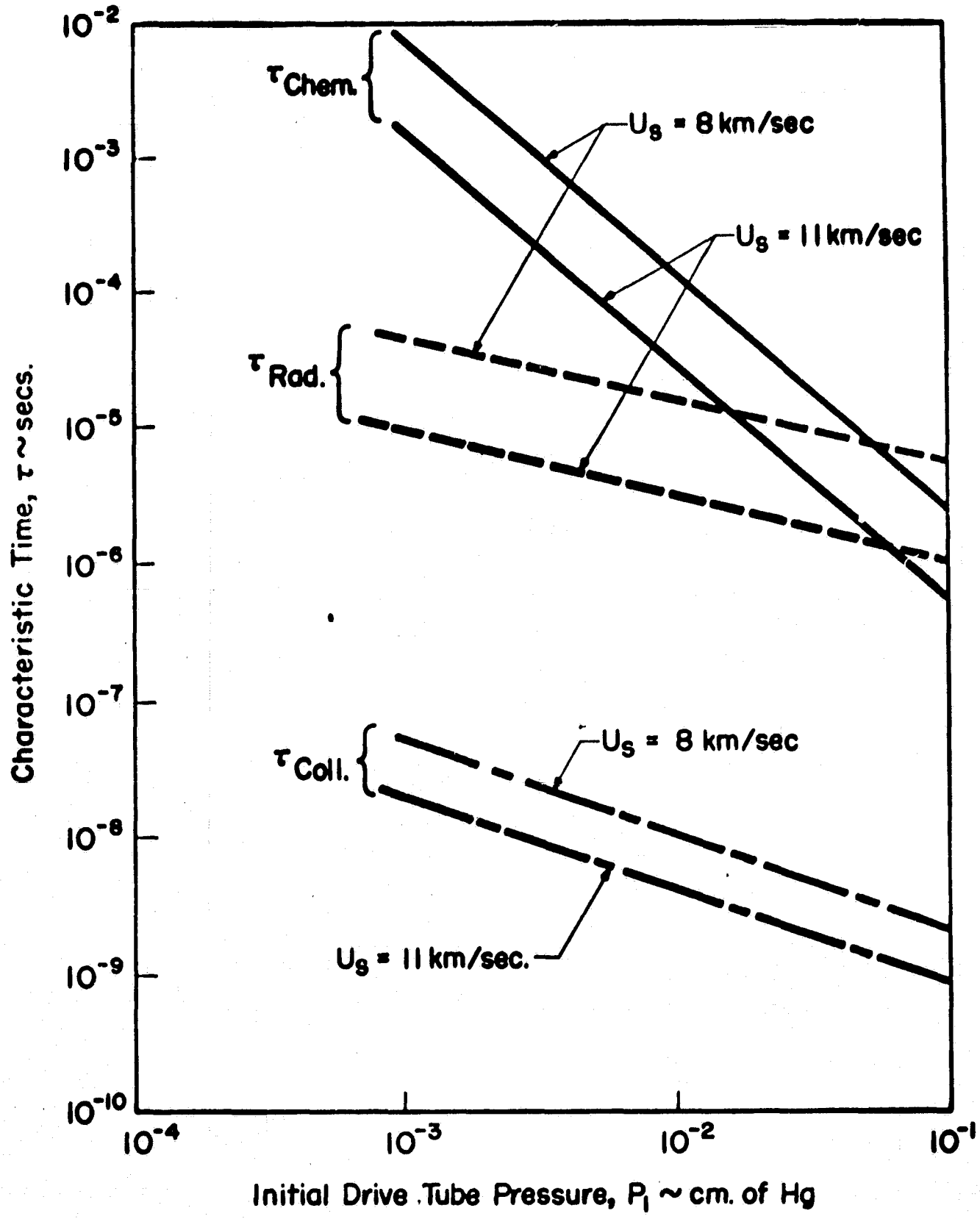

Fig. 5.--Characteristic Times Behind Reflected Shock Waves in Nitrogen

An initial pressure of ten microns represents about the lowest practical shock tube operating pressure, and an incident velocity of 11 km/sec should yield significant radiation effects in the reflected shock region. Furthermore, these conditions are comparable to those at the stagnation point of a vehicle travelling 16.5 km/sec at an altitude of about 67 kilometers. Therefore a reflected shock flow field which corresponds to an incident shock travelling at 11 km/sec into quiescent nitrogen at 10^{-3} cm of mercury has been selected as the initial calculation condition for this investigation.

CHAPTER VI

DISCUSSION OF RESULTS

A. Introduction

Ideally it would be desirable to obtain calculations for the flow field behind a reflected shock wave which include the nonequilibrium region behind the shock front, the near equilibrium inviscid region between the relaxation zone and the boundary layer, and the end-wall thermal boundary layer. However, attempts to obtain starting profiles for the boundary layer region at the condition of 11 km/sec and initial pressure of 10^{-3} cm of mercury using the above described tri-diagonal technique have met with only partial success. Not only is the rate of convergence of this technique extremely slow, but a minimum of twenty points inside the boundary layer is required for the finite differences to be accurate. Since the number of calculations required by the main flow field program increases faster than the number of points squared, any inclusion of a boundary layer represented by this number of points would result in excessive computer times. As a result all of the calculations discussed in this chapter have been carried out neglecting the end-wall boundary layer.

An inviscid calculation has been carried out for the flow field behind a reflected shock wave resulting from an incident shock wave propagating at 11 km/sec into quiescent nitrogen at 10^{-3} cm of mercury. The numerical solution was started at a time corresponding to 0.1 μsec after shock reflection with a constant property flow field equivalent to that behind the reflected shock front. Even at this short time, the ratio of translational shock thickness, based upon three to four mean free path lengths, to flow field length was 3×10^{-2}. The immediate post-shock conditions were determined assuming that the atoms and molecules were in local equilibrium but that the electron and ion mass fractions were frozen at their values in the incident shock zone. The incident region was considered to be in complete equilibrium and precursor effects were ignored. The starting time was chosen as being the shortest possible time compatible with a reasonable step size. Due to numerical stability requirements, shorter times would have required step sizes which would have resulted in excessively long computational times.

For this calculation the following set of chemical reaction rate constants has been used. The rates for the nitrogen dissociation reactions, Equations (129a-c), are those given by Marrone.[22] The forward rate for the atom-electron ionization process corresponds to the one

Reaction	Rate	
$N_2 + N_2 \rightleftharpoons 2N + N_2$	$k_b = 1.5 \times 10^{20} T_N^{-1.5}$	(129a)
$N_2 + N \rightleftharpoons 2N + N$	$k_b = 7.5 \times 10^{20} T_N^{-1.5}$	(129b)
$N_2 + M \rightleftharpoons 2N + M$	$k_b = 1 \times 10^{19} T_N^{-1.5}$	(129c)
$N + N^+ \rightleftharpoons 2N^+ + e$	$k_f = 2.34 \times 10^{11} T_N^{1/2} e^{-120000/T_N}$	(129d)
$N + e \rightleftharpoons N^+ + 2e$	$k_f = 4.16 \times 10^{13} T_e^{1/2} \left[1 + \frac{T_e}{60000}\right] \cdot e^{-120000/T_e}$	(129e)
$N + N \rightleftharpoons N^+ + e^- + N$	$k_f = 2.34 \times 10^{11} T_N^{1/2} e^{-120000/T_N}$	(129f)

experimentally obtained by AVCO.[24] Unfortunately, very little information exists as to the rates appropriate for reactions (129d) and (129f). Therefore, expressions corresponding to ten percent of the collision theory value have been selected. These should serve as an upper limit because actual rates seldom exceed ten percent of the collision theory value.[24]

B. Flow Field Properties

Figure 6 presents electron and heavy particle

temperature profiles for the reflected shock region. While the flow field was actually computed at each 5.7×10^{-4} μsec interval, the quarter microsecond intervals presented give a good indication of the thermal phenomena present. Initially the heavy particle temperature is at 75,000°K while that of the electrons is at 9300°K. However, collisions between the electrons and the heavy particles cause the electron temperature to increase rapidly, and by 0.25 μsec the electron temperature over a large part of the flow field has stabilized at about 19,500°K. This stabilization or pseudo-equilibrium of the electron temperature is caused by a balance between collision effects, which tend to increase the electron temperature, and ionization effects, which tend to decrease it. As a consequence of this quite high electron temperature, the gas radiates strongly with the result that the heavy body temperature has cooled to almost 30,000°K. In fact this decrease is mostly due to radiation cooling since at 0.25 μsec the dominating term in the overall energy equation is the radiation term. At this short time the ionization effects, while significant, are still small in comparison to the radiation effects.

By 0.50 μsec the temperature profiles begin to have shapes which are characteristic of flows in thermal non-equilibrium. The heavy body temperature behind the shock

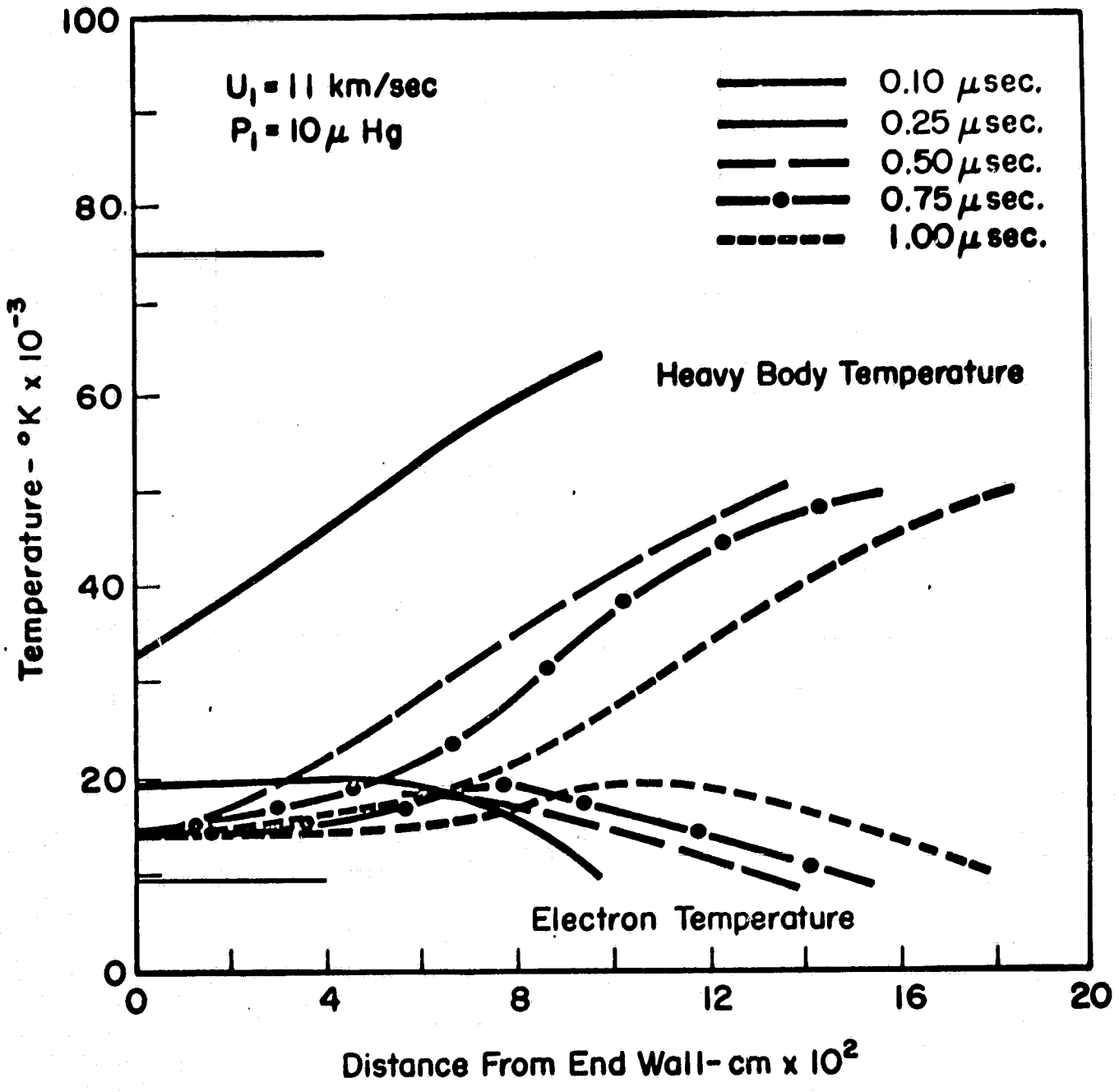

Fig. 6.--Electron and Heavy Particle Temperature Profiles Behind a Reflected Shock Wave in Nitrogen

front has decreased, due to shock wave attenuation, to about 49,000°K; and at the wall the gas has cooled to about 14,000°K. The electron temperature still increases from its value behind the shock wave to about 19,500°K and then gradually decreases towards the wall. As before this initial rise is due to collisions tending to equilibrate the heavy body and electron temperatures. About midway between the wall and the shock front the heavy particles have cooled sufficiently so that with respect to electron energy ionization predominates over elastic collision effects. The result is that the electron temperature remains lower than the heavy particle temperature throughout the entire flow field.

A similar analysis and explanation applies to the profiles at 0.75 μsec and 1.00 μsec except that more of the flow field is characterized by temperatures below 20,000°K with each increase in time. Nevertheless, even at 1.00 μsec the major portion of the flow field is still characterized by a large degree of thermal nonequilibrium. This feature can be described best by defining a degree of thermal nonequilibrium parameter χ_T as

$$\chi_T = \left| \frac{T_H - T_e}{T_H} \right| \times 100 \qquad (130)$$

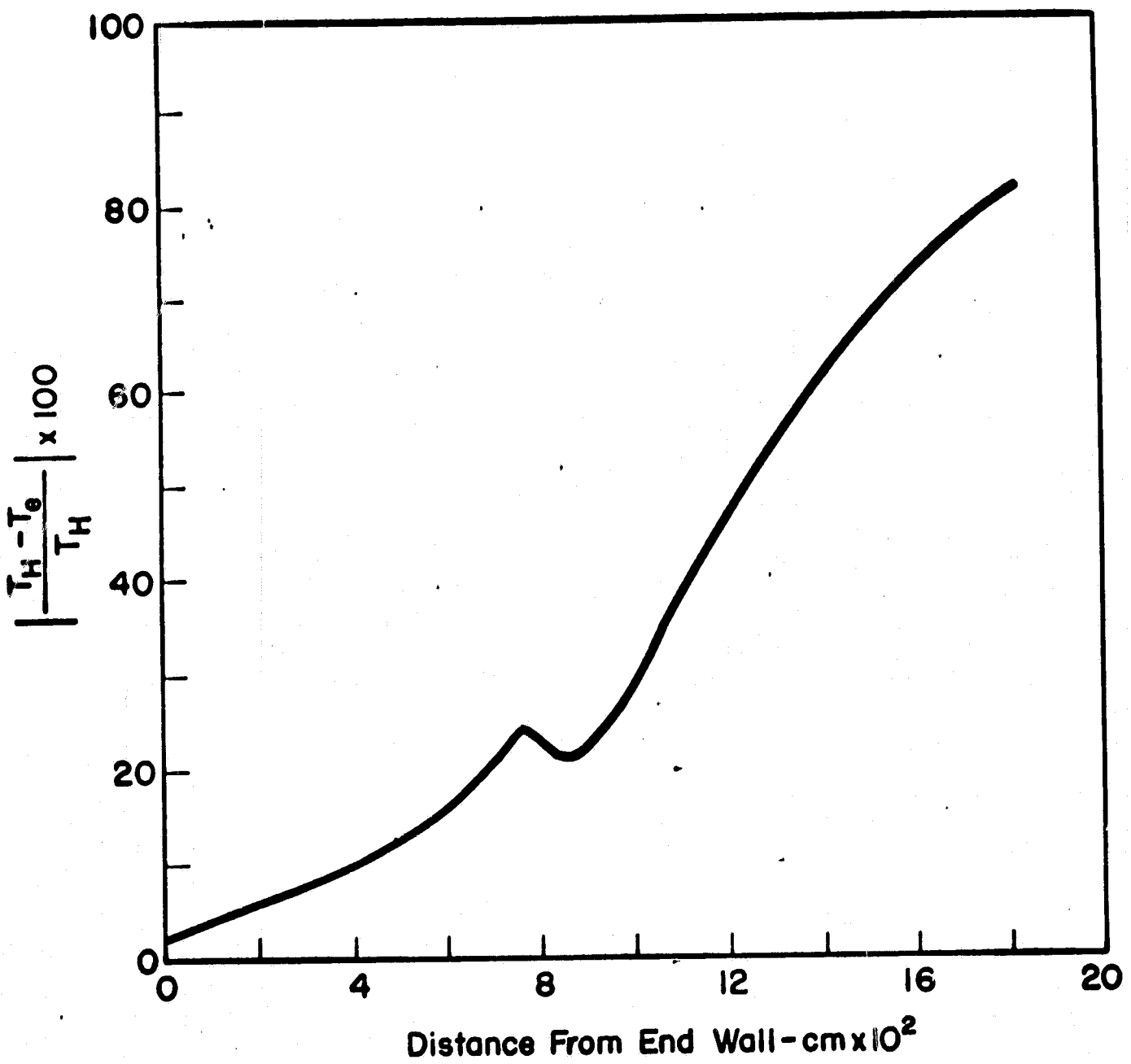

Fig. 7.--Degree of Thermal Nonequilibrium at 1.00 μsec After Reflection

Figure 7 shows this parameter plotted for a time after reflection of 1.00 μsec. As would be expected the degree of thermal nonequilibrium is greatest immediately behind the shock front and then decreases to its lowest value at the wall. The inflection which occurs at about 0.9 mm from the wall is due to the electron temperature being near its maximum value while the heavy particle temperature is rapidly decreasing. Now if it is assumed that significant nonequilibrium exists when χ_T is greater than ten percent, then clearly at 1.00 μsec over two-thirds of the flow field is still characterized by extensive thermal nonequilibrium.

As discussed in Chapter I, in a previous analysis[3] of the reflected shock region it was assumed that the flow could be approximated as being in chemical and thermal equilibrium at a time of 1.00 μsec. While the latter assumption might be valid when the initial pressure is greater than or equal to 0.10 cm of mercury, it obviously is not applicable to the conditions represented by the present calculation.

Some idea of the chemical phenomena occurring in the flow can be obtained by examining the species density profiles as a function of time. Figure 8 shows electron density curves, again at quarter-microsecond intervals. Each profile exhibits the same features in that there

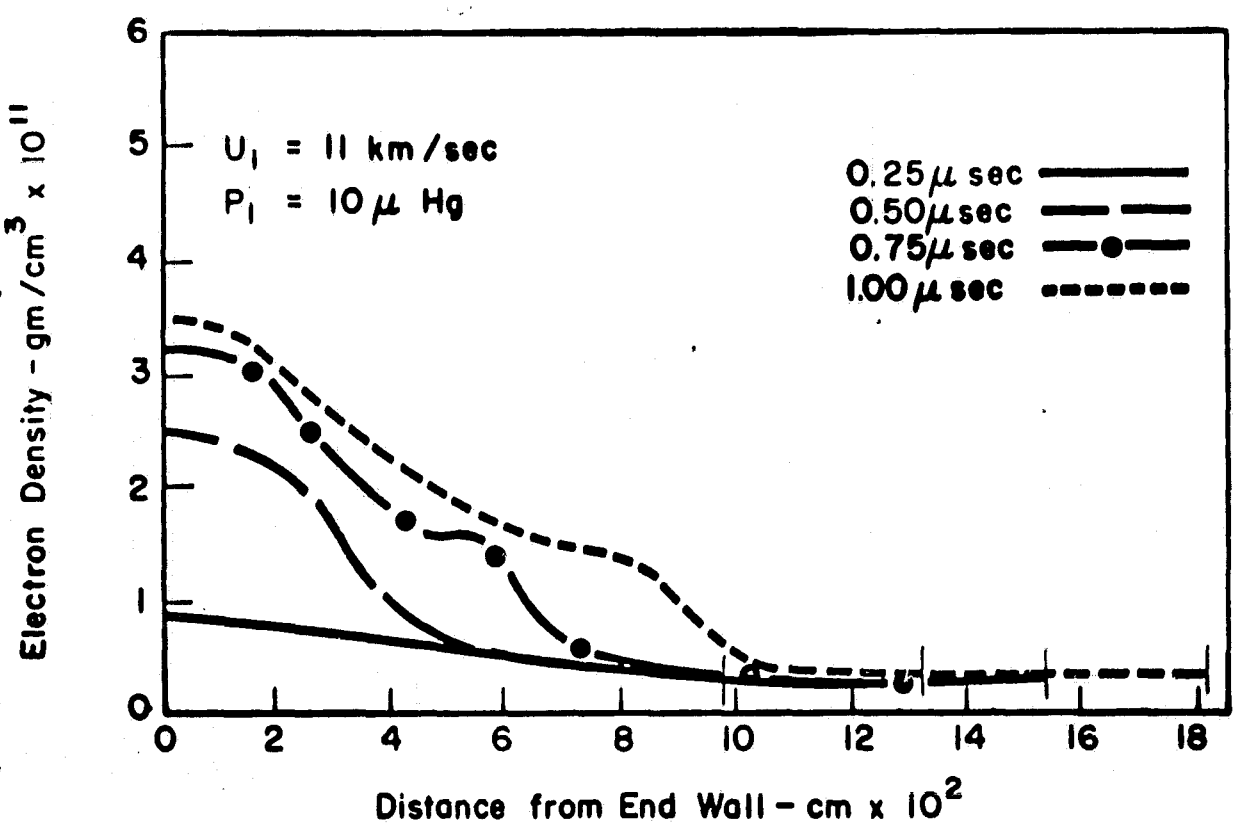

Fig. 8.--Electron Density Profiles Behind a Reflected Shook Wave in Nitrogen

exists a region behind the shock front of relatively constant density followed by an increase to the wall value. It is believed that this complex variation in the electron density is due to an interaction between the increase caused by chemical production and the effects due to the velocity induced in the flow.

Since nonequilibrium exists, the flow velocity between the shock wave and the wall is not necessarily zero. In fact, Figure 9 shows that behind the shock front there is a velocity towards the wall of about 2.5 km/sec, which subsequently increases and then decreases as the wall is approached. This velocity variation creates a build-up of particles and partially accounts for the initial rise in the electron density.

It should be noted that for the conditions of this calculation the mixture velocity given in Figure 9 is equal to the species velocity. The coincidence of these two velocities results from two effects. First the temperature is sufficiently high and the density sufficiently low that from a computational standpoint no nitrogen molecules exist. Second, no diffusion of the species occurs. Thus, the mixture velocity is the actual species velocity of the atoms, ions, and electrons.

Several other interesting features are exhibited in Figure 9. One of these is, of course, the fact that the

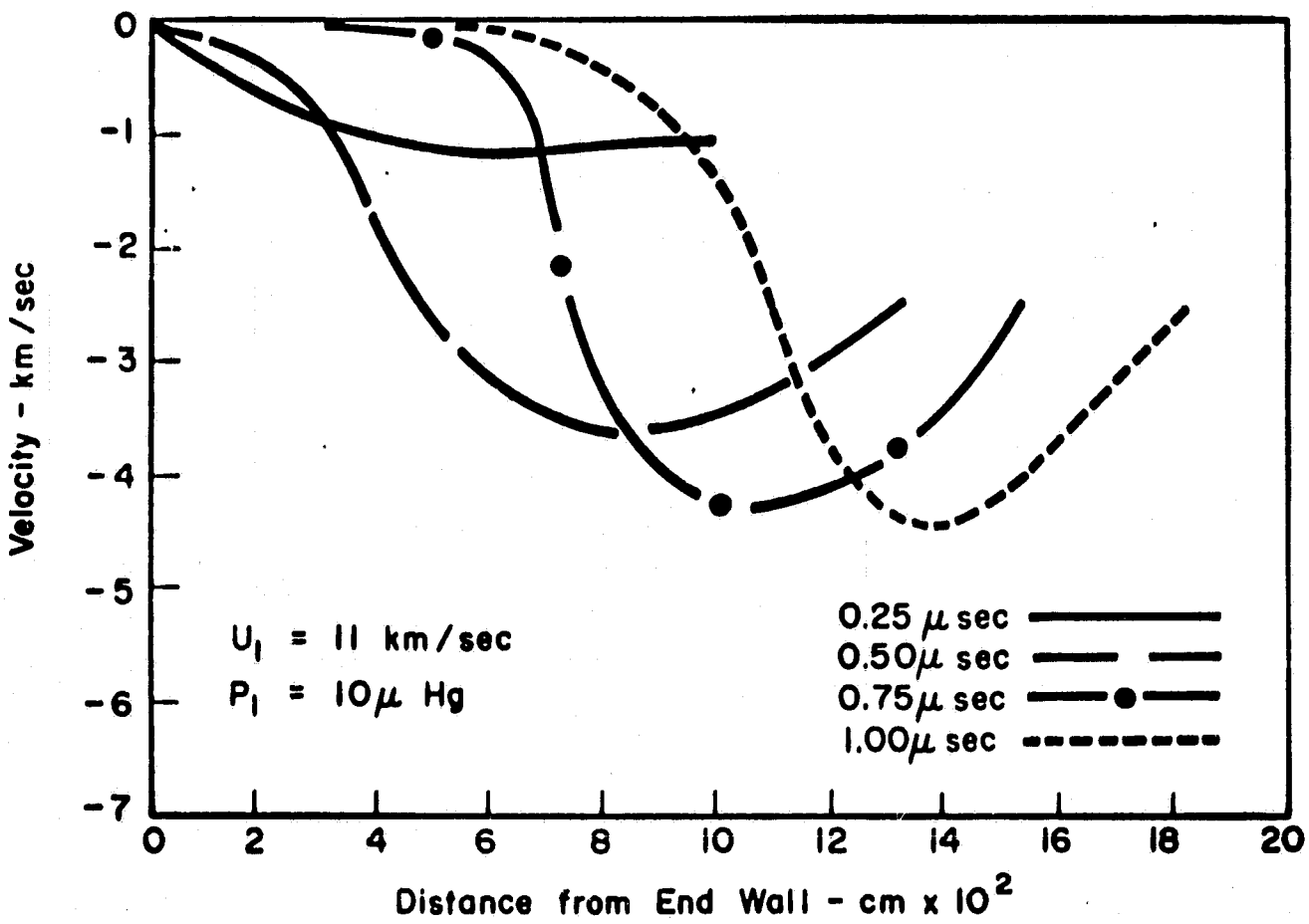

Fig. 9.--Velocity Profiles Behind a Reflected Shock Wave in Nitrogen

magnitude of the velocity increases from its value behind the shock before beginning its decrease to the wall value. This initial acceleration results because in the immediate post-shock region cooling occurs sufficiently rapidly and without a corresponding density increase so that there is an initial pressure decrease. As can be seen from the momentum equation the velocity is very sensitive to any pressure gradient, and such a pressure decrease creates an acceleration towards the wall.

The density distributions of atomic nitrogen are shown in Figure 10. Except for the 0.25 μsec curve they are all very similar. Each profile has a minimum value in the region behind the shock front followed by an increase toward the wall. In contrast to the electron density profiles, however, the increase is more abrupt and is followed by a relatively constant value. Also, the decrease due to the velocity in the region immediately behind the shock front is more evident than in the electron density case.

Further understanding of the chemical nonequilibrium phenomena can be obtained by comparison of the chemical production rates of electrons. Figure 11 presents such a comparison for a time of 0.20 μsec. The three curves shown indicate the rate at which electrons are being produced due to each of the three ionization reactions

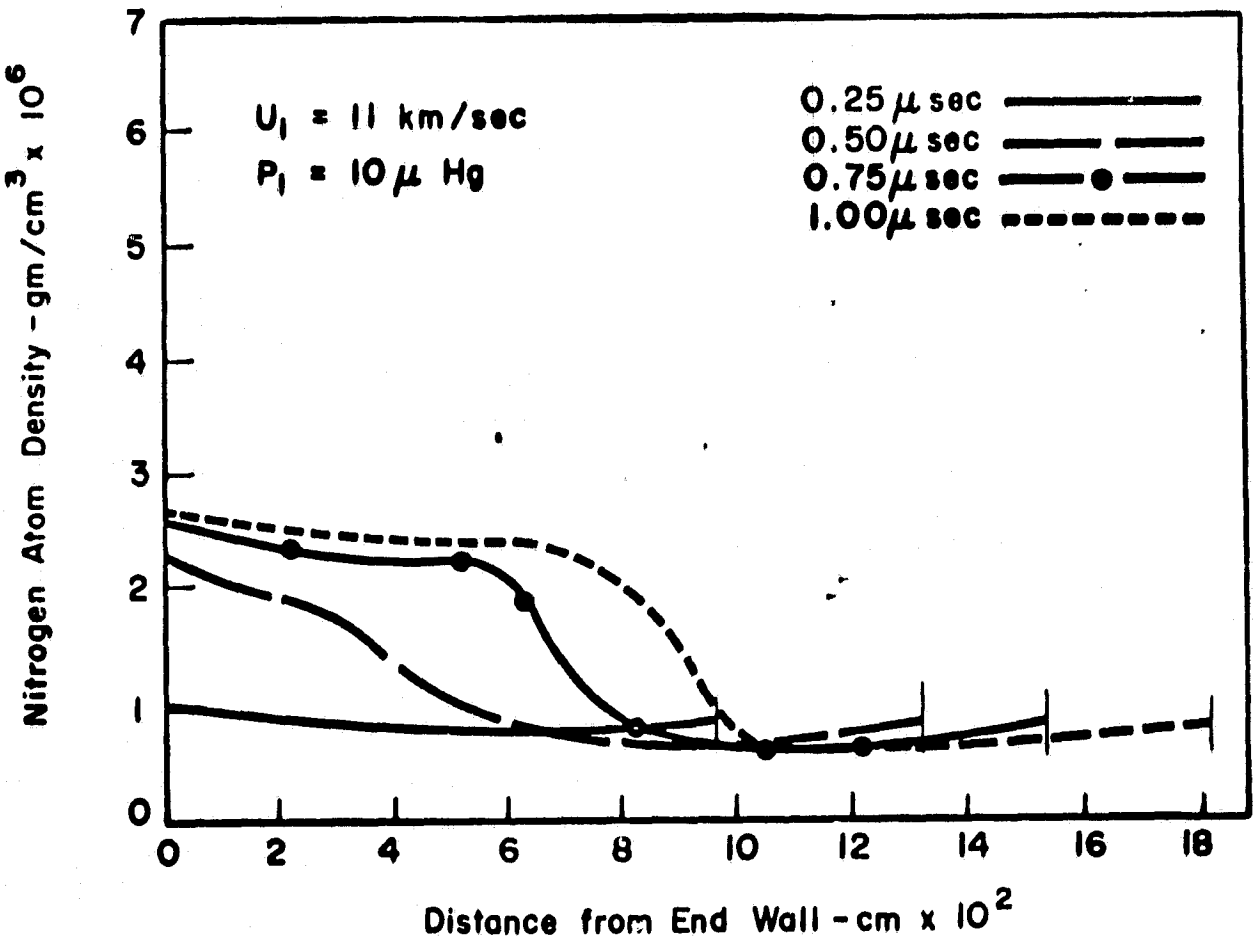

Fig. 10.--Nitrogen Atom Density Profiles Behind a Reflected Shock Wave in Nitrogen

considered -- i.e. atom-ion collisions, atom-atom collisions, and atom-electron collisions. The dominating reaction near the shock fron is unquestionably that resulting from atom-atom collisions. However, in the region near the wall where the concentration of electrons is higher, the electron-atom reaction production rate increases significantly, indicating that it is very sensitive to the number of electrons present. This domination of the atom-atom reaction in the region immediately behind the shock and of the electron-atom reaction becoming more significant in the cooler downstream regions has been predicted and observed in argon.[8,17] The present results indicate that similar behavior can be expected for ionizing nitrogen. Moreover, the explanation is relatively simple. The electron-atom ionization rate is extremely rapid if sufficient number of electrons exist. However, in the immediate post-shock region very few electrons exist with the result that initial production is due to atom-atom collisions. As soon as sufficient electrons have been produced the electron-atom rate becomes effective and soon starts to dominate the entire chemistry. This is shown more clearly in Figure 12.

Figure 12 presents the same basic information as Figure 11 but for a time of 1.00 μsec after reflection. Again the atom-atom reaction is predominant behind the

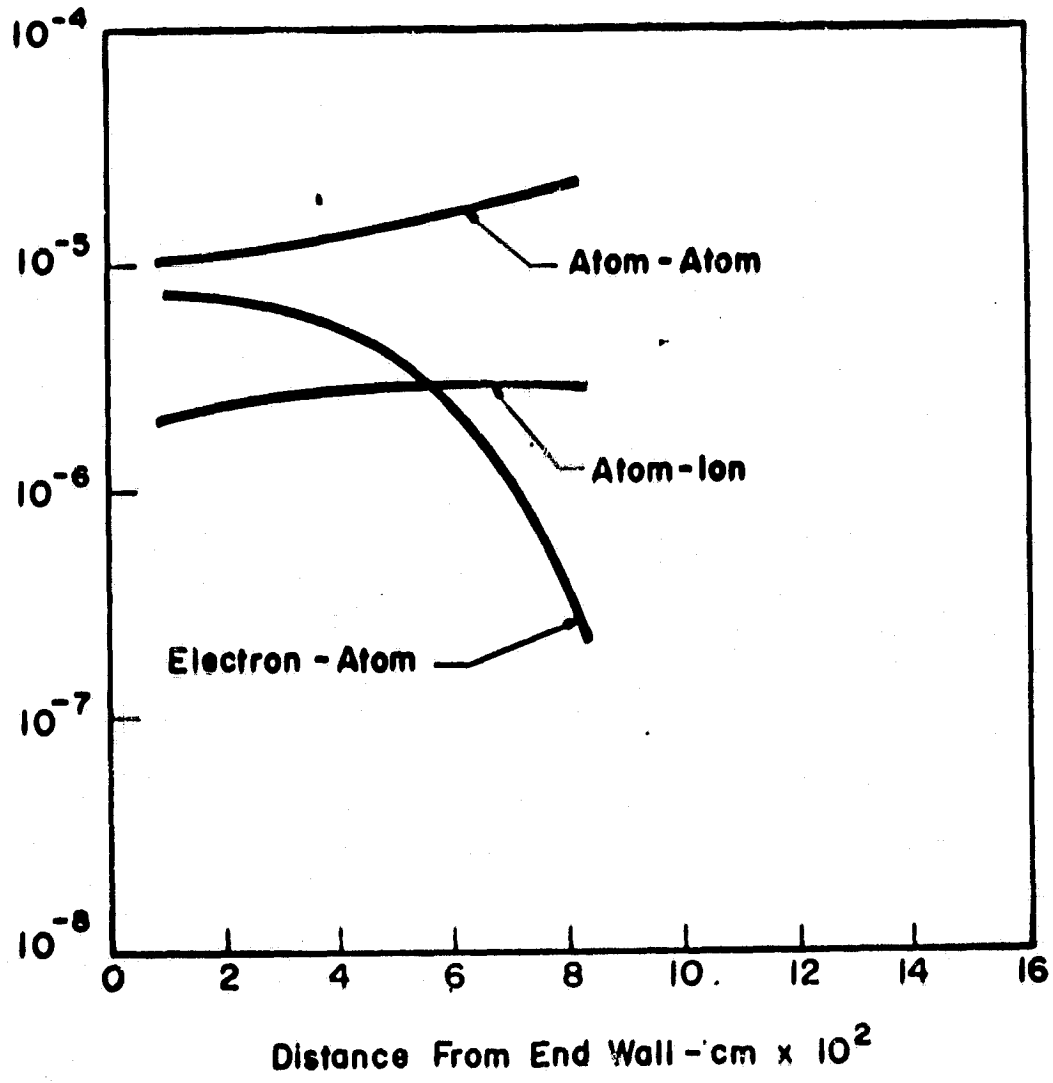

Fig. 11.--Comparison of Electron Production Rates at 0.20 Microseconds

shock front, and the electron-atom reaction predominates near the wall. Between the shock and the wall, however, the production rates oscillate. From Equations (63) and (64) the atom-atom and atom-ion electron production rates are dependent not only upon the concentrations of the colliding partners but also upon the electron and heavy particle temperatures. Since in the region immediately behind the shock the concentrations are relatively constant and the heavy body temperature is decreasing rapidly, a decrease in the atom-atom and atom-ion production rates would be expected. Between 0.08 and 0.10 cm (see Figures 9 and 10), however, a large increase in the concentrations occurs with the result that the atom-atom and atom-ion production rates sharply increase. They subsequently decrease again with the continued cooling of both the electron and heavy body temperatures and the overall approach of the flow towards chemical equilibrium.

Now Equation (64) shows that the only temperature affecting the production of electrons due to atom-electron collisions is the electron temperature. Thus in the immediate post-shock region the initial increase in the electron temperature causes the indicated rise in the electron-atom rate. The sharp increase near 0.10 cm is due to the rapid changes in the electron and atom concentrations. After the peak the rate tends to decrease, but at a pace slower than

the other two. This difference is probably due to the fact that the electron density is still increasing in this region while the electron temperature is decreasing slowly.

Another interesting feature becomes apparent from examining both Figures 11 and 12, and that is that nowhere is the atom-ion electron production rate ever significant. Thus future calculations might be simplified by ignoring the atom-ion chemical reaction completely.

One of the secondary purposes of this investigation was to determine whether or not a constant property equilibrium starting solution applied at a time of one microsecond would in general be valid. The equilibrium approximation assumes that the reflected shock wave always propagates at its equilibrium speed; and thus, for the present conditions this assumption would place the shock at 0.12 cm from the wall at 1.00 μsec after reflection. Examination of Figure 12 indicates that even in this limited region considerable nonequilibrium exists. Hence, the results of the present calculation indicate that at least for short times after reflection the equilibrium approximation is not generally valid.

However, for times on the order of ten microseconds the situation may be different. By that time the nonequilibrium region behind the shock constitutes only a small portion of the entire flow field. Furthermore, while the

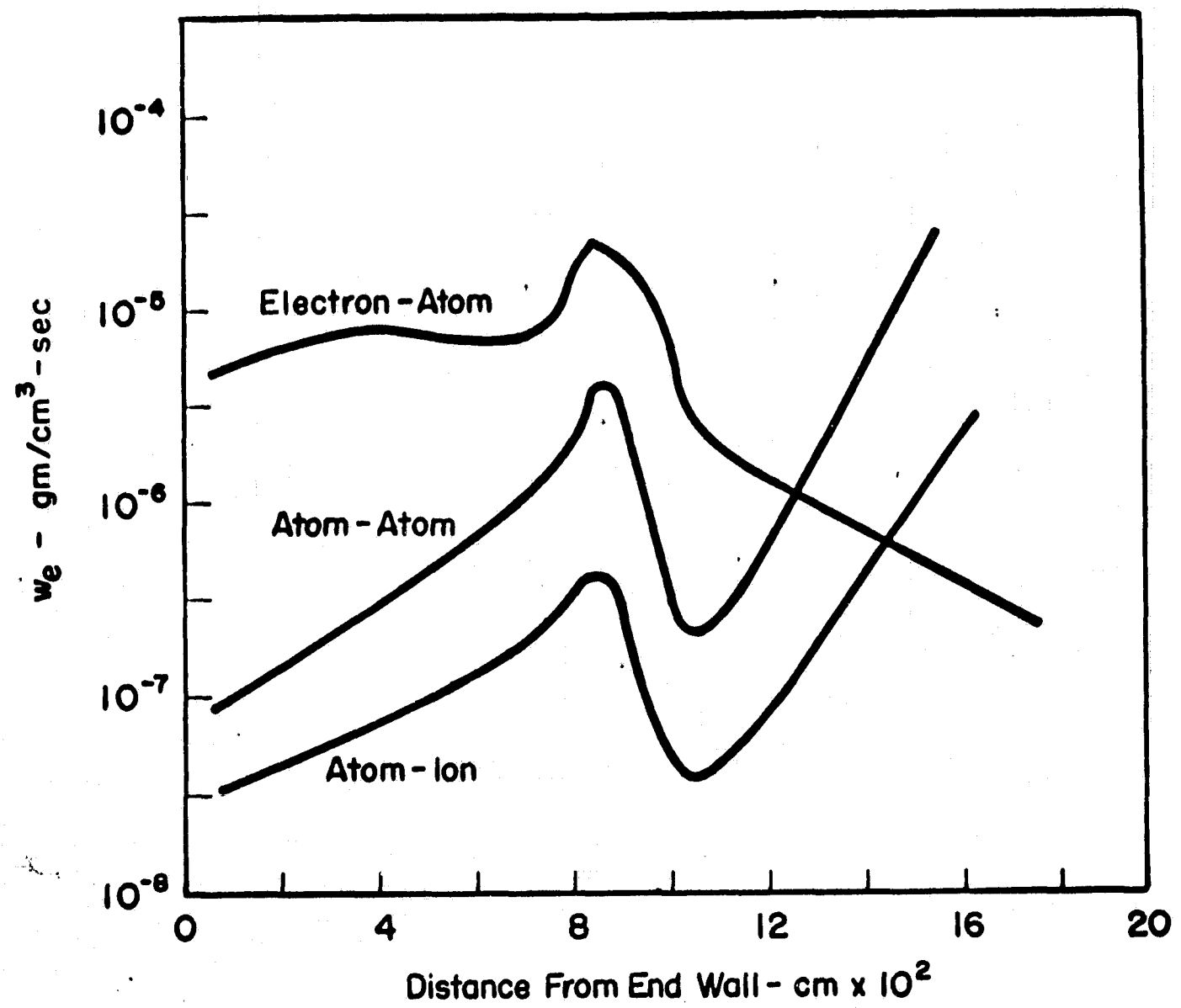

Fig. 12.--Comparison of Electron Production Rates at 1.00 Microseconds

reflected shock speed is initially higher than the equilibrium speed, its final steady state value is lower.[6] Thus, it might be possible that the length of the radiating region would be approximately the same for both the equilibrium and nonequilibrium calculations and that radiative transfer and flow field results would be equivalent. Thus, while the equilibrium approach is questionable at short times, it may be a valid approach for obtaining information at long times.

C. End-Wall Properties

R. K. Hanson[32] at Stanford University has made calculations concerning the variation in end-wall properties after the reflection of a shock wave. While he was primarily interested in developing theoretical techniques combined with experimental methods for determining various chemical reaction rates, his results indicate that end-wall properties can give at least qualitative information concerning the relaxation processes. Later he and Presley[6] carried out extensive calculations of the flow field and end-wall properties behind a reflected shock wave resulting from a 3 km/sec incident shock.

The present calculation has also yielded the variation of end-wall properties, and a portion of these results are presented in Figures 13 thru 16. It should be pointed out that the term wall property is used here to denote the

value of a given property exterior to the end-wall boundary layer. Figure 13 shows both the values of electron and heavy particle temperatures at the wall as a function of time. As would be expected the heavy body temperature initially decreases very rapidly and is accompanied by a rise in the electron temperature. At about 0.25 μ sec, however, the electron temperature peaks and begins to decrease. This turnaround is indicative of the increasing importance with time of electron-atom reactions, which tend to decrease the electron temperature. Between 0.35 and 0.45 μ sec the electron temperature slightly overshoots the heavy particle temperature. After this time the two temperatures are essentially the same with the electron temperature being slightly lower. Also both wall temperatures appear to be decreasing, although at a slow rate, towards some final equilibrium temperature. This temperature will be lower than the ideal value of 14,000°K due to the loss of energy by radiation.

In Figure 14, the change of the ion mass fraction at the wall is plotted. This curve is characterized by a rapid increase until about 0.40 μ sec. After that there exists a short duration plateau in $(\rho_I/\rho)_w$ followed by a gentle increase. This latter effect is the characteristic asymptotic approach to the equilibrium value.

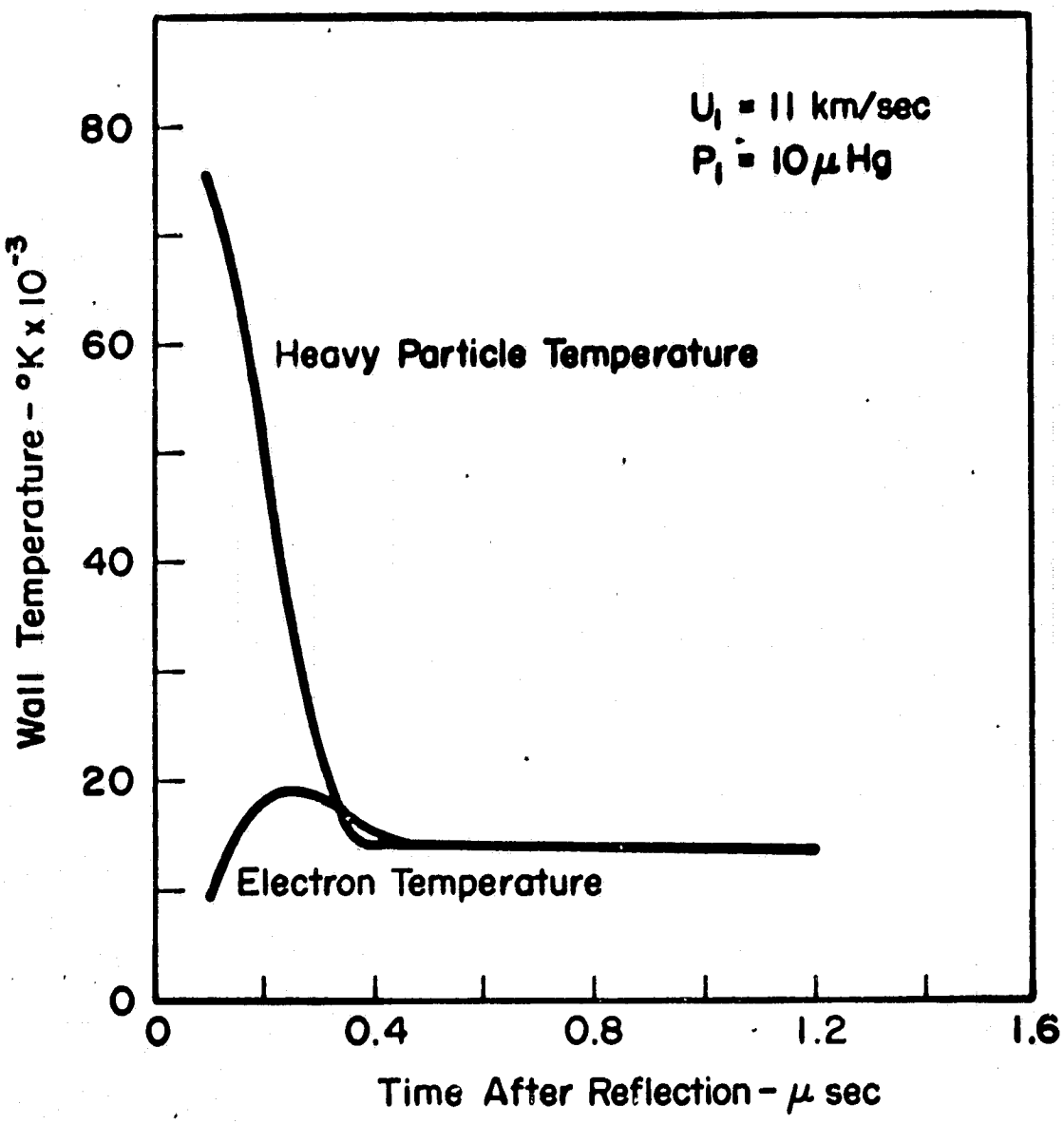

Fig. 13.--Electron and Heavy Particle Temperature at the Wall as a Function of Time After Reflection

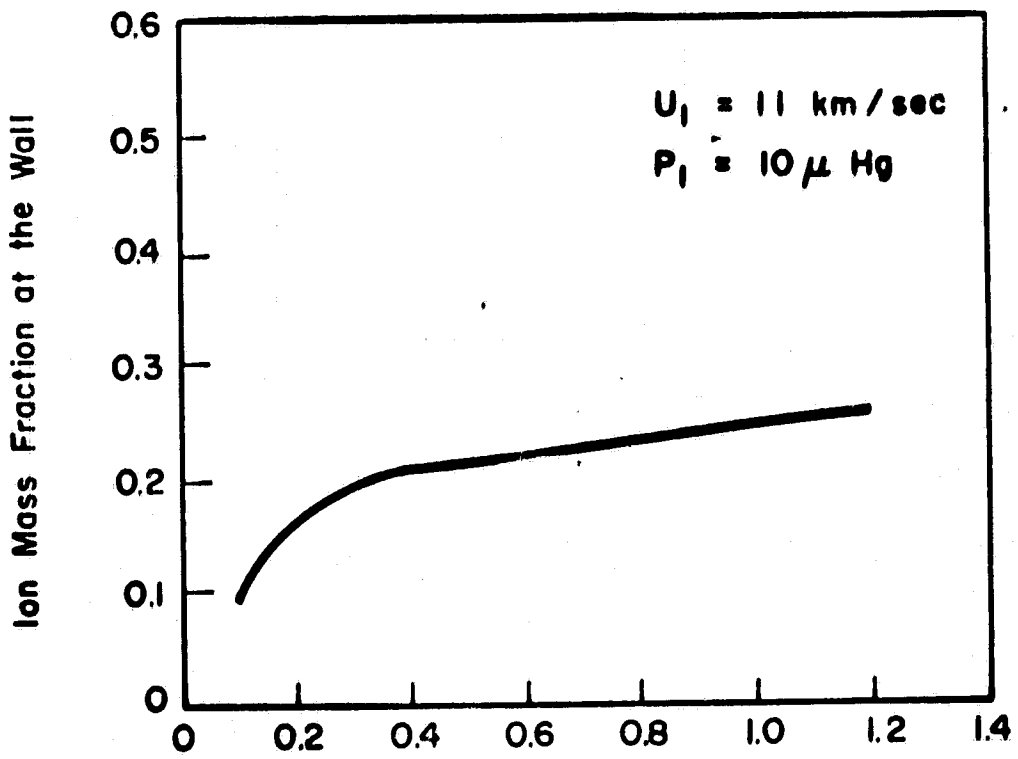

Fig. 14.--Variation of the Ion Mass Fraction at the Wall as a Function of Time After Reflection

The variation in end-wall pressure is presented in Figure 15, and in many ways it is the most interesting. From its initially relatively high value corresponding to frozen flow conditions, the end-wall pressure decreases to a minimum value at about 0.35 μsec and then increases. At about 0.70 μsec it attains a value which remains relatively constant for the rest of the calculation and which is almost identical to the ideal equilibrium value of 3.6×10^5 dynes/cm^2. This decrease followed by an increase to fairly steady value at first appears quite startling. However, some type of decrease is required because the initial post-shock pressure is higher than the corresponding equilibrium pressure. Furthermore this type of initial decrease has even been predicted for flows in which the initial pressure was lower than the equilibrium pressure.[6] This phenomena probably results from the fact that the initial rapid cooling is not immediately accompanied by a corresponding increase in density.

The end-wall density is presented in Figure 16. In this case, the curve exhibits a steady increase in value until about 0.70 μsec. After this time the value of the wall density remains relatively constant.

Examination of Figures 13-16 reveals that there appears to exist two characteristic times for the relaxation process. The wall temperature and ion mass fraction

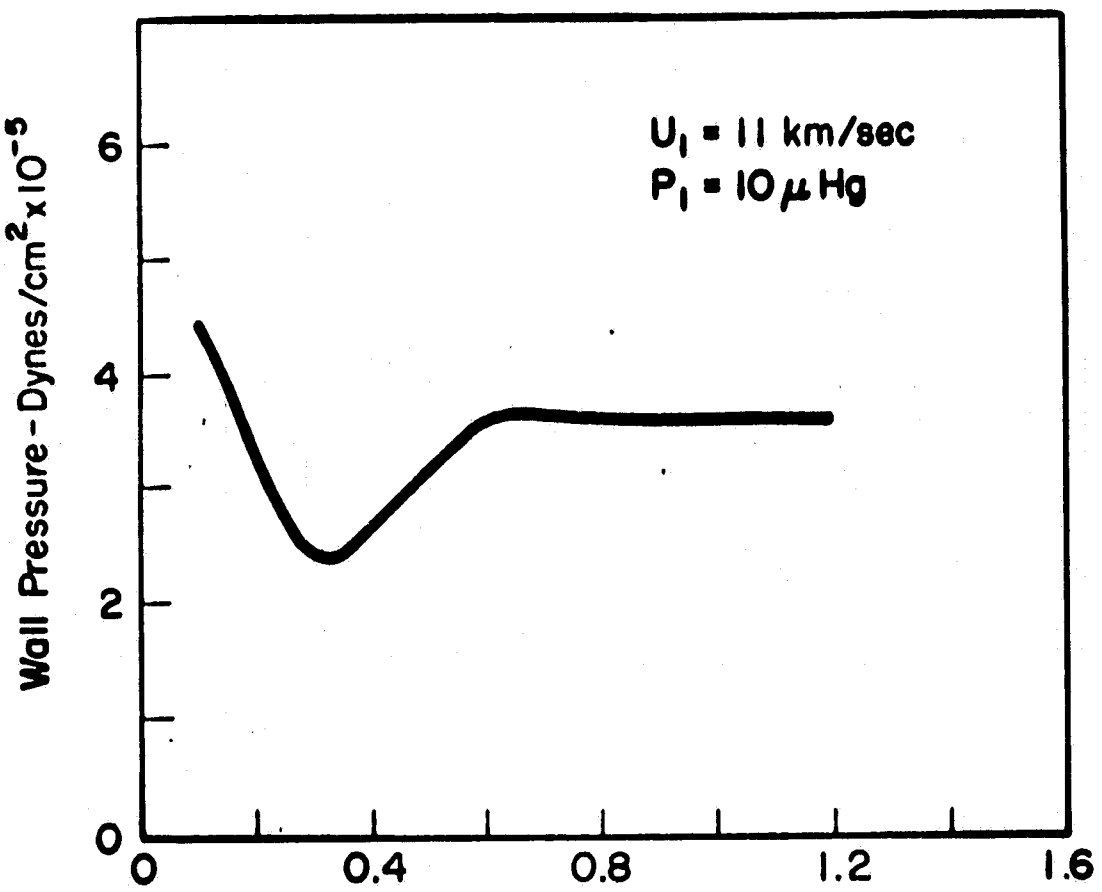

Fig. 15.--Variation in End-Wall Pressure as a Function of Time After Reflection

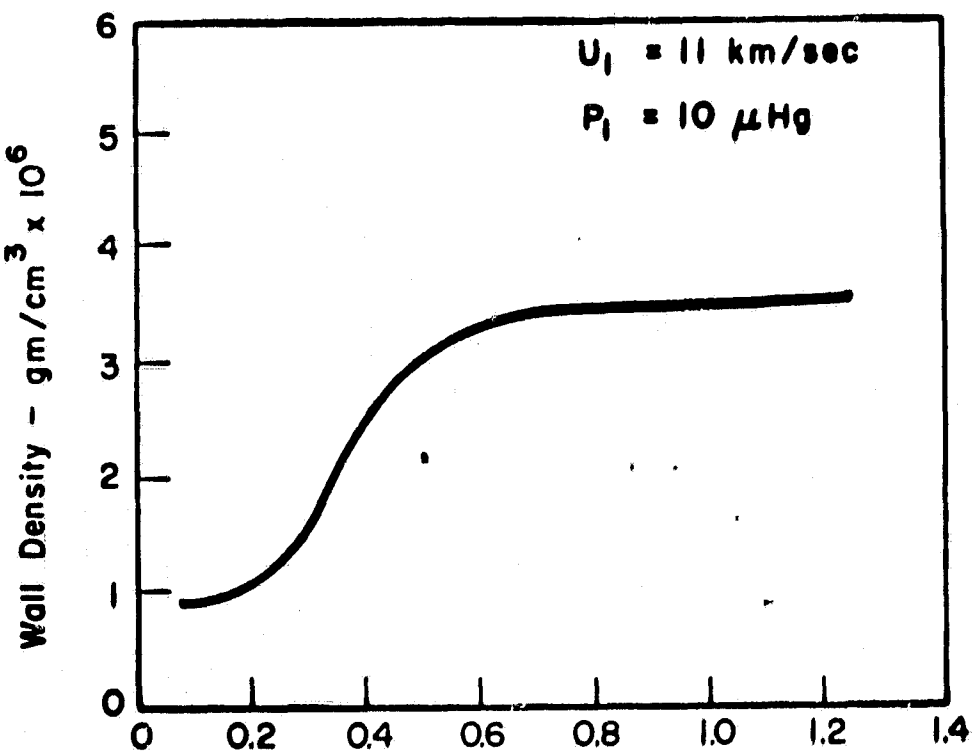

Fig. 16.--Variation in the Density at the Wall as a Function of Time After Reflection

curves indicate that the time required to reach a pseudo-steady state is about 0.45 μsec. On the other hand, the wall pressure and density solutions show a longer characteristic time that is on the order of 0.70 μsec. Presley and Hanson[6] also observed two characteristic times in their calculations for dissociating oxygen. They reasoned that since temperature and mass fraction are sensitive to chemical state, the characteristic time associated with them should be related to the chemical relaxation behind the reflected shock wave. They further asserted that since pressure and density are indicative of fluid dynamic phenomena, their characteristic time should be controlled by the chemical relaxation behind the incident shock wave. Since their analysis included nonequilibrium behind both shock waves, this seemed like a plausible explanation.

In the present set of calculations, however, the region behind the incident shock wave is assumed to be in complete equilibrium. Therefore, the existence of the second characteristic time cannot be attributed to incident shock relaxation. Instead it is felt that the two times in the present study are indicative of thermal relaxation and chemical relaxation respectively. The fact that the first time, 0.45 μ sec, is characteristic of thermal relaxation is apparent from Figure 13 because after that time the electron and heavy particle temperatures are essentially

the same.

Now in nonequilibrium steady state solutions of normal shock waves the pressure usually increases due to chemical relaxation. In Figure 15 the pressure initially decreases due to the cooling of the heavy particles by radiation and elastic collision interaction. After a short period of time chemical nonequilibrium effects do become important, and thus the increase in pressure after 0.30 μsec is probably due to chemical effects. This interpretation is further substantiated by Figure 16 which shows that the wall density increases sharply after 0.30 μsec. Such a density increase is usually representative of a chemical relaxation zone. Hence, it is concluded that for the present results the characteristic time required for end-wall pressure and density to reach steady values is indicative of the time required for chemical relaxation in the reflected shock region.

Furthermore, the trends evident in this calculation combined with those of Presley and Hanson[6] suggest that if thermal and chemical nonequilibrium behind a reflected shock wave were considered in conjunction with chemical nonequilibrium behind the incident wave, then end-wall properties could exhibit three characteristic times. One would represent thermal equilibration, a second would be characteristic of chemical relaxation behind the reflected

shock, and the third would be associated with chemical nonequilibrium effects behind the incident wave. Of course, until actual calculations are carried out the existence of three such times is only speculation, but it does represent an interesting area for further investigation.

D. Shock Trajectory

According to ideal constant property theory a reflected shock wave moves away from the end-wall at constant velocity. If, assuming complete equilibrium behind the incident shock wave, one considers the flow behind the reflected wave to be chemically frozen, then for the conditions of the present investigation a constant reflected shock speed of 4.163 km/sec results. On the other hand, if complete chemical and thermal equilibrium is assumed to exist in the reflected region, the Rankine-Hugoniot solution yields a reflected shock velocity of only 1.204 km/sec.

Since the present calculation assumes the flow to be initially chemically frozen, the nonequilibrium trajectory should at first correspond to the frozen case. Figure 17, which has plotted on it the frozen, equilibrium and nonequilibrium trajectories, shows this to be true. At about 0.20 μsec after reflection the effects of radiative cooling, collisional interaction, and ionization become

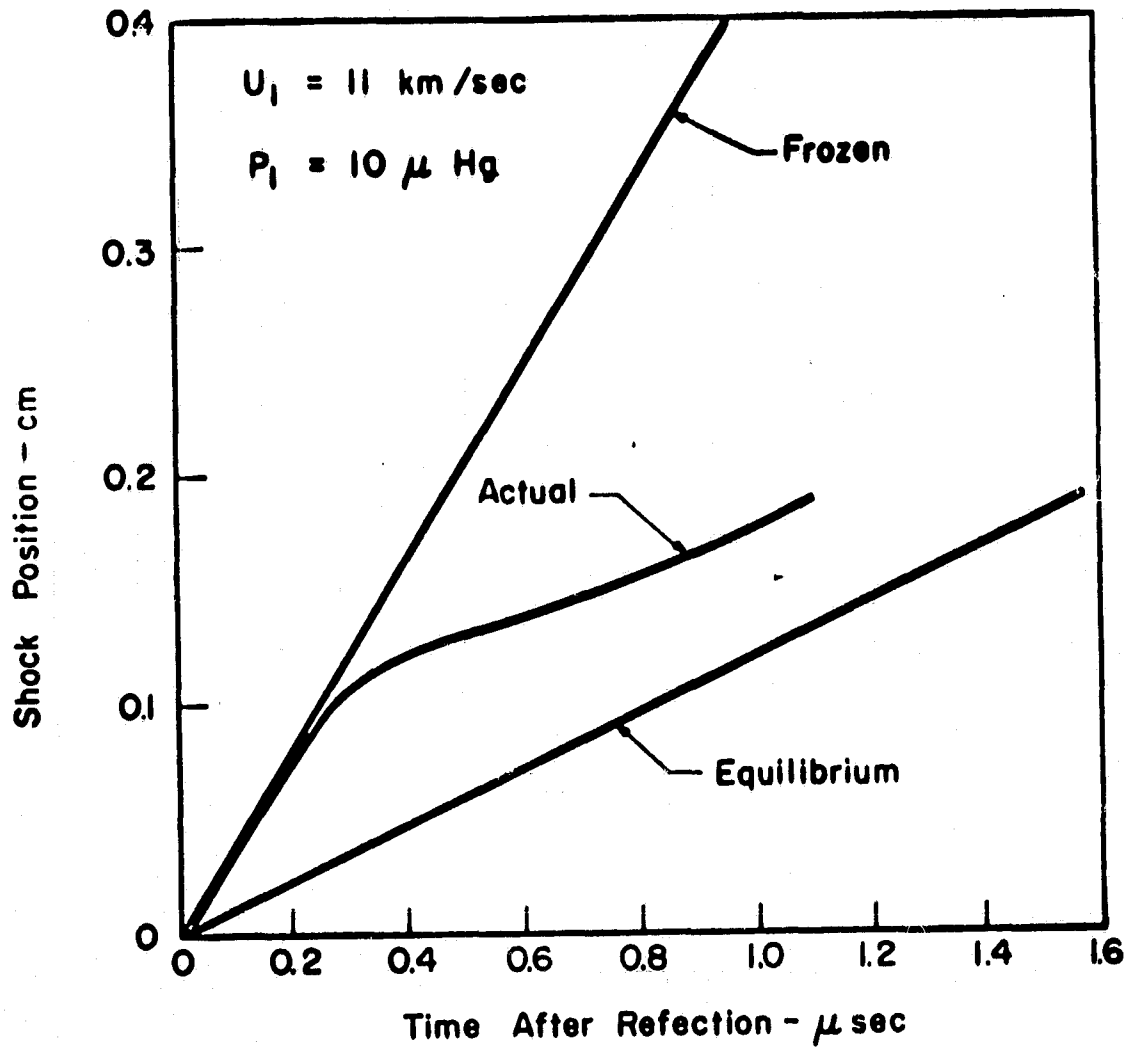

Fig. 17.--Position of Reflected Shock Wave as a Function of Time After Reflection

sufficiently strong so as to cause the density in the reflected shock region to increase. As a result, the shock velocity decreases and the trajectory deviates from the ideal frozen solution. By 0.70 μ sec, however, the shock velocity has essentially attained a steady value; and the position trajectory has approached a line parallel to the equilibrium solution. Eventually the effects of radiation cooling should cause the shock velocity to decrease even further,[5] but this effect is not exhibited in the present short time solution.

The most important point concerning the shock trajectory is obtained by comparing the actual shock position at one microsecond with that predicted by equilibrium theory. Since the slopes at that time are almost the same, the results indicate that an equilibrium solution could be started at that time using the equilibrium shock velocity. Nevertheless, the actual shock position should be located some forty-five percent further from the end-wall than predicted by equilibrium theory. Admittedly at times on the order of ten microseconds the difference in shock position resulting from the two calculations would be less than ten percent, but at small times the difference would be much greater. Thus, as in the discussion of the flow field properties, the shock trajectory results indicate that for the conditions of the present

calculations accurate short time results can be obtained only by explicitly considering nonequilibrium effects.

E. Radiative-Gasdynamic Coupling

In order to determine whether or not radiative-gasdynamic coupling effects exist at short times after reflection a calculation has been made including chemical and thermal nonequilibrium but without radiative cooling. Figure 18 compares the temperature profiles for this case with those for the radiation cooled case. Both sets of curves are for a time of 0.75 μ sec after reflection. One obvious difference between the two sets of results exists in the region near the wall. In the radiation cooled case, both the electron and heavy particle temperatures are characterized by temperatures below 20,000°K; but the non-cooled calculation exhibits heavy body temperatures greater than 25,000°K and electron temperatures around 22,000°K. Since the only difference in the two computations is the inclusion of radiative cooling, it can be deduced that radiative transfer has a very pronounced cooling effect.

Figure 18 also indicates that radiative cooling accelerates the relaxation processes. It was pointed out in the discussion of Figure 13 that at the wall thermal equilibration essentially exists for times longer than 0.45 μ sec. However, in the radiation uncoupled case the

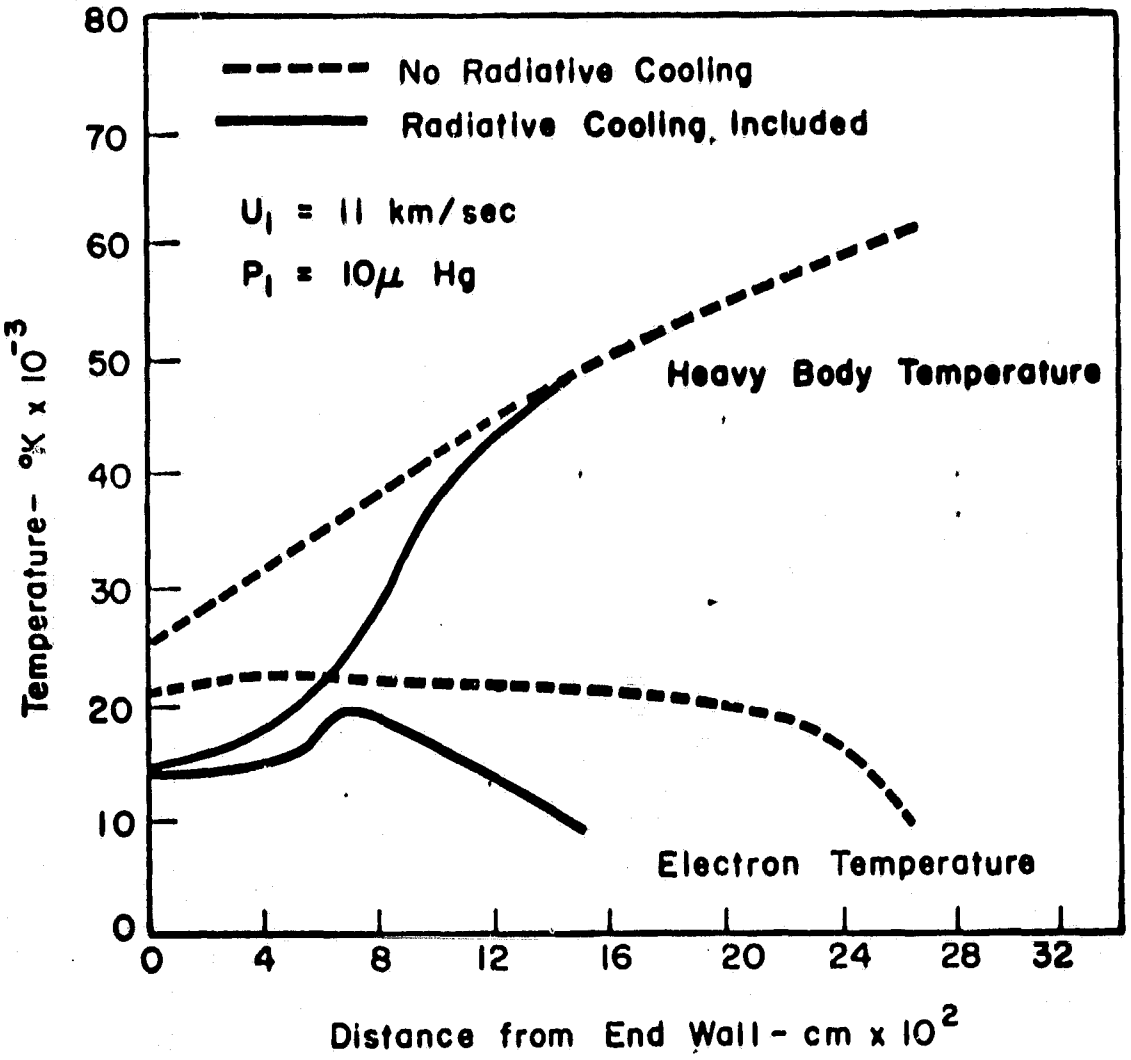

Fig. 18.--Comparison of Temperature Profiles at 0.75 μsec With and Without Radiative Cooling

heavy particle and electron temperatures at the wall are still over 4000°K apart at 0.75 μsec. Thus, it would appear that radiative cooling decreases the thermal relaxation time by better than a factor of two.

Furthermore, the radiation cooled results indicate that the final equilibrium temperature is around 14,000°K and that near the wall such a temperature is achieved approximately 0.70 μ sec after reflection. The uncoupled results show a temperature 10,000°K higher at 0.75 μ sec, again indicating that chemical and thermal relaxation are accelerated by radiative cooling. This acceleration partially occurs because the radiative loss term only appears in the overall energy equation. Thus, its inclusion serves to accelerate further the cooling of the heavy particles.

Additional evidence that radiative transfer affects the flow field can be obtained from Figure 18 by comparing the shock front position and immediate post-shock temperature resulting from each calculation. The fact that the shock front is almost twice as far from the end-wall in the uncooled case indicates that radiative cooling has a strong effect on the shock wave trajectory. Likewise, the existence of a considerably higher post-shock temperature in the uncoupled case indicates a higher reflected shock velocity, and thus, less shock wave attenuation.

The existence of extensive radiative gasdynamic coupling at short times after reflection is dramatically demonstrated in Figure 19, which compares the variation in end-wall pressure for the two cases. In the uncoupled case the wall pressure decreases slowly and steadily from its frozen value without the pronounced dip evident in the complete calculation. Obviously this rather marked decrease in pressure of almost a factor of two must be due entirely to the effects of radiation cooling. Since some investigators[32] have proposed using end-wall pressure measurements to determine chemical reaction rates, these comparisons are very important because they indicate that the prediction and interpretation of wall pressure results must include the effects of radiative transfer.

Now there does exist the possibility that if end-wall thermal conduction were included that the end-wall pressure behavior would be different. The initial effect of thermal conduction is to cause the shock wave to reflect at only one-half its ideal velocity, but as the shock moves away from the wall thermal conduction effects become less important and the shock velocity increases until the attenuative effects of radiation and chemistry become important.[33]

In order to ascertain whether or not this initial behavior could affect the results, a calculation has been

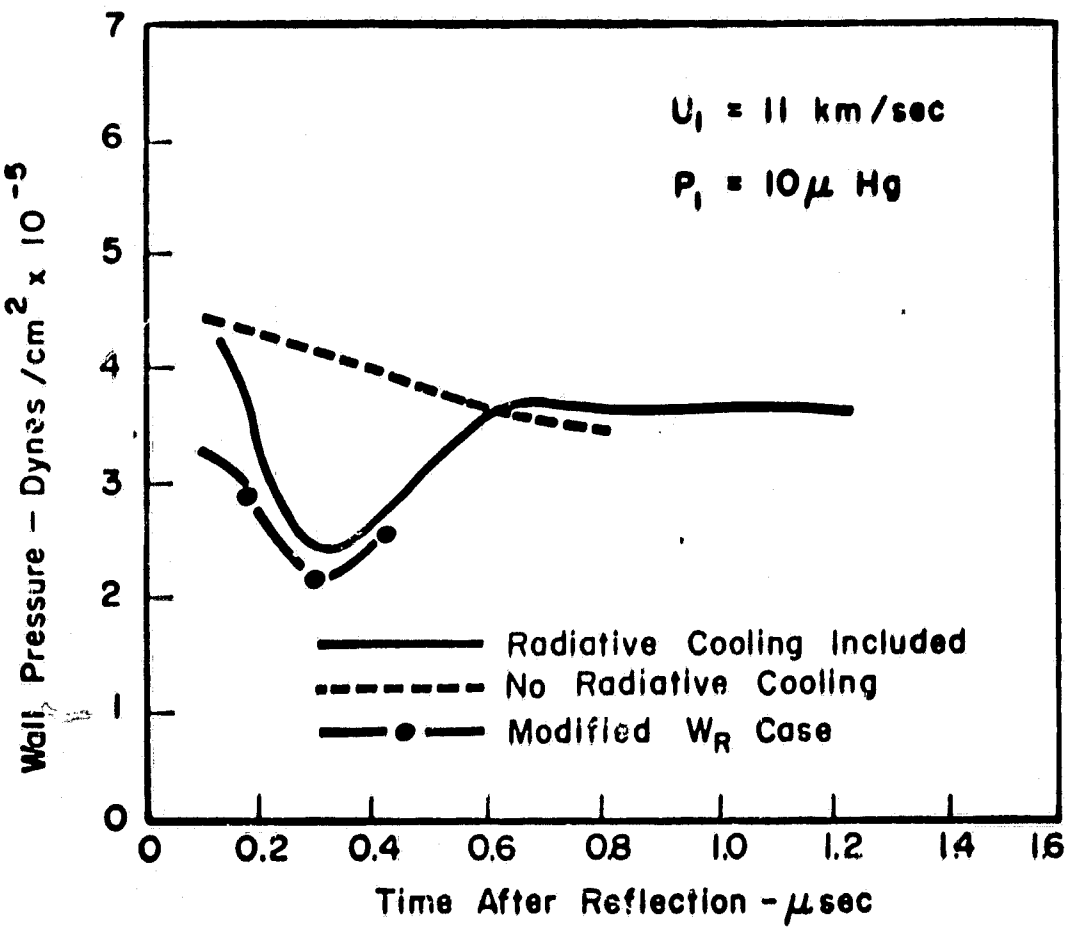

Fig. 19.--Comparison of the Variation of Wall Pressure With and Without Radiative Cooling

made with the initial reflected shock velocity one-half the ideal frozen value. For the 0.10 μsec starting time which was used, this velocity is conservative since the shock wave actually accelerates in that time. Thus, the results should show the maximum possible effect. The resulting end-wall pressure variation is shown on Figure 19, and it is almost identical to the radiative cooled case. Thus, in comparison to radiation cooling, shock velocity variations resulting from thermal conduction have only a small effect on the end-wall pressure behavior.

Finally, Figure 20 shows cooled and uncooled velocity profiles at 0.75 μsec. In the no radiative cooling case there is no evidence whatsoever of the velocity acceleration towards the wall that is so prevalent in the complete calculations. This velocity pattern, which results directly from the pressure variation, is an indirect manifestation of the radiative cooling effects that must be included in order to obtain valid results.

Thus, these results demonstrate that for the conditions of the present investigation radiative-gasdynamic coupling exists and is important in the reflected shock flow field for short times after reflection. They also show that if radiative cooling is ignored, completely erroneous trends may be obtained for the pressure and velocity variations.

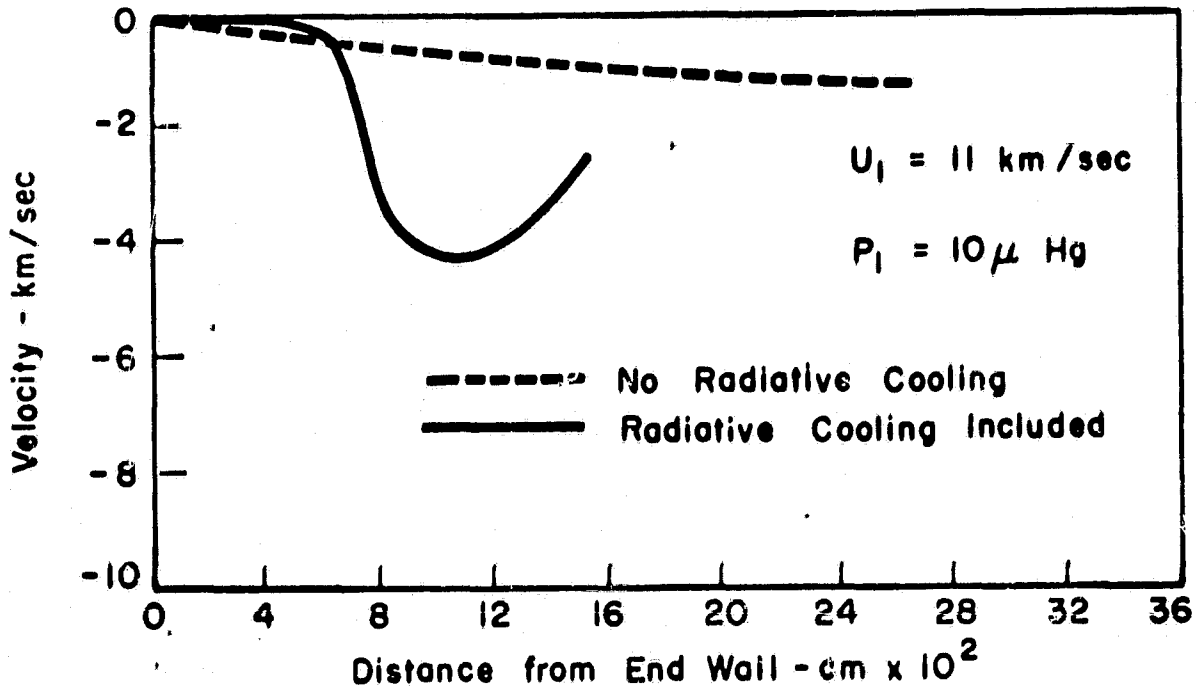

Fig. 20.--Comparison of Velocity Profiles at 0.75 μsec With and Without Radiative Cooling

F. End-Wall Radiative Heat Transfer

One of the major purposes of this investigation has been to examine the effects of chemical and thermal non-equilibrium upon the end-wall radiative heat transfer. The results corresponding to the 11 km/sec incident shock velocity and 10^{-3} cm of mercury initial pressure condition are shown on Figure 21. In this figure the heat transfer rate due to radiation from the visible continuum (1570 - 7870Å) and from infrared lines (7870 - 9552Å) has been plotted separately because as of this date these wavelength regions are the main ones for which heat transfer data have been obtained in shock tubes.[4]

Since the radiative transfer processes are related to the electron temperature, the end-wall radiative heat transfer should to some degree reflect any large variations in the electron temperature; and Figure 21 shows this to be the case. Initially, when the electron temperature is only slightly higher than its pre-shock value, the radiative heat transfer is negligible. However, the heat transfer from all wavelength regions increases very rapidly and actually achieves a temporary maximum value at about a quarter microsecond. As can be seen by comparison with Figures 6 and 13, this rapid rise in the radiative heat transfer rate corresponds almost exactly to the increase in electron temperature due to collision effects. From this

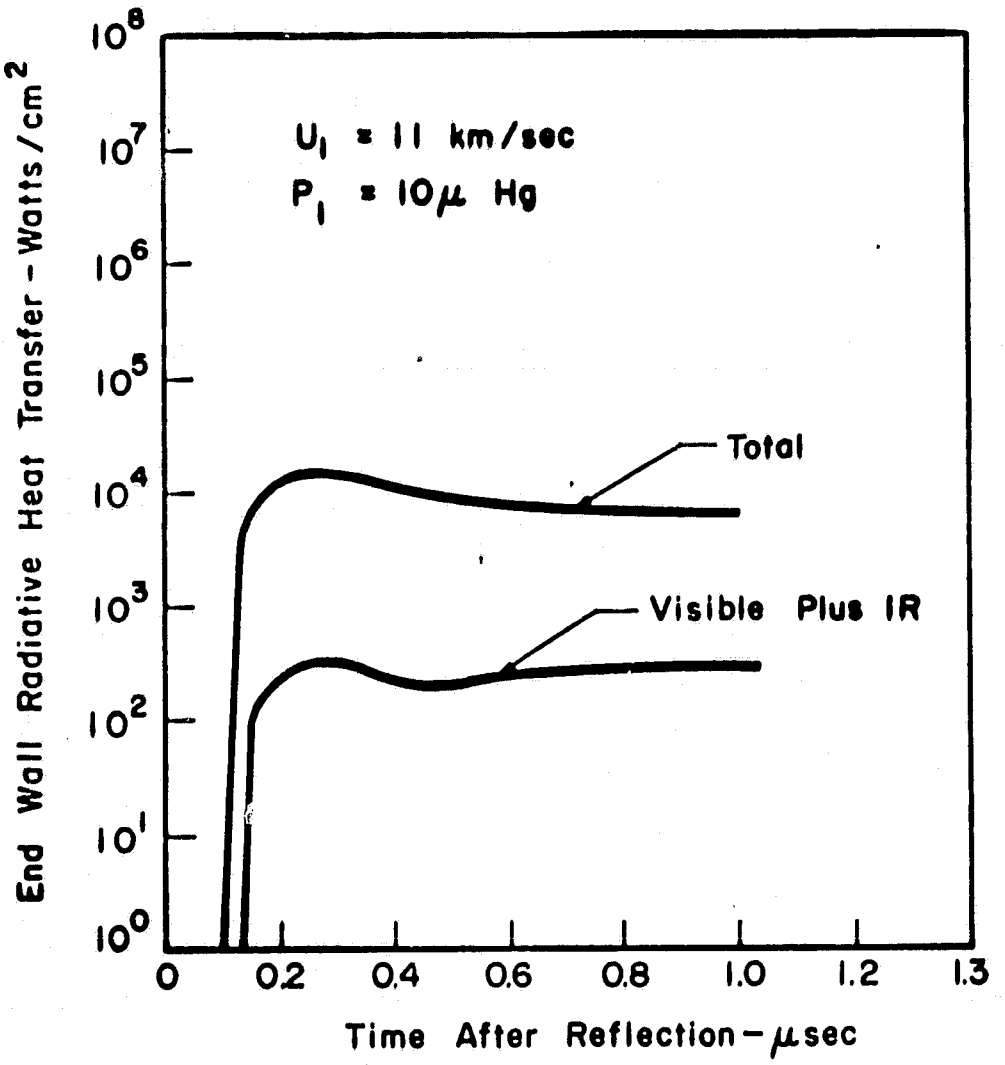

Fig. 21.--End-Wall Radiative Heat Transfer Behind a Reflected Shook Wave in Nitrogen

correspondence it can be concluded that during the initial period after reflection the end-wall radiative heat transfer varies in the same manner as the electron temperature.

After a quarter of a microsecond the total heat transfer, which is dominated by radiation from the almost opaque vacuum ultra-violet region, steadily decreases (at least during the period covered by the present calculation); but that portion from the visible and infrared part of the spectrum first decreases and then begins to slowly increase. This phenomena is due to the existence of two competing effects. First, during this time period the electron temperature is steadily decreasing, thus reducing the amount of energy being radiated by a given element of gas. Second, the slug of radiating gas is steadily increasing in size since the shock is moving away from the end-wall. Since the visible continuum is essentially a transparent region (see Figure 3), almost all radiative energy emitted in the visible in the direction of the wall will reach the wall. Consequently, it is possible, even with a decreasing electron temperature, for the radiative heat transfer from this region to increase with time simply because of the increased number of radiating particles.

Thus, for the conditions of the present investigation it appears that during the first microsecond after

reflection the total end-wall radiative heat transfer is closely coupled to the electron temperature. On the other hand, that portion originating in the visible continuum and from infrared lines appears to be influenced by both the electron temperature and the amount of gas which is radiating.

In order to ascertain whether or not two-temperature effects are important, a calculation of the end-wall radiative heat transfer for a time of 0.1 μsec has been made for the case where the electron temperature is equal to the heavy particle temperature. The result is an unrealistically large 10^{10} watts/cm^2, six orders of magnitude greater than the results from the complete calculation. The radiative cooling rate imposed upon the gas by this condition is on the order of 300,000°K per nanosecond. Since, for these conditions, a radiative heat transfer rate of 10^5 watts/cm^2 is high[4,5] and since the gas is initially at about 58,000°K, these results indicate that thermal nonequilibrium must be explicitly accounted for in the calculation of the flow field and the resulting end-wall radiative heat transfer at short times.

CHAPTER VII

CONCLUSIONS

The following general conclusions can be drawn from the present study of the effects of chemical and thermal nonequilibrium on the flow field behind a reflected shock wave in nitrogen.

(1) At short times after reflection a major portion of the reflected shock flow field exhibits a high degree of chemical and thermal nonequilibrium. These nonequilibrium effects exert a strong influence on the nature and character of the flow field behind the reflected shock wave. If accurate results are desired, their effects cannot be neglected.

(2) Immediately behind a reflected shock wave the important ionization process is atom-atom collisions. However, as soon as the number of electrons becomes significant, electron-atom collisions become the dominant ionization mechanism. The atom-ion reaction is always relatively unimportant.

(3) Initially in the reflected shock flow field the effect of radiative cooling and the loss of energy by the heavy particles due to collisions with the electrons are

sufficient to cause the end-wall pressure to decrease significantly. Only after thermal equilibration does the end-wall pressure exhibit the pressure rise usually associated with chemical relaxation.

(4) Radiative-gasdynamic coupling is quite pronounced at short times after reflection. In fact, completely erroneous velocity and pressure profiles are obtained if radiative transfer is omitted from the energy equation.

(5) Two-temperature effects must be explicitly included in order to obtain correct radiative-gasdynamic coupling results and to predict accurate end-wall radiative heat transfer rates.

In addition to the above general conclusions, the following remarks can be made concerning the present analysis.

(1) Behind the reflected shock wave, the initial cooling of the heavy particles is primarily due to radiative cooling and elastic collision effects.

(2) The velocity of the particles is strongly dependent upon the pressure. As a result, the initial decrease in pressure immediately behind the reflected shock front includes a temporary decrease in the particle velocity to a value lower than its immediate post-shock value. This velocity pattern has a slight effect on the density profiles.

(3) Examination of the variation in end-wall pressure, temperature, and density indicates that two characteristic times are associated with the relaxation processes. The first is indicative of thermal equilibration, while the second is related to chemical relaxation.

(4) During the first microsecond after reflection the total end-wall radiative heat transfer is closely coupled to the electron temperature.

Finally, the following suggestions are made for improvements and extensions to the present investigation.

(1) A better understanding of the phenomena behind a reflected shock wave could be obtained by extending the present analysis to other pressures and velocities.

(2) The generality of the present analysis could be improved by including in the reflected shock flow field the effects of chemical nonequilibrium in the incident shock region.

(3) It would be interesting to include in the present calculations the end-wall boundary layer.

(4) Since the present investigation has demonstrated that the inclusion of nonequilibrium effects in a computational scheme is tedious and lengthy, future investigations might attempt to determine approximations and simplifications which will decrease the computational effort while maintaining reasonable accuracy.

APPENDIXES

APPENDIX I

DERIVATION OF THE SPECIES CONSERVATION EQUATIONS FOR MOMENTUM AND ENERGY

In Chapter II the general equation of change was presented as

$$\frac{\partial}{\partial t}(N_i\overline{\phi_i}) + \sum_{j=1}^{3}\frac{\partial}{\partial x_j}(N_i\overline{\phi_i u_j}) - N_i\left\{\overline{\frac{\partial \phi_i}{\partial t}}\right.$$

$$\left. + \sum_{j=1}^{3}\overline{u_j\frac{\partial \phi_i}{\partial x_j}} + \sum_{j=1}^{3}F_j\overline{\frac{\partial \phi_i}{\partial u_j}}\right\} = N_i\overline{\Delta\phi_i} \qquad \text{(I-1)}$$

However the summation terms can be expressed in vector notation as

$$\sum_{j=1}^{3}\frac{\partial}{\partial x_j}(N_i\overline{\phi_i u_j}) = \frac{\partial}{\partial x_1}(N_i\overline{\phi_i u_1}) + \frac{\partial}{\partial x_2}(N_i\overline{\phi_i u_2})$$

$$+\frac{\partial}{\partial x_3}(N_i\overline{\phi_i u_3}) = \frac{\partial}{\partial \vec{r}}\cdot(N_i\overline{\vec{v}_i\phi_i}) \qquad \text{(I-2)}$$

$$\sum_{j=1}^{3}F_j\overline{\frac{\partial \phi_i}{\partial u_j}} = \left(\vec{F}\cdot\overline{\frac{\partial}{\partial \vec{v}_i}}\right)\phi_i \qquad \text{(I-3)}$$

where the order of $\vec{v}_i$ and ϕ_i given in Equation (I-2) will yield the correct result even if ϕ_i is a vector quantity.

For the conservation of momentum

$$\phi_i = m_i \vec{v}_i = m_i (\vec{V}_i + \vec{u}) \tag{I-4}$$

Thus

$$\frac{\partial}{\partial t}\left(N_i \overline{m_i(\vec{V}_i + \vec{u})}\right) = \frac{\partial}{\partial t}\left(\rho_i (\vec{u} + \vec{U}_i)\right) \tag{I-5}$$

and

$$\sum_{j=1}^{3} \frac{\partial}{\partial x_j}\left(N_i \overline{\phi_i u_j}\right) = \frac{\partial}{\partial \vec{r}} \cdot \left(N_i (\vec{V}_i + \vec{u}) m_i (\vec{V}_i + \vec{u})\right)$$

$$= \frac{\partial}{\partial r} \cdot \left(\rho_i \overline{(\vec{V}_i + \vec{u})(\vec{V}_i + \vec{u})}\right)$$

$$= \frac{\partial}{\partial \vec{r}} \cdot \left[\rho_i \overline{\vec{V}_i ; \vec{V}_i}\right] + \frac{\partial}{\partial \vec{r}} \cdot \left[\rho_i \overline{\vec{V}_i ; \vec{u}}\right] \tag{I-6}$$

$$+ \frac{\partial}{\partial r} \cdot \left[\rho_i \overline{\vec{u} ; \vec{V}_i}\right]$$

$$+ \frac{\partial}{\partial \vec{r}} \cdot \left[\rho_i \vec{u} ; \vec{u}\right]$$

However since the pressure tensor is

$$[P_i] = [\rho_i \overline{\vec{V}_i ; \vec{V}_i}] \tag{I-7}$$

and

$$\overline{\vec{V}_i} = \vec{U}_i \tag{I-8}$$

Equation (I-6) can be written

$$\sum_{j=1}^{3} \frac{\partial}{\partial x_j} (N_i \overline{\phi_i u_j}) = \frac{\partial}{\partial \vec{r}} \cdot [P_i] + \frac{\partial}{\partial \vec{r}} \cdot [\rho_i \vec{U}_i ; \vec{u}]$$

$$+ \frac{\partial}{\partial \vec{r}} \cdot [\rho_i \vec{u} ; \vec{U}_i] + \frac{\partial}{\partial \vec{r}} \cdot [\rho_i \vec{u} ; \vec{u}] \tag{I-9}$$

Likewise since $\vec{v}_1$, t, and $\vec{r}$ are independent variables

$$\overline{\frac{\partial (m_i \vec{v}_i)}{\partial t}} = 0 \tag{I-10}$$

$$\sum_{j=1}^{3} \overline{u_j \frac{\partial (m_i \vec{v}_i)}{\partial x_j}} = 0 \tag{I-11}$$

By expressing $\vec{F}$ as $\vec{X}_1/m_1$ the last term becomes

$$-N_i \left(\frac{\vec{X}_i}{m_i} \cdot \frac{\partial}{\partial \vec{v}_i}\right) \overline{m_i \vec{v}_i} = -N_i \vec{X}_i \qquad \text{(I-12)}$$

Thus the species momentum equation can be written

$$\frac{\partial}{\partial t}(\rho_i \alpha) + \frac{\partial}{\partial t}(\rho_i \vec{U}_i) + \frac{\partial}{\partial \vec{r}} \cdot [P_i] + \frac{\partial}{\partial \vec{r}} \cdot [\rho_i \vec{U}_i ; \vec{u}]$$

$$+ \frac{\partial}{\partial \vec{r}} \cdot [\vec{u} ; \rho_i \vec{U}_i] + \frac{\partial}{\partial \vec{r}} \cdot [\rho_i \vec{u} ; \vec{u}] - N_i \vec{X}_i \qquad \text{(I-13)}$$

$$= N_i \overline{\Delta \phi_i}$$

The various dyadics in this equation can be rewritten using the relationship that

$$\frac{\partial}{\partial \vec{r}} \cdot [\vec{a} ; \vec{b}] = \vec{b} \left(\frac{\partial}{\partial \vec{r}} \cdot \vec{a}\right) + \left(\vec{a} \cdot \frac{\partial}{\partial \vec{r}}\right) \vec{b} \qquad \text{(I-14)}$$

Hence, Equation (I-13) becomes

$$\rho_i \frac{\partial \vec{u}}{\partial t} + \vec{u} \frac{\partial \rho_i}{\partial t} + \frac{\partial}{\partial t}(\rho_i \vec{v}_i) + \frac{\partial}{\partial \vec{r}} \cdot [P_i] + \vec{u}\left(\frac{\partial}{\partial \vec{r}} \cdot \rho_i \vec{v}_i\right)$$

$$+ \left(\rho_i \vec{v}_i \cdot \frac{\partial}{\partial \vec{r}}\right)\vec{u} + \rho_i \vec{v}_i \left(\frac{\partial}{\partial \vec{r}} \cdot \vec{u}\right) + \left(\vec{u} \cdot \frac{\partial}{\partial \vec{r}}\right)\rho_i \vec{v}_i \qquad \text{(I-15)}$$

$$+ \vec{u}\left(\frac{\partial}{\partial \vec{r}} \cdot \rho_i \vec{u}\right) + \rho_i \left(\vec{u} \cdot \frac{\partial}{\partial \vec{r}}\right)\vec{u} - N_i \vec{X}_i$$

$$= N_i \overline{\Delta \phi_i}$$

Now in general, assuming that the elastic collisions are binary in nature, the volumetric rate of change in average value of some property ϕ_i can be expressed as

$$N_i \overline{\Delta \phi_i} = N_i \sum_j \Delta_j \overline{\phi_i} \qquad \text{(I-16)}$$

where $N_i \Delta_j \overline{\phi_i}$ represents the change due to encounters between particles of type i and particles of type j. According to Chapman and Cowling[34] the individual terms of Equation (I-16) can be expressed for elastic collisions as

$$N_i \Delta_j \bar{\phi}_i = \int\int\int\int (\phi_i' - \phi_i) f_i f_j g \, b \, db \, d\epsilon \, d\vec{v}_i \, d\vec{v}_j \qquad \text{(I-17)}$$

where prime denotes the quantity after collision. The parameters b and ϵ describe the geometry of the encounter, while g is the magnitude of the relative velocity between the two particles. The respective velocity distribution functions are indicated by f_i and f_j. For the momentum equation the elastic portion of the collision term is determined from Equation (I-17) using $\phi_i = m_i \vec{V}_i$ and $\phi_i' = m_i \vec{V}_i'$. The resulting expression will be designated as $\vec{P}_{ij}$.

Collisions involving charged particles, however, are characterized by small deflections and involve many particles at once. Thus, for electrons and ions the Boltzmann binary collision idea of Equation (I-17) is not strictly applicable. If, on the other hand, this fact is ignored and Equation (I-17) evaluated using an appropriate collision cross section, the result is the same as that obtained by using a more exact treatment such as the Fokker-Planck equation.[35] The reason is that the important deflections are small, simultaneous, and random and can be treated as if they were two-body sequential collisions. While this approach does encounter difficulties for like-particle interactions such as electron

self-equilibration, it should be adequate for the present analysis, which considers relaxation between species but assumes self-equilibration to be instantaneous. Now if the species continuity equation is multiplied by $\vec{u}$

$$\vec{u}\,\frac{\partial \rho_i}{\partial t} + \vec{u}\left(\frac{\partial}{\partial \vec{r}} \cdot \rho_i \vec{u}\right) + \vec{u}\left(\frac{\partial}{\partial \vec{r}} \cdot \rho_i \vec{V}_i\right) = \dot{w}_i \vec{u} \qquad \text{(I-18)}$$

then Equation (I-15) becomes

$$\rho_i \frac{\partial \vec{u}}{\partial t} + \rho_i \left(\vec{u} \cdot \frac{\partial}{\partial \vec{r}}\right)\vec{u} + \frac{\partial}{\partial t}\left(\rho_i \vec{V}_i\right) + \left(\vec{u} \cdot \frac{\partial}{\partial \vec{r}}\right)\rho_i \vec{V}_i$$

$$+ \frac{\partial}{\partial \vec{r}} \cdot [P_i] + \rho_i \vec{V}_i \left(\frac{\partial}{\partial \vec{r}} \cdot \vec{u}\right) + \rho_i \left(\vec{V}_i \cdot \frac{\partial}{\partial \vec{r}}\right)\vec{u} - N_i \vec{X}_i \qquad \text{(I-19)}$$

$$+ \dot{w}_i \vec{u} = \sum_j \vec{P}_{ij} + \vec{J}_i$$

where the collision term has been represented by two parts -- one part representing effects due to elastic collisions and one part for inelastic collisions.

By defining

$$\frac{D}{Dt} = \frac{\partial}{\partial t} + \vec{u} \cdot \frac{\partial}{\partial \vec{r}} \qquad \text{(I-20)}$$

Equation (I-19) becomes identical with Equation (4) in Chapter II.

For the species energy equation the suitable property function is

$$\phi = \frac{1}{2} m_i v_i^2 = \frac{1}{2} m_i (\vec{v}_i + \vec{u})^2 \qquad \text{(I-21)}$$

where the first term in Equation (I-1) becomes

$$\frac{\partial}{\partial t}(N_i \overline{\phi_i}) = \frac{\partial}{\partial t}\left(\frac{1}{2} N_i \overline{m_i v_i^2}\right) = \frac{\partial}{\partial t}\left(\frac{1}{2} N_i \overline{m_i v_i^2}\right)$$

$$+ \frac{\partial}{\partial t}(N_i m_i \overline{\vec{v}_i \cdot \vec{u}}) + \frac{\partial}{\partial t}(N_i \tfrac{1}{2} \overline{m_i u^2}) \qquad \text{(I-22)}$$

By definition

$$e_i = \overline{\tfrac{1}{2} v_i^2} \qquad \text{(I-23)}$$

so that

$$\frac{\partial (N_i \overline{\phi_i})}{\partial t} = \frac{\partial}{\partial t}(\rho_i e_i) + \frac{\partial}{\partial t}(\rho_i \vec{U}_i \cdot \vec{u}) + \frac{1}{2}\frac{\partial}{\partial t}(\rho_i u^2) \qquad \text{(I-24)}$$

The second term is

$$\frac{\partial}{\partial \vec{r}} \cdot \left(N_i \overline{\vec{v}_i \phi_i}\right) = \frac{\partial}{\partial \vec{r}} \cdot \left[N_i \overline{\vec{v}_i \tfrac{1}{2} m_i V_i^2}\right]$$

$$+ \frac{\partial}{\partial \vec{r}} \cdot \left(m_i N_i \overline{\vec{v}_i \left(\vec{V}_i \cdot \vec{u}\right)}\right) + \frac{\partial}{\partial \vec{r}} \cdot \left(N_i \overline{\vec{v}_i \tfrac{1}{2} m_i u^2}\right) \qquad \text{(I-25)}$$

By using the relationships

$$\vec{a}\left(\vec{b} \cdot \vec{c}\right) = \vec{c} \cdot \left(\vec{b} ; \vec{a}\right) \qquad \text{(I-26)}$$

$$\vec{q}_i = \tfrac{1}{2} \rho_i \overline{V_i^2 \vec{V}_i} \qquad \text{(I-27)}$$

this term becomes

$$\frac{\partial}{\partial \vec{r}} \cdot \left(N_i \overline{\vec{v}_i \phi_i}\right) = \frac{\partial}{\partial \vec{r}} \cdot \vec{q}_i + \frac{\partial}{\partial \vec{r}} \cdot \left(\rho_i e_i \vec{u}\right) + \frac{\partial}{\partial \vec{r}} \cdot \left(\vec{u} \cdot [P_i]\right)$$

$$+ \frac{\partial}{\partial \vec{r}} \cdot \left(\rho_i \vec{u} \cdot \left(\vec{U}_i ; \vec{u}\right)\right) + \frac{\partial}{\partial \vec{r}} \cdot \left(\tfrac{1}{2} \rho_i u^2 \vec{u}_i\right) \qquad \text{(I-28)}$$

As in the case of the species momentum equation the third and fourth terms are zero because $\vec{v}_1$, $\vec{r}$, and t are independent variables. The last term on the left-hand side of Equation (I-1) becomes

$$-N_i\left(\vec{F}_i\cdot\overline{\frac{\partial}{\partial\vec{v}_i}}\right)\phi_i = -N_i\left(\frac{\vec{X}_i}{m_i}\cdot\overline{\frac{\partial}{\partial\vec{v}_i}}\right)\left(\tfrac{1}{2}m_i v_i^2\right)$$

$$= -N_i\vec{X}_i\cdot\vec{U}_i - N_i\vec{X}_i\cdot\vec{u} \qquad \text{(I-29)}$$

In this manner the species energy equation becomes

$$\frac{\partial}{\partial t}(\rho_i e_i) + \frac{\partial}{\partial t}(\rho_i\vec{U}_i\cdot\vec{u}) + \frac{1}{2}\frac{\partial}{\partial t}(\rho_i u^2) + \frac{\partial}{\partial\vec{r}}\cdot\vec{q}_i$$

$$+\frac{\partial}{\partial\vec{r}}\cdot(\rho_i e_i\vec{u}) + \frac{\partial}{\partial\vec{r}}\cdot(\vec{u}\cdot[P_i]) + \frac{\partial}{\partial\vec{r}}\cdot(\rho_i\vec{u}\cdot(\vec{U}_i;\vec{u}))$$

$$+\frac{\partial}{\partial\vec{r}}\cdot\left(\frac{1}{2}\rho_i u^2\vec{u}_i\right) - N_i\vec{X}_i\cdot\vec{U}_i - N_i\vec{X}_i\cdot\vec{u} \qquad \text{(I-30)}$$

$$= E_i$$

where E_i is used to represent the change in energy due to collisions. Now by using the fact that

$$\frac{\partial}{\partial\vec{r}}\cdot[\vec{u}\cdot[P_i]] = \left[\frac{\partial}{\partial\vec{r}}\,;\vec{u}\right]:[P_i] + \vec{u}\cdot\left[\frac{\partial}{\partial\vec{r}}\cdot[P_i]\right] \qquad \text{(I-31)}$$

and using the specie momentum equation to eliminate $N_1\vec{X}_1\cdot\vec{u}$, the energy equation becomes

$$\frac{D}{Dt}(\rho_i e_i) + \frac{\partial}{\partial \vec{r}} \cdot \vec{q}_i + \rho_i e_i \left(\frac{\partial}{\partial \vec{r}} \cdot \vec{u}\right) + \rho_i \vec{U}_i \cdot \frac{D\vec{u}}{Dt}$$

$$+\left[\frac{\partial}{\partial \vec{r}} ; \vec{u}\right] : [P_i] - N_i \vec{X}_i \cdot \vec{U}_i = E_i - \vec{u} \cdot \Sigma \vec{P}_{ij} \qquad \text{(I-32)}$$

For the energy equation, Equation (I-17) yields for elastic collisions

$$N_i \Delta_j \overline{\phi_i} = \iiiint \frac{1}{2} m_i (v_i'^2 - v_i^2) f_i f_j g b \, db \, d\epsilon \, d\vec{v}_i \, d\vec{v}_j \qquad \text{(I-33)}$$

This equation can be divided into two terms as follows

$$N_i \Delta_j \overline{\phi_i} = \iiiint \frac{1}{2} m_i \{(\vec{v}_i' - \vec{u}_i)^2 - (\vec{v}_i - \vec{u}_i)^2\} f_i f_j g b \, db \, d\epsilon \, d\vec{v}_i \, d\vec{v}_j \qquad \text{(I-34)}$$

$$+ \vec{u}_i \cdot \left[\iiiint m_i (\vec{v}_i' - \vec{v}_i) f_i f_j g b \, db \, d\epsilon \, d\vec{v}_i \, d\vec{v}_j\right.$$

where the first term represents the rate of energy gain by species i due to elastic encounters between species i and j because of thermal motion of the particles. The second part represents the rate at which work is done on species i due to elastic interactions between species i and j because of directed motion of the particles. In this work the first term will be denoted as $\int_{ij}$ and the second as

$\vec{u}_i \cdot \vec{P}_{ij}$. Hence

$$E_i = \sum_j \xi_{ij} + \vec{u}_i \cdot \sum_j \vec{P}_{ij} + Q_i \qquad \text{(I-35)}$$

where the last term represents energy change due to elastic collisions.

Then breaking up the pressure tensor as

$$[P_i] = p_i [I] + [\tau_i] \qquad \text{(I-36)}$$

and expressing internal energy is terms of enthalpy

$$e_i = h_i - p_i/\rho_i \qquad \text{(I-37)}$$

Equation (I-32) becomes

$$\frac{D}{Dt}(\rho_i h_i) - \frac{Dp_i}{Dt} + \frac{\partial}{\partial \vec{r}} \cdot \vec{q}_i + \rho_i h_i \left(\frac{\partial}{\partial \vec{r}} \cdot \vec{u}\right)$$

$$+ \rho_i \vec{v}_i \cdot \frac{D\vec{u}}{Dt} + [\tau_i] : \left[\frac{\partial}{\partial \vec{r}} ; \vec{u}\right] - N_i \vec{X}_i \cdot \vec{v}_i \qquad \text{(I-38)}$$

$$= \sum_j \xi_{ij} + \vec{v}_i \cdot \sum_j \vec{P}_{ij} + Q_i$$

Equation (I-38) is the same as Equation (5) in Chapter I.

APPENDIX II

DISCUSSION OF STABILITY AND THE η -s COORDINATE SYSTEM

In any numerical solution to a system of differential equations, consideration must be given to the restrictions imposed upon step size, or in the case of two independent variables, step size ratio, in order to insure numerical stability. In general the determination of these restrictions is at best a tedious and complicated procedure. However, Von Neumann and Richtmyer[36] have shown that for fluid dynamical equations second derivative terms usually dominate the stability. For example, if an equation of the form

$$\frac{\partial T}{\partial s} = C \frac{\partial^2 T}{\partial \eta^2} \tag{II-1}$$

is written in finite difference form as

$$\frac{T(\eta, s+\Delta s) - T(\eta, s)}{\Delta s} = C \frac{T(\eta+\Delta\eta, s) - 2T(\eta, s) + T(\eta-\Delta\eta, s)}{(\Delta\eta)^2} \tag{II-2}$$

then their analysis indicates that the numerical solution

will be stable if

$$\frac{\Delta s}{(\Delta \eta)^2} \leq \frac{1}{2C} \qquad \text{(II-3)}$$

The word stable here means that any errors incurred at some given time do not amplify with time.

In the set of equations used in the present investigation expressions similar to the right-hand-side of Equation (II-1) appear in the energy equations via the thermal conduction terms. Since the present calculation neglects the end-wall boundary layer these terms should be small. Thus, in the electron energy equation the thermal conduction term was neglected in all calculations. Neglecting this term is further justified by the fact that the electron temperature gradients are always comparitively small. On the other hand the heavy particle temperature gradients are quite high in some regions, and thermal conduction may be important there. Also initial numerical experiments with the equations indicated that thermal conduction aided the stability of the overall energy equation in the same manner that viscosity aids shock problems.[33] Consequently, the thermal conduction term associated with atomic nitrogen was included in the calculations.

By assuming that the conduction term dominates the stability character, Equation (II-3) can be used to estimate the step size ratio required. Application of this technique to the overall energy equation yielded that for a $\Delta\eta$ of one, the non-dimensional time increment, Δs^*, had to be less than one-fourth. Numerical experiments revealed that this method predicted very accurately the stability restrictions, but to be conservative Δs^* was set equal to one-fifth in the actual computations. Physically, this value corresponds to a time increment of 5.7×10^{-10} seconds.

The reflected shock wave problem was formulated with the end-wall boundary layer included, and it was for this reason that the governing equations were recast into the η - s coordinate system. However, the representative calculation discussed in Chapter VI neglects the end-wall boundary layer; and, thus, a discussion of the advantages and disadvantages of using a density stretched coordinate system in an inviscid flow is in order.

It has been the experience of this investigator that external to the end-wall boundary layer the η - s system offers one small advantage but in turn introduces one major and several minor disadvantages. The advantage (previously discussed in Chapter V, Section B) is that the mass balance condition across the shock wave becomes algebraic in form

in the η - s system and can subsequently be solved directly to obtain the shock position. The major disadvantage is that the transformation places more computational points in regions of higher density. As a result at times of one microsecond and greater the finite difference grid points have shifted so that there are many points in the relatively steady region near the wall and very few in the highly nonequilibrium region near the shock front. Consequently, with increasing time the solution near the shock front becomes increasingly more inaccurate, and the problem is eventually doomed to become unstable. Exactly when such instability will set in depends upon the magnitude of the spatial variable step size. If the problem had been formulated in the x-t plane no such shifting would occur, and this problem would not exist. For the step size used in the present calculation ($\Delta\eta = 1.0$), this instability occurred at about 1.23 μsec after reflection.

Another disadvantage of the transformed system is that the corresponding x coordinates can only be obtained by integration, i.e.

$$x = \left[\frac{2\rho_2 s}{c_2}\right]^{1/2} \int_0^{\eta} \frac{1}{\rho}\, d\eta \qquad \text{(II-4)}$$

Thus, the accuracy of the x coordinate is dependent upon the accuracy of the flow field solution, the accuracy of the integration method, and the number of points considered. Obviously in an x-t system this situation does not exist.

Another minor disadvantage of using an η - s system is that it makes it difficult to formulate the equation variables in conservative forms. Here the term conservative form is used to denote the practice of treating as actual variables certain quantities such as ρu, $p + \rho u^2$, etc. The philosophy behind this approach is that these grouped variables change more slowly in the flow than the usual quantities (p, ρ , u, etc.) and thus lend themselves to more accurate numerical solution. In an x-t system this approach could be used.

The present set of calculations required the following execution times on the Ohio State University IBM 360, Model 75, computer.

Flow Time	Computer Time
0.10 - 0.68 sec	58 minutes
0.68 - 1.00 sec	58 minutes
1.00 - 1.23 sec	45 minutes
Total	2 hours 41 minutes

While the present results were obtained in the η - s coordinate system, it is felt that the computational time

would be relatively unaffected by changing to an x-t system.

In summary, it is the opinion of this investigator based on the experience gained from these results that inviscid reflected shock studies can be best carried out in a physical x-t coordinate system.

REFERENCES

1. Nerem, R. M. and Stickford, G. H., "Shock Tube Studies of Equilibrium Air Radiation," AIAA Journal, Vol. 3, No. 6, June 1965, pp. 1011-1018.

2. Nerem, R. M., Carlson, L. A., and Hartsel, J. E., "Chemical Relaxation Phenomena Behind Normal Shock Waves in a Dissociated Freestream," AIAA Journal, Vol. 5, No. 5, May 1967, pp. 910-916.

3. Anderson, Jr., J. D., "Radiative Transfer Effects on the Flow Field and Heat Transfer Behind a Reflected Shock Wave in Air," Physics of Fluids, Vol. 10, No. 8, August 1967, pp. 1785-1793.

4. Golobic, R. A. and Nerem, R. M., "Shock Tube Measurements of End-Wall Radiative Heat Transfer in Air," AIAA Journal, Vol. 6, No. 9, September 1968, pp. 1741-1747.

5. Nerem, R. M., Golobic, R. A., and Carlson, L. A., "Radiation-Gasdynamic Coupling Behind Reflected Shock Waves in Air," Presented at the 12th International Applied Mechanics Congress, Stanford University, August 26-31, 1968.

6. Presley, L. L. and Hanson, R. K., "Exact Solutions of Reflected Normal Shock-Wave Flow Fields with Nonequilibrium Chemical Reactions," AIAA Paper 68-732, AIAA Fluid and Plasma Dynamics Conference, Los Angeles, California, June 24-26, 1968.

7. Oettinger, P. E. and Bershader, D., "A Unified Treatment of the Relaxation Phenomena in Radiating Argon Plasma Flows," AIAA Journal, Vol. 5, No. 9, September 1967, pp. 1625-1632.

8. Chapin, C. E., "Nonequilibrium Radiation and Ionization in Shock Waves," AA&ES 67-9, June 1967, Purdue University, Lafayette, Indiana.

9. Camac, M. and Kemp, N. H., "A Multitemperature Boundary Layer," Research Report 184, August 1964, Avco-Everett Research Laboratory, Everett, Mass.

10. Chapman, S. and Cowling, T. G., The Mathematical Theory of Non-Uniform Gases, 2nd ed., University Press, Cambridge, 1964, p. 48.

11. Demetriades, S. T., "Determination of Energy-Loss Factors for Slow Electrons in Hot Bases," The Physical Review, Vol. 158, No. 2, June 1967, pp. 215-217.

12. Jaffrin, M. Y., "Shock Structure in a Partially Ionized Gas," Physics of Fluids, Vol. 8, No. 4, April 1965, pp. 606-625.

13. Jaffrin, M. Y. and Probstein, R. F., "Structure of a Plasma Shock Wave," Physics of Fluids, Vol. 7, No. 10, October 1964, pp. 1658-1674.

14. Clauser, F. H., ed., Symposium of Plasma Dynamics, Addison-Wesley, Reading, Massachusetts, 1960, pp. 119-157.

15. Cravath, A. M., "The Rate at Which Ions Lose Energy in Elastic Collisions," Physical Review, Vol. 36, 1930, p. 248.

16. Morse, T. F., "Energy and Momentum Exchange Between Nonequilibrium Gases," Physics of Fluids, Vol. 6, No. 10, October 1963, pp. 1420-1427.

17. Petschek, H. and Byron, S., "Approach to Equilibrium Ionization Behind Strong Shock Waves in Argon," Anals of Physics, Vol. 1, 1957, pp. 270-315.

18. Hansen, C. F., "Approximations for the Thermodynamic and Transport Properties of High-Temperature Air," NASA TR-R-50, 1959.

19. Fay, J. A., "Hypersonic Heat Transfer in the Air Laminar Boundary Layer," AMP 71, March 1962, Avco-Everett Research Laboratory, Everett, Massachusetts.

20. Dorrance, W. H., Viscous Hypersonic Flow, McGraw-Hill, New York, 1962, p. 283.

21. Chapman, S. and Cowling, T. G., The Mathematical Theory of Non-Uniform Gases, 2nd ed., University Press, Cambridge, 1964, p. 245.

22. Marrone, P. V., "Inviscid Nonequilibrium Flow Behind Bow and Normal Shock Waves, Part I. General Analysis and Numerical Examples," CAL Report No. QM-1626-A-12 (I), May 1963, Cornell Aeronautical Laboratory, Inc., Buffalo, New York.

23. Chu, C. W., "Use of Equilibrium Constants in Nonequilibrium Flow Computations," AIAA Journal, Vol. 3, No. 6, June 1967, pp. 1193-1194.

24. Wilson, J., "Ionization Rate of Air Behind High Speed Shock Waves," Research Report 222, October 1965, Avco-Everett Research Laboratory, Everett, Mass.

25. Vanderslice, J. T., Mason, E. A., and Lippincott, E. R., "Interactions Between Ground-State Nitrogen Atoms and Molecules. The N-N, N-N_2, and N_2-N_2 Interactions," Journal of Chemical Physics, Vol. 30, No. 1, January 1959, pp. 129-136.

26. Shkarofsky, I. P., Bachynski, M. P., and Johnston, T. W., "Collision Frequency Associated With High Temperature Air and Scattering Cross-Sections of the Constituents," Planetary Space Science, Vol. 6, 1961, pp. 24-46.

27. Fay, J. A. and Kemp, N. H., "Theory of Stagnation-Point Heat Transfer in a Partially Ionized Diatomic Gas," AIAA Journal, Vol. 1, No. 12, December 1963, pp. 2741-2751.

28. Chapman, S. and Cowling, T. G., The Mathematical Theory of Non-Uniform Gases, 2nd ed., University Press, Cambridge, 1964, p. 244.

29. Schulz, G. J. and Brown, S. C., "Microwave Study of Positive Ion Collection by Probes," Physical Review, Vol. 98, No. 6, June 1955, pp. 1642-1644.

30. Dix, D. M., "Energy Transfer Processes in a Partially Ionized Two-Temperature Gas," AIAA Journal, Vol. 2, No. 12, December 1964, pp. 2081-2090.

31. Knight, D. D., "Electron Thermochemical Nonequilibrium Effects in Re-Entry Boundary Layers," AIAA Paper No. 69-82, Seventh Aerospace Sciences Meeting, New York, January 20-22, 1969.

32. Hanson, R. K., "An Experimental and Analytical Investigation of Shock-Wave Reflection in a Chemically Relaxing Gas," SUDAR No. 345, May 1968, Stanford University, Stanford, California.

33. Hay, G. D., "An Approximate Small-Time Solution for a Transparent Radiating Gas Behind a Reflected Shock Wave," M.Sc. Thesis, The Ohio State University, Columbus, Ohio, 1968.

34. Chapman, S. and Cowling, T. G., The Mathematical Theory of Non-Uniform Gases, 2nd ed., University Press, Cambridge, 1964, p. 62.

35. Shkarofsky, I., Johnston, T., and Bachynski, M., The Particle Kinetics of Plasmas, Addison-Wesley, Reading, 1966, pp. 14-16.

36. Von Neumann, J. and Richtmyer, R. D., "A Method for the Numerical Calculation of Hydrodynamic Shocks," Journal of Applied Physics, Vol. 21, No. 3, March 1950, pp. 232-237.

RADIATIVE TRANSFER, CHEMICAL NONEQUILIBRIUM, AND TWO-TEMPERATURE EFFECTS BEHIND A REFLECTED SHOCK WAVE IN NITROGEN

By

Leland Arnold Carlson, Ph.D.

The Ohio State University, 1969

Professor Robert M. Nerem, Adviser

The fundamental equations and boundary conditions governing the flow between a reflected shock wave and a shock-tube end-wall have been formulated including chemical nonequilibrium, two-temperature, and radiative-gasdynamic coupling effects. In obtaining these equations one dimensionality has been assumed, and precursor effects on the gas in front of the shock wave have been ignored. The radiative properties of the gas have been represented by an approximate non-gray absorption coefficient model. Furthermore, the gas in front of the reflected wave has been considered to be in complete equilibrium. In addition, the exchange of momentum and energy due to elastic collisions between particles has been included, and the associated collision integrals have been formulated and evaluated in closed form.

The resulting equations have been transformed into a boundary layer type of coordinate system, and a solution technique based upon a forward-in-time finite-difference scheme has been postulated. A calculation neglecting the end-wall boundary layer has been carried out for a reflected shock wave resulting from an incident shock travelling at 11 km/sec into quiescent nitrogen at a pressure of 10^{-3} cm of mercury.

The results show that in the region immediately behind the shock wave the electron temperature is much lower than the heavy particle temperature, but that near the wall the two temperatures are equal after 0.45 sec. Furthermore, during the first microsecond after reflection radiative cooling is strong enough to cause the end-wall pressure to decrease by a factor of almost two before increasing to its equilibrium value. This cooling also induces a velocity acceleration towards the wall and accelerates chemical and thermal relaxation. The atom-electron reaction is shown to be the predominant ionization mechanism except near the shock front, where atom-atom ionization is important. Finally, comparison calculations demonstrate that two-temperature effects must be included to accurately predict end-wall radiative heat transfer rates and radiative-gasdynamic coupling effects.